Fall 12-20-2019

Molecular Insights into Major Peripheral T-cell Lymphoma Entities with Advances in a Representative Model System

Tayla B. Heavican
University of Nebraska Medical Center

MOLECULAR INSIGHTS INTO MAJOR PERIPHERAL T-CELL LYMPHOMA ENTITIES WITH ADVANCES IN A REPRESENTATIVE MODEL SYSTEM

by

Tayla B. Heavican

A DISSERTATION

Presented to the Faculty of the University of Nebraska Graduate College in Partial Fulfillment of the Requirements for the Degree of Doctor of Philosophy

Pathology and Microbiology Graduate Program

Under the Supervision of Professor Javeed Iqbal

University of Nebraska Medical Center
Omaha, Nebraska

October, 2019

Supervisory Committee:

Javeed Iqbal, Ph.D.

Michael R. Green, Ph.D.

Kai Fu, M.D., Ph.D.

Ricia Kate Hyde, Ph.D.

ACKNOWLEDGEMENTS

I would like to begin by expressing my gratitude towards my advisor, Dr. Javeed Iqbal. He has provided continued support and motivation throughout my graduate program. I want to thank him for not only encouraging me to collaborate, present at conferences, publish research findings and be involved within our own campus, but for also providing me with many opportunities to do so. The environment he created challenged me to think and interpret data critically, exercise and enhance my leadership skills by guiding others in the laboratory, generate and maintain professional relationships with experts in our field, convey scientific findings through different platforms and competitively apply for fellowships, which has helped in preparing me for future endeavors. I would also like to extend my sincere appreciation to all other members of my Supervisory Graduate Committee, Drs. Kai Fu, Michael Green and Kate Hyde. Thank you for your continued support and suggestions in project design, execution and presentation. Further, I am grateful for your guidance throughout my comprehensive exam and dissertation preparation.

I would like to thank and acknowledge all past and present members of the Iqbal Laboratory for their companionship and shared knowledge during my graduate education. To start, I would like to thank Dr. Alyssa Bouska; I will be forever grateful for all she has taught me during the numerous projects we have completed together. There are too many to list, but in particular, I am thankful to have had her guidance throughout the design, execution, analysis, preparation and submission of my first manuscript. She has been essential to not only me, but to our entire laboratory in establishing protocols, performing bioinformatics analysis and ensuring daily life in the laboratory runs smoothly, just to name a few. Next, I would like to thank Dr. Waseem Lone for his help in the murine projects and performance of functional assays. I have countless memories, but am forever grateful for all of the hours we spent in the animal facility together

learning everything first-hand. I would also like to thank my fellow graduate students Jiayu Yu and Tyler Herek for help in establishing protocols, performing experiments and monitoring animals. I also extend my thanks to recent students Sunandini Sharma and Sahil Sethi for their help in bioinformatics analyses. Lastly, I would like to thank Cindy Lachel for being the first to teach and welcome me when I joined the laboratory.

I would like to extend my appreciation to Dr. John Chan and his laboratory at City of Hope National Medical Center. Drs. Chan and Timothy McKeithan have provided hours of valuable input on project design and experimental techniques, in addition to sharing their extensive knowledge as experts in our field. I would like to thank Dr. Yuping Li for all of her help in managing to successfully collaborate across the country. I would also like to thank her for her efforts and time spent on the murine project and manipulation of primary human cells, specifically. I would like to thank previous Chan Laboratory members Drs. Weiwei Zhang, Qiang Gong, Chao Wang and Joseph Rohr for helping in data analyses and project initiation.

Dr. Catalina Amador, it has truly been a pleasure to learn from and work side-by-side with her on a number of projects throughout my graduate program. In particular, I would like to thank her for the countless hours spent helping to optimize antibodies and reviewing slides, whether that be human or murine.

I would like to thank Jacob Robinson and Tyler Gilbreath for their efforts in completing much of the immunohistochemistry. I have been fortunate to work with Lijun Sun and other members of the Tissue Science Facility at the University of Nebraska Medical Center. In addition, I would like to acknowledge Dr. James Eudy, Alok Dhar and Timothy Szalewski of the Next Generation Sequencing Core at the University of Nebraska Medical Center and Dr. Bhavana Dave and Jadd Stevens of the Human Genetics Laboratory at the University of Nebraska Medical Center. I would also like to thank all staff in Comparative Medicine at the University of Nebraska Medical Center for

their continuous support in monitoring animals and learning new techniques. Further, my gratitude is extended to Dr. Chan-Wang Lio at the La Jolla Institute for Immunology for his collaboration and for providing the expertise necessary to complete the hydroxymethylation profiling.

I would like to extend my appreciation to all other local, national and international collaborators I had the pleasure of interacting with throughout the past five years. I would like to acknowledge that much of this research would not have been possible without your collaborations in case collection, review and data sharing to provide more comprehensive analyses in this field which is often hindered by the rarity of the disease. In particular, I would like to thank members of the Nebraska Lymphoma Study Group, International PTCL Consortium and Lymphoma Leukemia Molecular Profiling Project. I have been fortunate to have met many of you in person at conferences and hope to continue our professional collaborations.

I would also like to thank the Pathology and Microbiology Graduate Program, and in particular Dr. Rakesh Singh and Tuire Cechin, for your continued support. I am also grateful to have been funded for two years through the University of Nebraska Medical Center Assistantship Fellowship.

Lastly, I cannot express enough gratitude to my friends and family. I am fortunate to have built a number of relationships with fellow graduate students through EMPOWER, Student Senate and Graduate Student Association and will forever be thankful for the support we were able to provide each other. I am also grateful to have an extremely strong support system (“Squad”) outside of school who have been vital in helping me maintain a healthy work-life balance, while also always encouraging me when I need it and happy to sit through a trial run of a presentation. I especially want to acknowledge my boyfriend, Joseph Foral. I am thankful to have found someone who is understanding of late nights spent writing or who will spend a weekend with me in the

laboratory while I finish an experiment. I am forever grateful to have found someone who was willing to travel across the world with me and listen to me give the same presentation five times in seven days. However, most of all, I am thankful for his constant support and encouragement when I need it most. I want to end by thanking my parents, Todd and Cindy Heavican, and sister, Cailey Noonan. You have provided me with a lifetime of love, stability and encouragement leading me to where I am today, and for that, I am forever grateful.

MOLECULAR INSIGHTS INTO MAJOR PERIPHERAL T-CELL LYMPHOMA ENTITIES WITH ADVANCES IN A REPRESENTATIVE MODEL SYSTEM

Tayla B. Heavican, Ph.D.

University of Nebraska, 2019

Supervisor: Javeed Iqbal, Ph.D.

Peripheral T-cell lymphoma (PTCL) is a group of complex clinicopathological entities associated with an aggressive clinical course. Angioimmunoblastic T-cell lymphoma (AITL) and PTCL-not otherwise specified (PTCL-NOS) are the two most frequent categories accounting for more than 50% of PTCLs. Gene expression profiling (GEP) defined molecular signatures for AITL and delineated biological and prognostic subgroups within PTCL-NOS (PTCL-GATA3 and PTCL-TBX21). Genomic copy number analysis and targeted sequencing revealed unique genomic abnormalities and oncogenic pathways, indicating distinct oncogenic evolution. PTCL-GATA3 exhibited higher genomic complexity characterized by frequent loss or mutation of tumor suppressor genes targeting the CDKN2A/B-TP53 axis and *PTEN*-PI3K pathways. PTCL-TBX21 had fewer abnormalities, primarily targeting cytotoxic effector genes, and was enriched in mutations of genes regulating DNA methylation. AITL showed lower genomic complexity compared to other PTCL entities, suggesting it is epigenetically driven, yet frequent co-occurring gains of chromosome 5 and 21 were observed. Thus, to further explore the underlying pathobiology of AITL, we established an AITL-like murine model. We have found TET2 to be the most recurrent mutation in AITL with evidence that it may be a founder mutation. The generated murine model had a loss of Tet2 in $CD4^+$ T-cells, resulting in the long-term development of an aggressive T-cell lymphoma with a T_{FH} phenotype, similar to AITL. These mice developed lymphomas characterized by massive

splenomegaly, marked generalized lymphadenopathy, hepatomegaly and occasional involvement of other parenchymal organs. Serial RNA-sequencing analysis of the pre-neoplastic and neoplastic $CD4^+$ T-cells revealed increased PI3K-AKT signaling and decreased Foxo1 signaling likely mediated through ICOS in the neoplastic cells, promoting T_{FH} cell expansion. Overall, we demonstrated that novel GEP-defined PTCL subgroups likely evolve by distinct genetic pathways and that AITL is driven more by epigenetic alterations, such as loss of Tet2 as it resulted in an aggressive T-cell lymphoma with a T_{FH} phenotype. These findings emphasize the critical need for genetically faithful model systems for studying these common PTCL entities in order to improve therapeutic options.

TABLE OF CONTENTS

LIST OF FIGURES

LIST OF TABLES

LIST OF ABBREVIATIONS

HSC	Hematopoietic stem cell
BM	Bone marrow
LT-HSC	Long-term hematopoietic stem cell
ST-HSC	Short-term hematopoietic stem cell
MPP	Multi-potent progenitor
CMP	Common myeloid progenitor
CLP	Common lymphoid progenitor
MEP	Megakaryocyte-erythrocytes progenitor
GMP	Granulocyte-macrophage progenitor
NK	Natural killer
DN	Double-negative
DP	Double-positive
SP	Single-positive
RAG1	Recombination-activation gene 1
RAG2	Recombination-activation gene 2
TCR	T-cell receptor
MHC	Major histocompatibility complex
APC	Antigen presenting cell
TH_1	T-helper 1
TH_2	T-helper 2
T_{FH}	T follicular helper
iTreg	Induced T regulatory
IFN	Interferon
LCK	Leukocyte C-terminal Src kinase

ITAMS	Immunoreceptor tyrosine-based activation motifs
ZAP-70	ζ-chain-associated protein kinase 70
LAT	Linker for activation of T-cells
GRB2	Growth factor receptor-bound protein 2
SLP76	SH2-domain-containing leukocyte protein of 76 kDa
PLCγ1	Phospholipase Cγ1
ITK	IL-2-inducible T-cell kinase
PIP2	Phosphatidylinositol 4,5-bisphosphate
DAG	Diacylglycerol
IP_3	Inositol (1,4,5)-triphosphate
MAP	Mitogen-activated protein
PKCθ	Protein kinase Cθ
NFAT	Nuclear factor of activated T-cells
NF-κB	Nuclear factor-κB
ICOS	Inducible T-cell co-stimulator
PI3K	Phosphatidylinositol 3-kinase
mTOR	Mammalian target of rapamycin
JNK	c-Jun N-terminal kinases
PTCL	Peripheral T-cell lymphoma
NHL	Non-Hodgkin’s lymphoma
WHO	World Health Organization
GEP	Gene expression profiling
IPTCL	International peripheral T-cell lymphoma
PTCL-NOS	Peripheral T-cell lymphoma-not otherwise specified
AITL	Angioimmunoblastic T-cell lymphoma
NKTCL	Natural killer T-cell lymphoma

ATLL	Adult T-cell leukemia/lymphoma
EATL	Enteropathy-associated T-cell lymphoma
ALK	Anaplastic lymphoma kinase
ALCL	Anaplastic large cell lymphoma
IPI	International prognostic index
OS	Overall survival
IHC	Immunohistochemistry
H&E	Hematoxylin and eosin
LN	Lymph node
EBV	Epstein-Barr virus
ISH	In situ hybridization
FDC	Follicular dendritic cells
TME	Tumor microenvironment
COO	Cell of origin
GSEA	Gene set enrichment analysis
GC	Germinal center
DC	Dendritic cell
NGS	Next generation sequencing
MN	Myeloid neoplasms
5-mC	5-methylcytosine
5-hmC	5-hydroxymethylcytosine
5-fC	5-formylcytosine
5-caC	5-carboxylcytosine
α-KG	α-ketoglutarate
AML	Acute myeloid leukemia
D2-HG	D2-hydroxyglutarate

VAF	Variant allele frequency
WT	Wild-type
CHOP	Cyclophosphamide, doxorubicin, vincristine and prednisone
ENKTL	Extranodal natural killer T-cell lymphoma
CN	Copy number
FFPE	Formalin-fixed paraffin embedded
FF	Fresh frozen
CGH	Comparative genomic hybridization
CNA	Copy number abnormality
aCGH	Array comparative genomic hybridization
CTCL	Cutaneous T-cell lymphoma
FBS	Fetal bovine serum
DNA	Deoxyribonucleic acid
RNA-seq	RNA-sequencing
mRNA	Messenger ribonucleic acid
FPKM	Fragments per kilobase million
FDR	False discovery rate
HC	Hierarchical clustering
PTCL-NC	Peripheral T-cell lymphoma-not classifiable
SNP	Single nucleotide polymorphism
TS	Tumor suppressor
ALL	Acute lymphocytic leukemia
SRBC	Sheep red blood cells
PBS	Phosphate buffered saline
NSG	NOD *scid* gamma
DEG	Differentially expressed gene

CHAPTER 1: INTRODUCTION

1.1 T-cell Development

As summarized in **Figure 1**, T-cells originate from hematopoietic stem cells (HSCs). HSCs reside in the bone marrow (BM) and give rise to all blood cells through asymmetric cell division. Asymmetric cell division maintains a balance, as one daughter cell is committed to self-renewal to preserve the HSC population (long-term HSC (LT-HSC)) and the other advances to further cellular differentiation[1] (short-term HSC (ST-HSC)). LT-HSCs give rise to ST-HSCs, which differentiate into multi-potent progenitor cells (MPPs), as ST-HSCs have a brief self-renewal period. As a MPP, the cell has lost self-renewal capability and is committed to differentiating into an oligopotent progenitor, either a common myeloid progenitor (CMP) or a common lymphoid progenitor (CLP). The cytokine milieu of the BM, in addition to the BM cellularity and microenvironment, contribute to differentiation into CMPs or CLPs[2]. CMPs, which are $IL7R^-$, give rise to megakaryocyte-erythrocyte progenitors (MEPs) and granulocyte-macrophage progenitors (GMPs)[3]. Subsequently, MEPs and GMPs are able to differentiate into megakaryocytes, erythrocytes, granulocytes, monocytes, macrophages and dendritic cells[3]. Alternatively, CLPs, which are $IL7R^+$, Lin^-, $Sca\text{-}1^{low}$ and $c\text{-}Kit^{low}$, give rise to T-cells, B-cells, natural killer (NK) cells and dendritic cells[4].

Unlike other blood cell lineages that develop and mature in the BM, T-cells develop and mature in the thymus[5]. Thymic T-cell production requires that CLPs from the BM migrate via the blood to the thymus and although it is not completely understood as to when the thymus accepts the progenitors, it is believed to be at least partially controlled by the available thymic microenvironment niches including P-selectin (PSGL-1), CXCL12, CCL21 and CCL25[6]. In addition to IL7, Notch signaling is responsible for committing the CLPs to a T-cell fate[7], whereas Wnt signaling is more critical in thymic T-cell transitioning[8]. Before becoming a mature T-cell, the cell will go through a series of

three states, including double-negative (DN), double-positive (DP) and single-positive (SP)[9]. The first stage is DN, which occurs in the outer cortex region of the thymus[10]. The DN stage consists of four sub-stages (DN 1-4) that are distinguishable by expression of cell surface receptors CD44 and CD25 (DN1: $CD44^+$, $CD25^-$; DN2: $CD44^+$, $CD25^+$; DN3: $CD44^-$, $CD25^+$; DN4: $CD44^-$, $CD25^-$), as CD4 and CD8 are not yet expressed[9]. While transitioning through the DN stages, the cell expresses a re-arranged β-chain, mediated by recombination-activation gene 1 (RAG1) and RAG2 and a pre-Tα chain which together comprise a pre-T-cell receptor (TCR) that must interact with the CD3 complex (γ, δ, ε and ζ chains) as active signaling is require for β-chain selection[9]. This process excludes the small percentage of T-cells that differentiate into γδ T-cells as they express γ and δ TCR chains rather than α and β TCR chains. Following β chain selection, recombination of the α chain occurs, producing a mature αβ TCR. An αβ TCR is required for transition from DN4 to the DP stage, in which the cells now express both CD4 and CD8[9]. Next, the cells undergo additional selection in the deeper cortex region[10]. The positive selection process consists of the TCR interacting moderately with a self-peptide-major histocompatibility complex (MHC), with TCRs binding MHC class II complexes becoming $CD4^+$ T-cells and those binding MHC class I complexes becoming $CD8^+$ T-cells[9]. On the contrary, “neglect”, if no MHC complex is recognized, or negative selection occurs if the signaling between the TCR and MHC complex is too weak or too high, ultimately resulting in cellular apoptosis in nearly 95% of DP cells[9]. The cells that were positively selected for continue their transition to the medulla region of the thymus[10]. During this transition, the cells interact with medullary endothelial and dendritic cells, which leads to a SP state as either $CD4^+$ or $CD8^+$ with restricted MHC class II or class I complexes, respectively[9]. Once thymic migration is complete, the SP cells travel in the periphery and through secondary lymphoid organs until activated by antigen recognition[11].

$CD4^+$ T-cells serve a variety of roles in the immune system, including activation of innate immunity, B-cells, cytotoxic T-cells and macrophages[12]. The function of a T-cell depends on which helper/effector subset the naïve mature $CD4^+$ T-cell differentiates into. Subset differentiation is dependent upon cytokine milieu, transcription factors and epigenetic modifications upon stimulation of the naïve T-cell from interaction between an antigen presenting cell (APC), most often a dendritic cell, and its TCR, and subsequent CD3 activation[12]. The major $CD4^+$ subsets include T-helper 1 (TH_1), TH_2, TH_{17}, T follicular helper (T_{FH}), induced T regulatory (iTreg) and TH_9. TH_1 and TH_2, and more recently T_{FH} cells have been heavily investigated with identification of major cytokines and transcription factors. Interferon (IFN) γ and TBX21 induce TH_1 cell differentiation, whereas TH_2 is induced by IL4 and GATA3 and T_{FH} cells by IL6/IL21 and BCL6. Although these subsets have unique expression patterns and functions, it is recognized that plasticity exists and thus the subsets can be re-programmed depending on the microenvironment.

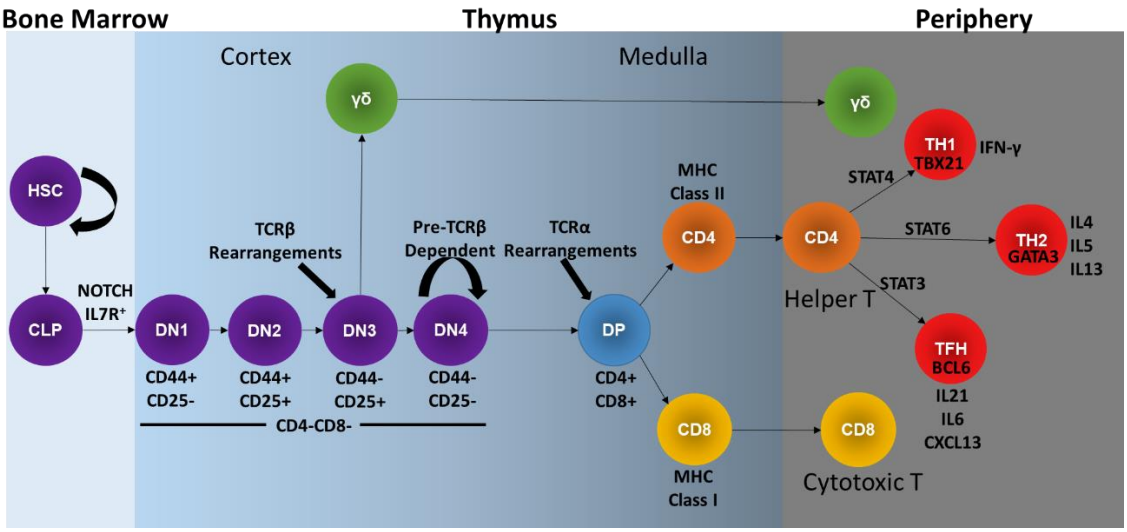

Figure 1: Stages of T-cell development and differentiation.

T-cells originate as HSCs in the BM. With expression of NOTCH and IL7R, cells are steered towards the CLP lineage. The cell then enters the cortex region of the thymus in which it will undergo a series of DN stages (1-4). These stages are identified based on unique expression patterns of CD44 and CD25. If the cell is able to continue through the differentiation process and successfully undergoes TCR β and α rearrangement, it will achieve a DP state, expressing both CD4 and CD8. Depending which MHC class molecule the cells recognizes will determine if it will become a SP CD4 or CD8 cell. In the periphery, the $CD4^+$ cells are capable of further differentiation into helper subsets, dependent upon stimuli from effector cytokines and transcription factors. $CD8^+$ cells serve a cytotoxic function. *This figure has been modified with permission from: Iqbal J., de Leval L. (2019) Pathology and Molecular Pathogenesis of T-Cell Lymphoma. In: Lenz G., Salles G. (eds) Aggressive Lymphomas. Hematologic Malignancies. Springer, Cham.*

1.2 T-cell Receptor Activation and Signaling

TCRs are activated following an immune synapsis between a T-cell and an APC. The interaction between the $CD4^+$ T-cell and MHC class II presenting antigen needs to exceed a certain affinity threshold to induce the TCR signaling cascade. Sustained TCR activation and signaling occurs when co-stimulatory factors, such as CD28, are engaged. As shown in **Figure 2**, in the initial steps of TCR signaling, CD3/TCR ligates with a cognate antigen, and CD4 and the MHC class II complex interact at the plasma membrane. The intracellular domain of CD4 recruits the leukocyte C-terminal Src kinase (LCK), increasing proximity to the TCR and promoting phosphorylation of the immunoreceptor tyrosine-based activation motifs (ITAMS) on the cytoplasmic CD3ζ chains. Zeta-chain-associated protein kinase 70 (ZAP-70) is recruited to the TCR and is phosphorylated by LCK, and in turn phosphorylates the linker for activation of T-cells (LAT), which is a transmembrane scaffolding adaptor. The tyrosine phosphorylation of LAT creates docking sites for adaptor molecules such as growth factor receptor-bound protein 2 (GRB2), GADS, SH2-domain-containing leukocyte protein of 76 kDa (SLP76), and NCK, in addition to the activation of effector signaling molecules phospholipase Cγ1 (PLCγ1), IL-2-inducible T-cell kinase (ITK) and VAV1. VAV1 is important in the stimulation of Rho/Rac GTPases through Rac and Cdc42 activation, which is essential for actin polymerization and cytoskeleton remodeling. Phosphorylation of PLCγ1 catalyzes the enzymatic cleavage of phosphatidylinositol 4,5-bisphosphate (PIP2) into diacylglycerol (DAG) and inositol (1,4,5)-triphosphate (IP_3). This cleavage results in increased intracellular calcium storage as well as activation of downstream signalers such as mitogen-activated protein (MAP) kinases and protein kinase Cθ (PKCθ) by DAG and calcineurin by IP_3. These downstream effector signaling pathways result in the activation of nuclear factor of activated T-cells (NFAT) and nuclear factor-κB (NF-κB),

both of which are critical in a number of T-cell responses, such as proliferation, migration, cytokine production and effector functions[13].

Co-stimulatory factors are critical in maintaining TCR activation, T-cell subset differentiation and effector function. CD28 is a co-stimulatory factor expressed on both naïve and activated T-cells, whereas inducible T-cell co-stimulator (ICOS) is primarily expressed on activated T-cells[14]. CD28 has two cytoplasmic motifs, YMNM and PYAP[14]. The YMNM motif associates with the p85 subunit of phophatidylinosital 3-kinase (PI3K)[15]. PI3K regulates AKT signaling, which promotes T-cell proliferation and survival through activating downstream targets like mammalian target of rapamycin (mTOR) and NF-κB. The PYAP motif of CD28 interacts with LCK and GRB2 to enhance IL-2 induction and ultimately increase NFAT nuclear translocation[15]. CD28 has also been shown to induce RAS activation leading to activation of JUN through phosphorylation of c-Jun N-terminal kinases (JNK)[15]. ICOS possesses a YMFM SH2 binding motif, similar to the SH2 binding motif YMNM of CD28, that attracts both p85 and p50α PI3K subunits[15]. As compared to CD28 co-stimulation, co-stimulation of ICOS results in higher AKT signaling as the p50α subunit is more active than the p85 subunit; however, ICOS does not interact with LCK or GRB2 so does not enhance IL-2 production as CD28 does[15] nor does ICOS activate JNK[14]. Rather, ICOS increases specific interleukin production (IL-4, IL-10 and IL-21) through PI3K signaling, which is essential in T-helper subset differentiation[15].

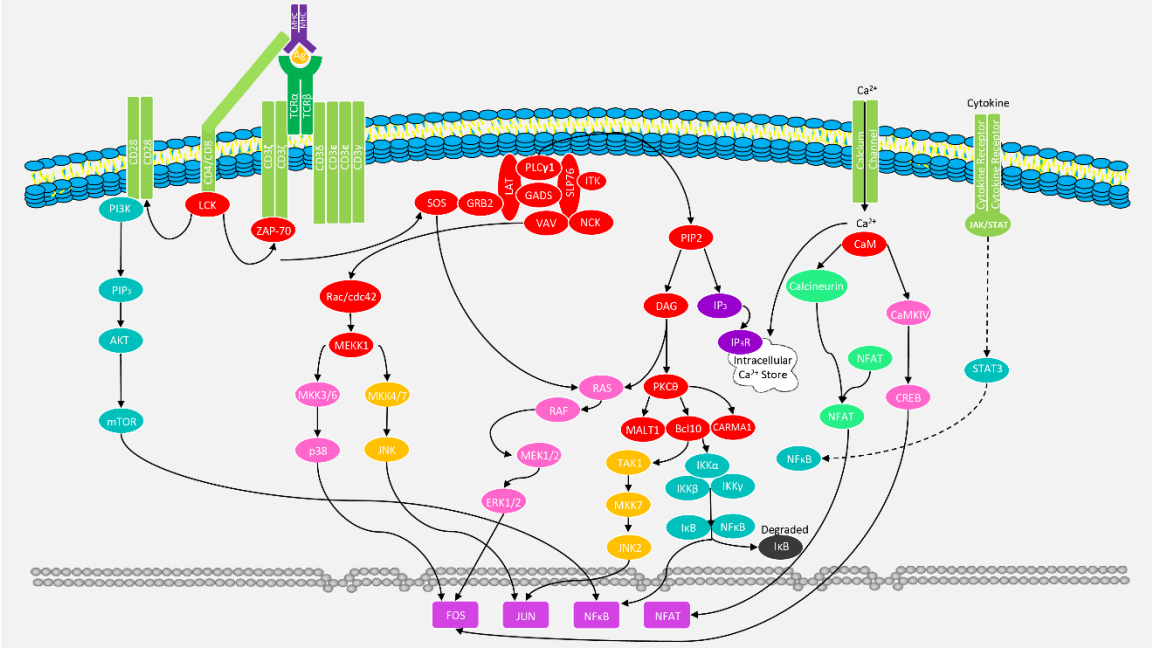

Figure 2: T-cell receptor activation and downstream signaling cascades.

Schematic of pathways commonly observed to be dysregulated in peripheral T-cell lymphoma downstream of initial TCR activation. *This figure has been modified with permission from: Iqbal J, Wilcox R, Naushad H, Rohr J, Heavican TB, Wang C, et al. Genomic signatures in T-cell lymphoma: How can these improve precision in diagnosis and inform prognosis? Blood Rev. 2015.*

1.3 Clinical Characteristics and Classification of Peripheral T-cell Lymphomas

Peripheral T-cell lymphomas (PTCLs) are a rare heterogeneous group of Non-Hodgkin's lymphomas (NHLs). Depending on geographic region, PTCLs can account for 10-20% of all NHLs, being more frequent in Asian countries than Western countries[16]. The World Health Organization (WHO) currently recognizes more than 25 distinct entities of PTCL. Unfortunately, diagnosis of PTCLs is difficult for even expert hematopathologists; however, advances in genomic profiling have helped establish classification criteria and the identification of novel molecular subgroups and provisional entities[17]. Current PTCL classification schemes incorporate morphologic, immunophenotypic, and genetic data, and more recently the addition of gene expression profiling (GEP).

In 2008, a collaborative international PTCL (IPTCL) study of 1,320 cases from North America, Europe, and Asia was published, in which four pathologists completed diagnostic review based on histology, immunophenotypic, and molecular genetic data[16]. After consensus review, approximately 10% of cases were identified as misclassified[16]. Of the cases evaluated, PTCL-not otherwise specified (PTCL-NOS) and angioimmunoblastic T-cell lymphoma (AITL) were the most common PTCL subtypes, accounting for nearly 25% and 20%, respectively[16]. As mentioned earlier, there are significant geographic associations with PTCL frequencies. North America and Europe had similar frequencies of PTCL-NOS, which were at higher levels than in Asian countries[16]. In contrast, Asian countries had higher frequencies of natural killer T-cell lymphoma (NKTCL) and adult T-cell leukemia/lymphoma (ATLL)[16]. Compared to the other regions, Europe had the highest frequency of AITL and enteropathy-type PTCL now referred to as enteropathy-associated T-cell lymphoma (EATL)[16].

PTCLs, specifically PTCL-NOS and AITL, are most often diagnosed in the elderly population. In the IPTCL study, the largest study to date, the median age of all PTCLs was 62 years, with PTCL-NOS and AITL having amongst the highest median age overall at 60 and 65 years, respectively[16]. However, it is important to note that some PTCLs affect younger populations, such as subcutaneous panniculitis-like, hepatosplenic and anaplastic lymphoma kinase (ALK)-positive anaplastic large cell lymphoma (ALCL) whose median ages were in the lower thirties[16]. This large consortium of cases also revealed that males were more commonly affected in all PTCL subtypes evaluated, with the largest being 75% in subcutaneous panniculitis-like. At diagnosis, an Ann Arbor stage (I, II, III or IV) was given based on the number of involved sites, location of involved sites and symptoms. With a higher Ann Arbor stage being more involved, it was observed that 69% of PTCL-NOS and 89% of AITL had an Ann Arbor stage of III or IV[16]. The international prognostic index (IPI) was reported for the PTCL subtypes with an IPI of 2/3, which is considered low-high intermediate, most common for PTCL-NOS (57%) and AITL (59%)[16].

Unfortunately, overall survival (OS) for PTCL patients is quite dismal and improvement has been limited in recent decades due to lack of sufficient model systems for many PTCL subtypes, except ALK^+ ALCL as seen in **Figure 3**. ATLL has been reported to have the poorest OS, followed by AITL and PTCL-NOS, which have a 50% survival rate of less than three years[16]. The study further incorporated IPI into OS and observed that at five years, 50% of PTCL-NOS and 56% of AITL patients with an IPI of 0/1 were alive compared to 11% of PTCL-NOS and 25% of AITL with an IPI of 4/5[16]. Further, a significant trend between OS and IPI was observed within the PTCL-NOS cohort with 4/5 having the worst outcome followed by 3, 2 and 0/1[16].

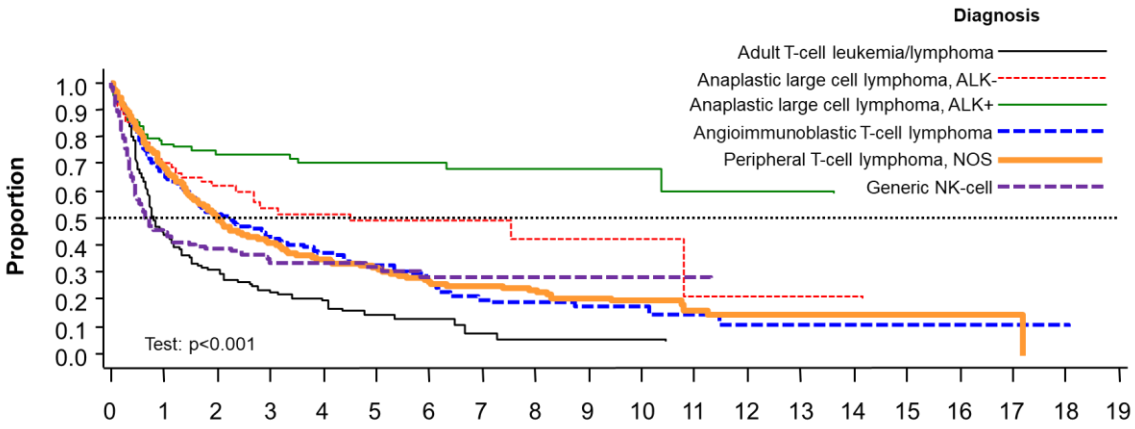

Figure 3: Poor overall survival trends in major PTCL entities.

Overall, peripheral T-cell lymphomas have poor OS. The two most frequent entities, AITL and PTCL-NOS, have a 50% OS rate of less than 3 years. *This figure has been modified with permission from: Vose J, Armitage J, Weisenburger D. International peripheral T-cell and natural killer/T-cell lymphoma study: pathology findings and clinical outcomes. Journal of clinical oncology : official journal of the American Society of Clinical Oncology. 2008;26(25):4124-4130.*

With recognition of misclassification in a large percent of PTCLs, additional immunohistochemistry (IHC) stains and molecular assays have become routine in clinics to increase accurate diagnosis. As shown in **Figure 4**, hematoxylin and eosin (H&E) staining of AITL lymph nodes (LN) often reveals an effaced normal architecture with increased vascularization, immunoblasts and B-cells[18]. The B-cells of AITL biopsies are often positive for Epstein-Barr virus (EBV), which is detected by in situ hybridization (ISH). It is valuable to note that the EBV infection is not observed in the neoplastic T-cells of AITL[17]; however, the infected B-cells have been shown to undergo malignant transformation in some patients. Expansion of follicular dendritic cells (FDCs) is also a common feature of AITL, often identified by IHC staining of CD21 or CD23[18]. Similar to other major PTCL subtypes, AITL is typically CD3 and CD4 positive. CD10 and/or cytoplasmic CXCL13 are commonly performed, with the later considered to be more specific for AITL[18]. With the recent addition of the provisional entity PTCL-T_{FH}, T_{FH} markers have become more routine and valuable in classification. The T_{FH} antibodies include PD-1, ICOS, BCL6, and less often CXCR5 and CD200[17]. Compared to other PTCLs, AITL is rarely positive for CD30 and CD8[18].

PTCL-NOS is a “wastebasket” diagnosis for PTCL cases that do not fit the classification requirements of other PTCL subtypes; therefore, the morphology and IHC staining is quite heterogeneous. In recent years, two molecular subgroups within PTCL-NOS have been identified, PTCL-GATA3 and PTCL-TBX21, which were acknowledged in the 2016 WHO Classification of Lymphoid Neoplasms[19]. Although both of these subgroups histologically display an effaced normal architecture, the size of the neoplastic cells vary. PTCL-GATA3 neoplastic T-cells tend to be larger in size compared to PTCL-TBX21 which is represented by smaller-sized neoplastic cells with a richer tumor microenvironment (TME) of proliferative and inflammatory immune cells, similar to

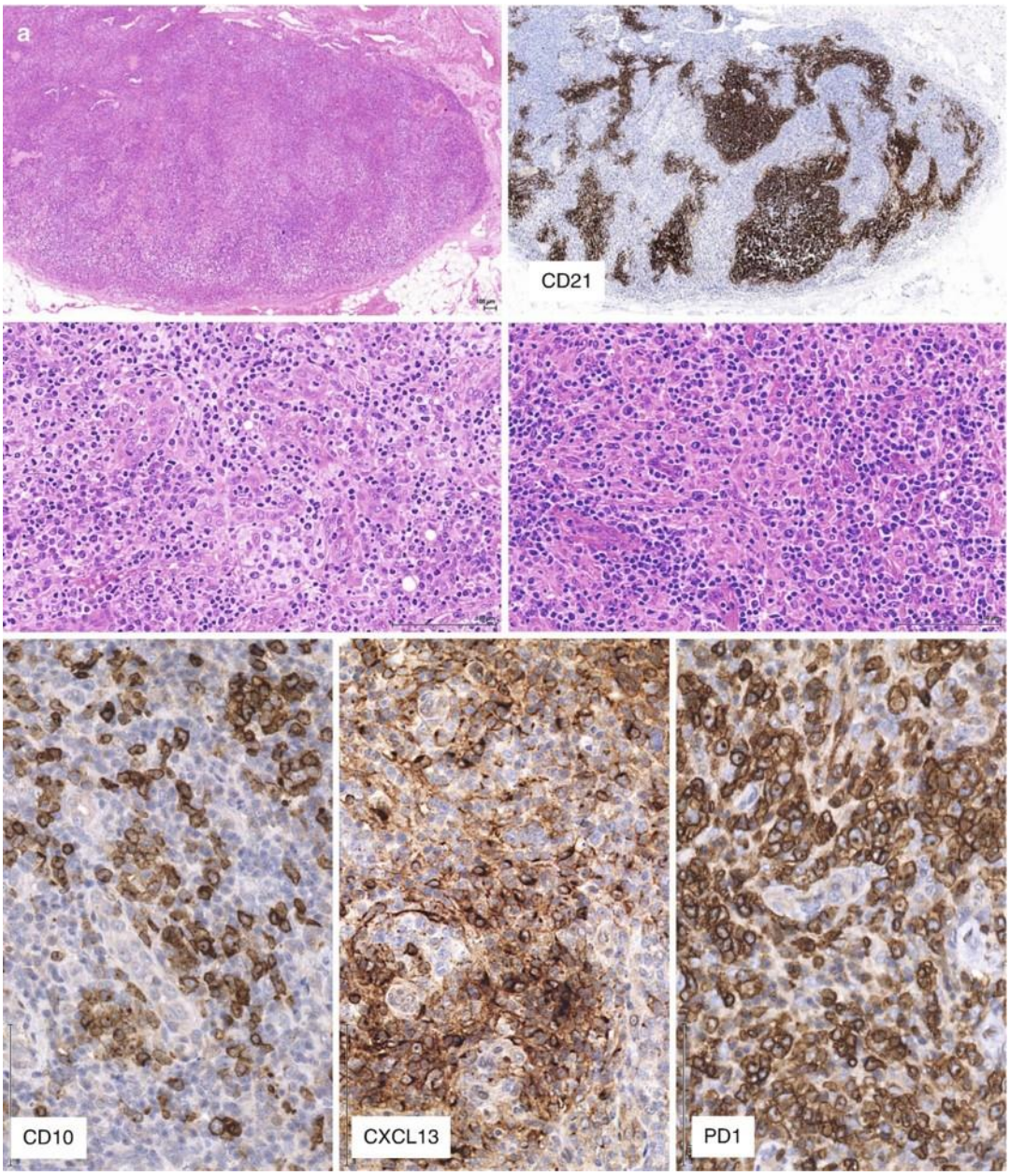

Figure 4: Histopathological features of angioimmunoblastic T-cell lymphoma.

A. Low-power view of an AITL LN showing complete effacement of the normal architecture. CD21 is representative of the increased FDC meshwork often observed in AITL. The left middle panel demonstrates the increased vascularization frequently observed, whereas the middle right panel is showing a case enriched with immunoblasts and histiocytes. CD10, CXCL13 and PD1 are IHC markers used to identify T_{FH} cells, and in this case the neoplastic population. *This figure has been included with permission from: Iqbal J., de Leval L. (2019) Pathology and Molecular Pathogenesis of T-Cell Lymphoma. In: Lenz G., Salles G. (eds) Aggressive Lymphomas. Hematologic Malignancies. Springer, Cham.*

AITL[20]. Through a large case evaluation of 173 PTCL-NOS biopsies with subgroup (PTCL-GATA3 or PTCL-TBX21) classification, we were able to identify four distinct morphological patterns[20] (**Figure 5**). Pattern 1 was identified as a monotonous pattern of either sheets of intermediate-sized cells with abundant clear cytoplasm whereas large clusters or sheets of large cells represented Pattern 2, both of which were predominant in the PTCL-GATA3 subgroup[20]. The PTCL-TBX21 subgroup was enriched in either Pattern 3 or Pattern 4[20]. Pattern 3 appeared as a polymorphous infiltrate of variably-sized neoplastic cells interspersed in a mixed inflammatory background of variable proportions of small lymphocytes, eosinophils, plasma cells and histiocytes, whereas Pattern 4 was observed as small atypical tumor cells with clusters of epithelioid histiocytes in a Lennert pattern[20].

Similar to AITL, PTCL-NOS neoplastic cells are typically CD3 positive. The heterogeneity of these cases results in varying patterns of CD4 and CD8 expression, with PTCL-GATA3 most often expressing CD4 alone and PTCL-TBX21 with a higher frequency of double expressing $CD4^+$ and $CD8^+$ neoplastic cells[20]. The PTCL-TBX21 subgroup is also enriched in cytotoxic markers such as TIA-1 and Granzyme B[20]. PTCL-NOS cases often have the loss of CD5, CD7 and CD52 expression. CD30 expression can be observed in PTCL-NOS; however, inclusion of other IHC markers is critical in differentiating from ALCL, as are EBV and T_{FH} markers in distinguishing from AITL. In our recent publication, we developed an IHC algorithm for further sub-classifying the PTCL-NOS cases into either the PTCL-GATA3 or PTCL-TBX21 subgroups[20]. The algorithm requires the IHC staining of TBX21, CXCR3, GATA3, and CCR4[20]. Optimal cutoffs were determined and cases with ≥20% expression of TBX21 and/or CXCR3 were classified as PTCL-TBX21 and cases with ≥50% expression of GATA3 and/or CCR4

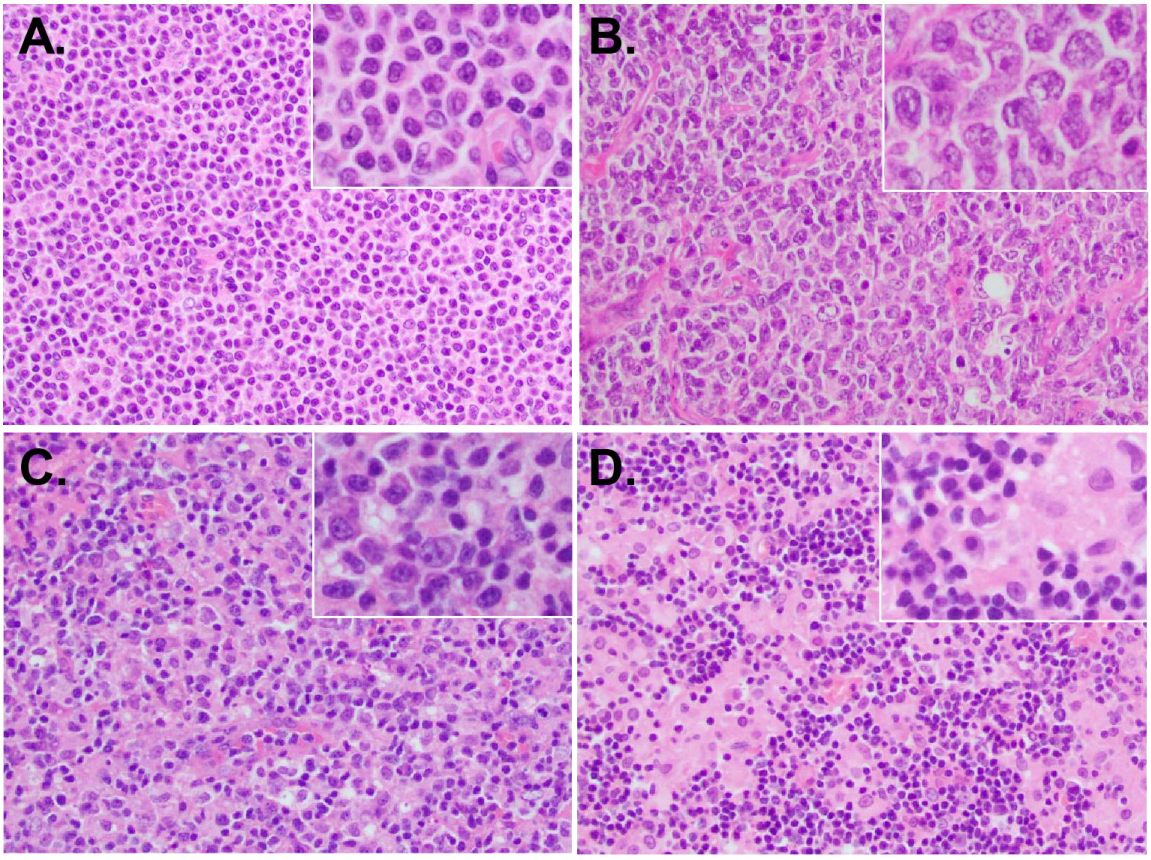

Figure 5: Four distinct morphologic patterns observed in peripheral T-cell lymphoma-not otherwise specified.

PTCL-GATA3 was significantly associated with a monomorphic, monotonous, tumor cell rich morphology with a minimal inflammatory background characterized by: **A.** small-intermediate cells with abundant cytoplasm (pattern 1) or **B.** clusters or sheets of large cells (pattern 2). In contrast, PTCL-TBX21 was significantly associated with a polymorphous morphology, characterized by **C.** neoplastic cells interspersed in a mixed inflammatory background (pattern 3), or **D.** the classic lymphohistiocytic (Lennert) lymphoma morphology composed of small tumor cells within clusters of epithelioid histiocytes (pattern 4). *This figure has been included with permission from: Amador C, Greiner TC, Heavican TB, Smith LM, Galvis KT, Lone WG, et al. Reproducing the Molecular Subclassification of Peripheral T-cell Lymphoma-NOS by Immunohistochemistry. Blood. 2019.*

were classified as PTCL-GATA3[20] (**Figure 6**). This tree-method algorithm resulted in an 85% diagnosis consensus within the GEP-defined training cohort[20].

Previous GEP studies using the Affymetrix HG-U133 Plus2 array lead to the derivation of unique gene signatures to classify PTCLs[21]. The identification of molecular signatures was valuable in providing additional means of classification since traditional methods still provided high misclassification rates, as approximately 20% of cases had a changed diagnosis between AITL and PTCL-NOS alone following GEP[21]. Since AITL often has a small neoplastic population, the derived signature was enriched in genes associated with angiogenesis and vascularization, which are common components of the AITL TME[21]. The two PTCL-NOS subgroups, PTCL-GATA3 and PTCL-TBX21, were originally identified by GEP as two sub-clusters that formed within the PTCL-NOS entity by unsupervised hierarchical clustering[21]. Under further analysis, an enrichment of GATA3 and its known targets was observed in one cluster and TBX21 and its known targets were enriched in the second PTCL-NOS cluster[21]. Examining the two clusters closer revealed a subset of PTCL-TBX21 cases expressing a cytotoxic signature[21], which has since been validated by IHC. The PTCL-GATA3 signature genes associated with increased mTOR, MYC and PI3K activity, whereas the PTCL-TBX21 signature genes associated with interferon IFN signaling, a $CD8^+$ T-cell profile and NF-κB[21]. The GEP data has helped to improve classification and provided insight into the cellular origins and dysregulated pathways in the major PTCL subtypes.

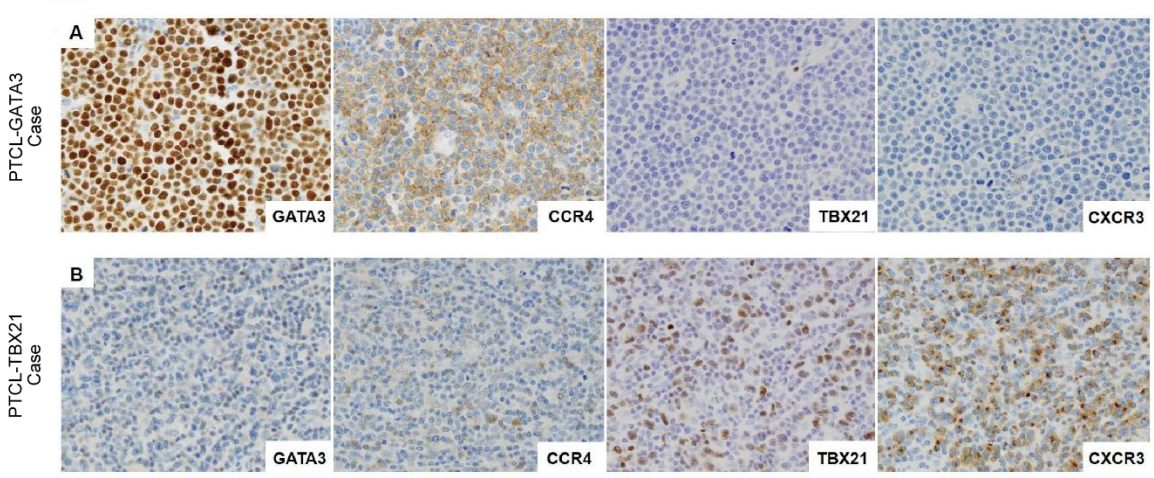

Figure 6: Immunohistochemistry staining of four antibodies to classify PTCL-GATA3 and PTCL-TBX21 subgroups.

A. Positive immunostains for GATA3 (nuclear) and its corresponding target protein CCR4 (membranous) in a PTCL-GATA3 case. This case is negative for TBX21 and CXCR3. **B.** Positive immunostains for TBX21 (nuclear) and its target protein CXCR3 (membranous) in a PTCL-TBX21 case. This case is negative for GATA3 and CCR4. Original magnification 600x. *This figure has been included with permission from: Amador C, Greiner TC, Heavican TB, Smith LM, Galvis KT, Lone WG, et al. Reproducing the Molecular Subclassification of Peripheral T-cell Lymphoma-NOS by Immunohistochemistry. Blood. 2019.*

1.4 Cellular Origin of Angioimmunoblastic T-cell Lymphoma and Peripheral T-cell Lymphoma-Not Otherwise Specified

Advances in technology, such as GEP, has provided evidence in identifying the cell of origin (COO) for major PTCL entities and subgroups. These findings have increased the appreciation that T-cell lineage differentiation is a factor in delineating PTCL entities. Sufficient evidence has shown that AITL is derived from T_{FH} cells, a subset of $CD4^+$ T-cells. The first insight into T_{FH} cells as the COO for AITL came from the observation of increased CXCL13 expression by IHC in AITL biopsies, which was further validated at the mRNA level in microarray studies[22,23]. In addition to CXCL13, GEP analysis revealed increased expression of other T_{FH}-related genes including PD1, BCL6, ICOS, CXCR5 and IL21[22-25]. Further, comparisons with published gene signatures using Gene Set Enrichment Analysis (GSEA) demonstrated that AITL was enriched in T_{FH} signatures compared to signatures representative of TH_1 and TH_2 T-cell subsets, which are more enriched in PTCL-NOS[22].

Although T_{FH} cell differentiation is quite well understood, the transformation of the T_{FH} cells to a malignant state as seen in AITL is not well understood and limited model systems have hindered further exploration. T_{FH} cells are critical in the germinal center (GC) reaction and GC B-cell differentiation. As illustrated in **Figure 7**, to initiate T_{FH} cell differentiation, a naïve $CD4^+$ T-cell must interact with a dendritic cell (DC). Upon interaction, ICOS is activated on the $CD4^+$ T-cell resulting in engagement of the TCR and subsequent PI3K signaling. Further, PI3K activation and increased IL6 expression result in BCL6 induction. Upon these events, PD1 and CXCR5 are upregulated and the cell becomes a T_{FH} precursor, which migrates to the B-cell follicle border to initiate the critical antigen-specific B-cell interaction. In the GC, T_{FH} cells undergo maturation,

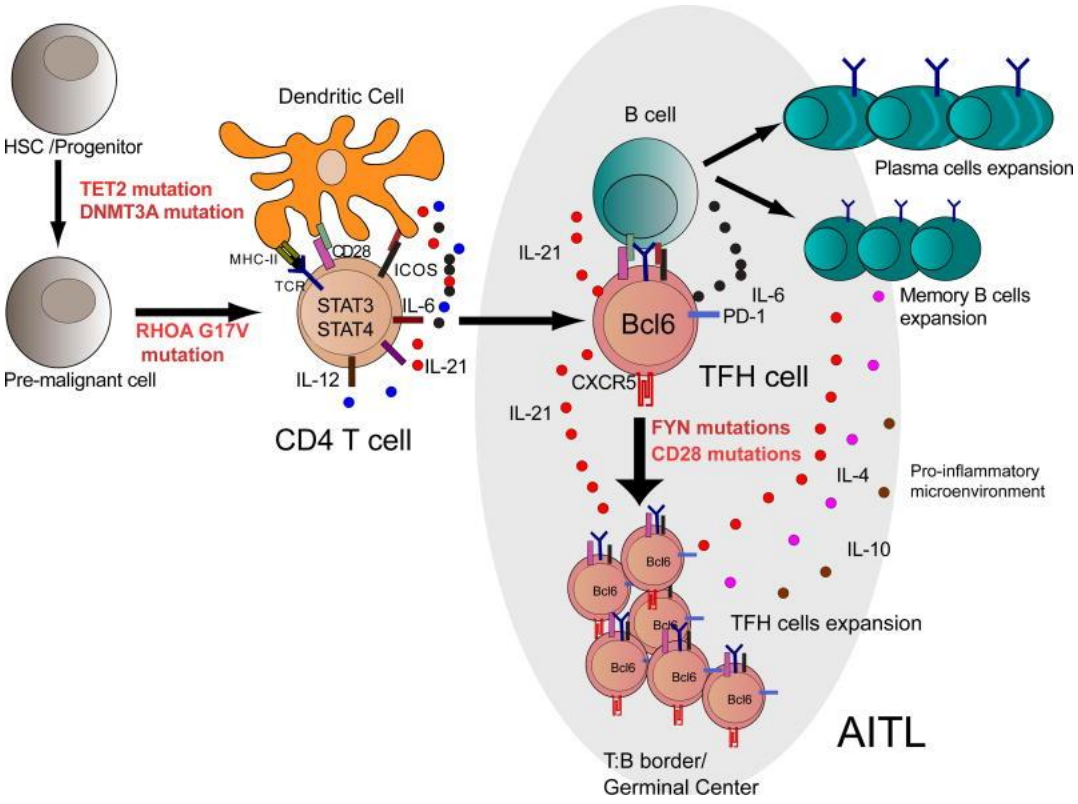

Figure 7: Schematic of T_{FH} cell differentiation and interaction with B-cells.

T_{FH} cell differentiation is initiated by the interaction of a naïve $CD4^+$ T-cell and a dendritic cell. This interaction activates ICOS, resulting in TCR engagement and PI3K activation. The PI3K activation and increased IL6 expression induce BCL6 expression. Subsequently, PD1 and CXCR5 are upregulated, classifying the cell as a T_{FH} precursor, in which it begins migration to the B-cell follicle border. In the GC, the T_{FH} and B-cell interact, shifting expression of key molecules, such as in increase in CXCR5, PD1, BCL6, MAF, ASCL2 and SAP and a reduction in CCR7, S1PR1 and PSGL1. Help from the T_{FH} cells allows the B-cells to differentiate into plasma cells or memory B-cells. In turn, the B-cells are critical in the T_{FH} cell maturation itself, allowing the mature T_{FH} cell to enter another GC reaction or else become a memory T_{FH} cell. *This figure has been included with permission from: Cortes JR, Palomero T. The curious origins of angioimmunoblastic T-cell lymphoma. Curr Opin Hematol. 2016;23(4):434-443.*

resulting in changes of expression molecules, such as high expression of CXCR5, PD1, BCL6, MAF, ASCL2 and SAP and reduced expression of CCR7, S1PR1 and PSGL1[26]. Once a T_{FH} cell has fulfilled its function, resulting in final B-cell differentiation to either plasma cells or memory B-cells, the T_{FH} cell is able to transition on to another GC and maintain its T_{FH} function, or else it may develop into a memory T_{FH} cell[27].

As mentioned earlier, GEP revealed two molecular subgroups within PTCL-NOS, PTCL-GATA3 and PTCL-TBX21[21]. The PTCL-GATA3 subgroup had increased expression of GATA3, the master transcription factor for the TH_2 subset, whereas the PTCL-TBX21 subgroup had increased expression of TBX21, the master transcription factor for the TH_1 subset[21]. Corresponding target genes of each transcription factor (GATA3 and TBX21) were also increased in the respective subgroups[21]. The PTCL-GATA3 subgroup exhibited poorer OS compared to the PTCL-TBX21 subgroup[21], suggesting the tumor milieu is different and may contribute to advanced or more aggressive lymphomagenesis. However, it is also of value to acknowledge that the PTCL-TBX21 subgroup is considered to be heterogeneous and may contain additional subgroups, such as a cytotoxic subgroup[21].

TH_1 cells are critical in immunity against intracellular pathogens. IFNγ and IL12 upregulation are crucial in promoting TH_1 differentiation. The enhanced IL12 signaling is responsible for activation of STAT4. In turn, STAT4 activates TBX21 (T-bet). IFNγ signaling is further enhanced, as TBX21 is also responsible for its transcription. On the other hand, TBX21 also plays a vital role in maintaining the TH_1 phenotype by repressing GATA3 expression. In *in vitro* culture systems, the addition of IL12, IL2 and α-IL4 have polarized naïve $CD4^+$ T-cells to TH_1 cells. In contrast, TH_2 cells are critical in humoral immunity responses. TH_2 differentiation is driven by expression of IL4. IL4 is responsible for phosphorylating STAT6, inducing GATA3 expression. GATA3 itself promotes the

transcription of IL4, IL5 and IL13, all of which are key TH_2 effector cytokines[28]. IL4 is able to promote further TH_2 differentiation by forming an autocrine feedback loop, which can be enhanced by expression of NFAT, Jun and c-MAF[29]. *In vitro*, the addition of IL4, IL2 and α-IFNγ is sufficient to polarize naïve $CD4^+$ T-cells to TH_2 cells. Interestingly, both TH_2 and T_{FH} cells have known interactions with B-cells and can display a similar phenotype. In particular is the increased expression of IL4; however, the means by which IL4 expression is regulated between the two $CD4^+$ T-cells subsets is unique[30]. Some investigations have demonstrated that under certain settings, T_{FH} cells can differentiate from TH_2 cells in a GC dependent manner[31].

1.5 Genetic and Epigenetic Modifications in Angioimmunoblastic T-cell Lymphoma and Peripheral T-cell Lymphoma-Not Otherwise Specified

In recent years, next generations sequencing (NGS) has revealed the mutation spectrum of AITL and PTCL-NOS. Although studies have ranged in sample size and the molecular subgroups of PTCL-NOS were not distinguished until our recent publication detailed in **Chapter 2**, the mutation rate of four genes has been observed at consistently higher frequencies, these including TET2, DNMT3A, IDH2 and RHOA[32-36]. The epigenetic regulator TET2 was found mutated in upwards of 70-80% of all AITL cases and closer to 30-40% in PTCL-NOS. Interestingly, mutations of TET2 have been found in the un-involved HSC compartment of patients, as well as in the B-cells[37]. These findings have led to the idea that TET2 mutations likely arise in early cell populations, such as the HSC, and require the accumulation of additional mutations and/or the long-term effects of epigenetic alterations to become malignant. TET2 mutations are commonly observed in myeloid neoplasms (MN) and less frequently in mature B-cell lymphomas[38], further suggesting that the accumulation of additional mutations may determine disease development. TET2 is a member of the TET family which catalyzes the successive oxidation of 5-methylcytosine (5-mC) to 5-hydroxymethylcytosine (5-hmC), 5-formylcytosine (5-fC) and 5-carboxylcytosine (5-caC), mediated by the presence of α-ketoglutarate (α-KG) and Fe(II). Thus, when loss of TET2 function occurs due to mutation, an increase in 5-mC levels and corresponding decrease in 5-hmC levels has been observed.

A second epigenetic regulator, IDH2, was mutated in approximately 40% of AITL; however, it is rarely observed in PTCL-NOS. Interestingly, mutations of IDH2 are almost exclusively observed at amino acid arginine 172 in AITL, most often resulting in an amino acid change to lysine or serine, and are identified only in the neoplastic T-cells;

whereas, other neoplasms have frequent mutations at amino acid arginine 140. Also of note, in other neoplasms, such as acute myeloid leukemia (AML), TET2 and IDH2 mutations are mutually exclusive; however, they tend to significantly co-occur in AITL. The normal function of IDH2 is to catalyze the oxidative decarboxylation of isocitrate, producing α-KG, NADP and carbon dioxide for the Krebs cycle. The $IDH2^{R172}$ mutation observed in AITL is a gain-of-function mutation, which has been shown to result in neomorphic activity that converts α-KG to D-2-hydroxyglutarate (D2-HG). This results in a loss of the necessary levels of α-KG needed for α-KG-dependent dioxygenases, such as the TET family, to function. Thus, if IDH2 mutation alone can inhibit TET2 function, the co-occurring mutations likely have a dynamic role in AITL lymphomagenesis.

The third epigenetic regulator frequently mutated is DNMT3A. Similar to IDH2, mutations in DNMT3A are observed in nearly 40% of AITL cases and to a lesser extent in PTCL-NOS. Unlike TET2, which is critical in the DNA de-methylation process, DNMT3A is a catalytically active DNA methyltransferase that performs *de novo* DNA methylation[39], which is critical in regulating gene expression. Like TET2, DNMT3A mutations are often observed at higher than expected variant allele frequencies (VAF) relative to estimated tumor content. This increased VAF suggests that these mutations are likely occurring early and are not specific to the neoplastic T-cells, as has been demonstrated in TET2. The majority of DNMT3A mutations occur in the methyltransferase domain, leading to the loss of function of the domain and ultimately hypomethylation. A hotspot mutation has been identified at arginine 882 in MNs. As detailed in Chapter 2, our work revealed this same site to be a hotspot mutation in PTCL-NOS, however less common in AITL.

A recurrent mutation in RHOA has been identified in upwards of 70% of AITL and 20% of PTCL-NOS. The mutation observed is heterozygous and almost exclusively a

change of glycine 17 to valine. Similar to $IDH2^{R172}$ mutations, the $RHOA^{G17V}$ mutation is considered tumor-specific, thus confined to the neoplastic T-cell population. RHOA is a member of the RHO family small GTPases. This family has known importance for many cellular functions, including migration, survival, proliferation and signal transduction. Although investigations of the $RHOA^{G17V}$ mutation have found it to inhibit wild-type (WT) function by acquiring a dominant-negative function, its role in terms of T-cell transformation is still quite unknown. Recent in vivo studies have found that the $RHOA^{G17V}$ mutation in $CD4^+$ T-cells resulted in increased T_{FH} cell proliferation and increased expression of ICOS and PI3K, but also often severe autoimmunity[40,41].

Mutations of genes involved in TCR activation and signaling have been observed in AITL and PTCL-NOS, however at frequencies closer to 5-15%[33,42]. Of interest are mutations in FYN, VAV1[43], PLCG1 and CD28[33,42]. Although these mutations were considered to be gain of function, more in depth investigations must be performed to identify their unique functions, especially in terms of T-cell lymphomagenesis. These initial investigations found that many of these variants resulted in increased T-cell activation through upregulation of important signaling cascades including MAPK, NFAT, NF-κB and PI3K[33,42].

1.6 Treatment Overview of Peripheral T-cell Lymphoma

PTCLs are rare and aggressive diseases often associated with poor clinical outcome. Although our understanding of the underlying pathobiology of PTCL has improved in recent years, this has not translated to improvement in therapeutic options and OS for PTCL patients, as these patients are quick to relapse with short progression free periods. Further limiting advances in therapies is the fact that these are such rare diseases, resulting in few patients for clinical trials. Unfortunately, the standard front-line therapy for AITL and PTCL-NOS remains to be a cyclophosphamide, doxorubicin, vincristine, and prednisone (CHOP) or a CHOP-like regimen. When reasonable, CHOP is followed up by an autologous or allogenic stem cell transplant[18]. Autologous stem cell transplants have been found to be more effective in younger individuals with primary disease as compared to allogenic stem cell transplants which are meant for relapsed/refractory disease. More recently, CHOP in combination with etoposide has been administered to PTCL patients, but results have not shown significant differences compared to CHOP alone[44]. Additional agents have been tested for primary and relapsed/refractory PTCL, including romidepsin[45], belinostat[46], pralatrexate[47], gemcitabine[48] and bortezomib[49]; however, more agents are currently under review in clinical trials. Of note, brentuximab vedotin, an antibody-drug conjugate targeting CD30, is an approved drug for ALCL and $CD30^+$ PTCL[50].

Romidepsin: histone deacetylase inhibitor, approved for patients with relapsed/refactory PTCL.

Belinostat: histone deacetylase inhibitor, approved for patients with relapsed/refactory PTCL.

Pralatrexate: antimetabolite, approved for patients with relapsed/refactory PTCL.

Gemcitabine: antimetabolite, in trials for relapsed/refractory PTCL.

Bortezomib: proteasome inhibitor, in trials for relapsed/refractory PTCL.

1.7 Dissertation Significance and Aims

With appreciation of the background information provided on T-cell development, the newly defined molecular subgroups of PTCL and acknowledgement of limited advances in therapeutic options, this thesis sought to reveal the underlying molecular differences distinguishing PTCL subgroups and generate a more representative model system for investigating T-cell lymphoma. Chapter 1 provided an overview of T-cell development and what is currently known about the two most common PTCL entities, PTCL-NOS and AITL. Importantly, two novel molecular subgroups were identified within the heterogeneous PTCL-NOS entity, PTCL-GATA3 and TBX21. A molecular signature for AITL was also generated, more clearly defining the entity. These newly defined cases were subjected to genomic analysis as detailed in Chapter 2 with the aim of revealing unique copy number abnormalities, mutations and oncogenic pathways, supporting that these are distinct diseases with identification of potential therapeutic targets. A better understanding of what was occurring at the molecular level in these diseases and acknowledgement of insufficient model systems, as no cell lines or animal models currently exist, led to the aim of generating a murine model system representative of AITL, which is detailed in Chapter 3. A murine model with a similar cellular phenotype (T_{FH}) was achieved, allowing for a better understanding of the effects of long-term loss of a crucial epigenetic regulator, TET2, leading up to lymphomagenesis. The findings from this thesis have provided evidence to the field of T-cell lymphoma that PTCL-GATA3 and PTCL-TBX21 are two unique subgroups with notable genomic differences, likely contributing to the differences in cellular origin and disease prognosis. Further, generation of a model system provides encouragement for exploring the underlying pathobiology by being able to look at sequential changes and altered pathways leading to lymphomagenesis as discussed in Chapter 4.

CHAPTER 2: GENETIC DRIVERS OF ONCOGENIC PATHWAYS IN MOLECULAR SUBGROUPS OF PERIPHERAL T-CELL LYMPHOMA

This chapter has been reformatted with permission from: Heavican TB, Bouska A, Yu J, Lone W, Amador C, Gong Q, et al. Genetic drivers of oncogenic pathways in molecular subgroups of peripheral T-cell lymphoma. Blood. 2019.

2.1 INTRODUCTION

PTCL accounts for 10-15% of NHL in the western world and ~20% of NHL in Asia or Central and South America[17]. The current WHO classification recognizes ~30 distinct PTCL entities including AITL, ALCL, ATLL and extra-nodal NK/T-cell lymphoma of nasal type (ENKTL) with distinct clinicopathological characteristics[17]. PTCL patients exhibit poor response to standard chemotherapy[51], with the exception of ALK and *DUSP22* translocated ALCL cases[52]. AITL is the most common PTCL entity, with distinct clinicopathological features[53,54] including a dysregulated immune system evidenced by polyclonal hypergammaglobulinemia and autoimmune manifestations, while also displaying strong immunosuppression in the tumor with the frequent presence of EBV infected B-cells[53]. We and others have demonstrated T_{FH} cells as the cell-of-origin and characteristic activation of the NF-κB pathway[21,22,55]. AITL has frequent mutations of genes regulating the epigenome (TET2, $IDH2^{R172}$ and DNMT3A*)* and proximal TCR and costimulatory signaling pathways[32,33,56-58]. However, the complex underlying pathobiology of AITL remains poorly defined.

Approximately 30-50% of PTCL cases cannot be further classified, and are designated PTCL-NOS[17,51]. Thus, PTCL-NOS includes a heterogeneous group of cases that is difficult to diagnose and treat[51]. Using GEP, we identified diagnostic and prognostic molecular signatures for major PTCL entities and identified two novel molecular subgroups within PTCL-NOS[21,55,59]. These subgroups were characterized by

differential expression of master TH_1 or TH_2 cell differentiation regulators (TBX21 or GATA3, respectively) with corresponding target genes[21,60], and significant differences in oncogenic transcriptional signatures and clinical outcome[21]. Although these subgroups have been alluded to in the 2016 WHO classification scheme[17], the genetic basis of this distinction is unknown. We investigated the genetic etiology of the subgroups using extensive GEP, genomic copy number (CN) analysis and mutation analysis of candidate driver genes within abnormal loci. Furthermore, we evaluated potential therapeutic targets affecting oncogenic pathways in these molecular subgroups.

2.2 MATERIALS AND METHODS

Patient Materials

One hundred and nineteen PTCL cases were included in the study (35 AITL, 69 PTCL-NOS and 15 PTCL-T_{FH}). Twenty-nine were formalin fixed paraffin embedded (FFPE)[61], with the remaining samples being fresh frozen (FF). PTCL specimens were collected from the Nebraska Lymphoma Study Group registry and Tissue Bank, the IPTCL Consortium or from generous collaborations. Twenty-five of the PTCL-NOS cases from a previous study[62] had corresponding comparative genomic hybridization (CGH) data and GEP data that allowed for GATA3/TBX21 subgroup classification. For three PTCL-NOS cases, copy number abnormalities (CNAs) were obtained from NGS data[63] and included in **Figure 15**. The clinical and pathological characteristics are tabulated in **Table 1**. **Table 1** shows detailed information regarding sample description, array CGH (aCGH) platform, molecular classification, ABSOLUTE (V1.0.06) purity and IHC data. One hundred and five of the cases were included in previous profiling studies[21,55,61,62] and were reviewed by at least two pathologists to reach a consensus diagnosis. Additional PTCL series were included for comparative analysis[64-68]. This study was approved by the Institutional Review Board of the University of Nebraska Medical Center.

Case	Classification	CN Platform	GEP Platform	Tissue Source	% Large Neoplastic T-cell	Absolute Purity	CD3	CD4	CD8	CD30	CD10	PD1	CXCL13	ICOS	CXCR5	SAP	BCL6
AITL1	AITL	OncoScan	HG-U133 Plus2	Fresh Frozen	22.5	24.00%	+	+	-		+						
AITL2	AITL	OncoScan	HG-U133 Plus2	Fresh Frozen	45	24.00%	+	+	-	-	-						
AITL3	AITL	OncoScan	HG-U133 Plus2	Fresh Frozen		22.00%	+	+	-		Partial		+				+
AITL4	AITL	OncoScan	HG-U133 Plus2	Fresh Frozen		18.00%											
AITL5	AITL	OncoScan	HG-U133 Plus2	Fresh Frozen	62.5	23.00%	+	+	-	+							
AITL6	AITL	OncoScan	HG-U133 Plus2	Fresh Frozen		21.00%	+	+	-	-							
AITL7	AITL	OncoScan	HG-U133 Plus2	Fresh Frozen		19.00%	+	+	-	Weak	Weak	Weak					
AITL8	AITL	OncoScan	HG-U133 Plus2	Fresh Frozen		31.00%	+	+	-	-	Weak	Weak	+				-
AITL9	AITL	OncoScan	HG-U133 Plus2	Fresh Frozen		18.00%	+	+	-	-	Partial						
AITL10	AITL	OncoScan	HG-U133 Plus2	Fresh Frozen		15.00%	+	+	-	-	-	+					
AITL11	AITL	OncoScan	HG-U133 Plus2	Fresh Frozen		18.00%	+										
AITL12	AITL	OncoScan	HG-U133 Plus2	Fresh Frozen		18.00%	-										
AITL13	AITL	OncoScan	HG-U133 Plus2	Fresh Frozen	70	25.00%	+	+	-								
AITL14	AITL	OncoScan	HG-U133 Plus2	Fresh Frozen		22.00%	+	-	-	+	+						
AITL15	AITL	OncoScan	HG-U133 Plus2	Fresh Frozen		21.00%	+	+	-	-	-	Weak					
AITL16	AITL	OncoScan	HG-U133 Plus2	Fresh Frozen		43.00%	+	+	-		+						
AITL17	AITL	OncoScan	HG-U133 Plus2	Fresh Frozen		17.00%	+	+	-	Weak		+					
AITL18	AITL	OncoScan	HG-U133 Plus2	Fresh Frozen		18.00%	+	+	-	Weak		+					
AITL19	AITL	OncoScan	HG-U133 Plus2	Fresh Frozen		23.00%	+	+	-	-		+					
AITL20	AITL	OncoScan	HG-U133 Plus2	Fresh Frozen		20.00%	+	+	-	-							
AITL21	AITL	SNP 250K	HG-U133 Plus2	Fresh Frozen	50	30.00%	+	+	-	-	-						
AITL22	AITL	SNP 250K	HG-U133 Plus2	Fresh Frozen	40	28.00%	+	|	-		-						
AITL23	AITL	SNP 250K	HG-U133 Plus2	Fresh Frozen	40	25.00%	+	+	-		+						
AITL24	AITL	SNP 250K	HG-U133 Plus2	Fresh Frozen	32.5	38.00%	+	|	-		+						
AITL25	AITL	SNP 250K	HG-U133 Plus2	Fresh Frozen		24.00%	+	+			+						
AITL26	AITL	SNP 250K	HG-U133 Plus2	Fresh Frozen		23.00%	+	+	-	|	+						
AITL27	AITL	SNP 250K	HG-U133 Plus2	Fresh Frozen	50	35.00%	+	+	-								
AITL28	AITL	SNP 6.0	RNA-Sequencing Illumina	Fresh Frozen	80	18.00%	+	+	-	-	+	+					+
AITL29	AITL	SNP 6.0	RNA-Sequencing Illumina	Fresh Frozen	80	50.00%	+	+	-		-	+					+
AITL30	AITL	SNP 6.0	RNA-Sequencing Illumina	Fresh Frozen	80	27.00%	+	+	-	+ Scattered	-	+					+
AITL31	AITL	SNP 6.0	RNA-Sequencing Illumina	Fresh Frozen		27.00%	+	+	+		+	+					
AITL32	AITL	SNP 6.0	RNA-Sequencing Illumina	Fresh Frozen		18.00%	+/-	+	-		+	+					
AITL33	AITL	SNP 6.0	RNA-Sequencing Illumina	Fresh Frozen		66.00%	+	+	-/+		-/+	+					
AITL34	AITL	SNP 6.0	RNA-Sequencing Illumina	Fresh Frozen		21.00%	+				+/-	+					+
AITL35	AITL	SNP 6.0	RNA-Sequencing Illumina	Fresh Frozen	80	24.00%	+/-	+	-	-	+	+					
PTCL-NOS1*	PTCL-GATA3	OncoScan	DASL Illumina	FFPE		18.00%	+	+	+		-	-	-				-
PTCL-NOS2*	PTCL-GATA3	OncoScan	DASL Illumina	FFPE		16.00%	+	+	-/+	-/+	-	+	-				-
PTCL-NOS3*	PTCL-GATA3	OncoScan	DASL Illumina	FFPE		20.00%	+	-/+	-	-	-	+	-				-
PTCL-NOS4	PTCL-GATA3	OncoScan	DASL Illumina	FFPE		23.00%	+	+	-	-	-	+	-				-
PTCL-NOS5*	PTCL-GATA3	OncoScan	DASL Illumina	FFPE		26.00%	+	+	-	+/-	-	-	-				-
PTCL-NOS6*	PTCL-GATA3	OncoScan	DASL Illumina	FFPE		23.00%	+	-	+		-	Rare+	Rare+				Rare+
PTCL-NOS7*	PTCL-GATA3	OncoScan	DASL Illumina	FFPE		70.00%	+	+	-	-	-	-	-				-
PTCL-NOS10	PTCL-GATA3	Agilent SurePrint	HG-U133 Plus2	Fresh Frozen		28.00%	Reviewed in Dobay et al, Haematologica 2017										
PTCL-NOS11	PTCL-GATA3	Agilent SurePrint	HG-U133 Plus2	Fresh Frozen		27.00%	Reviewed in Dobay et al, Haematologica 2017										
PTCL-NOS12	PTCL-GATA3	Agilent SurePrint	HG-U133 Plus2	Fresh Frozen		68.00%	Reviewed in Dobay et al, Haematologica 2017										
PTCL-NOS13	PTCL-GATA3	Agilent SurePrint	HG-U133 Plus2	Fresh Frozen		29.00%	Reviewed in Dobay et al, Haematologica 2017										
PTCL-NOS14	PTCL-GATA3	Agilent SurePrint	HG-U133 Plus2	Fresh Frozen		70.00%	Reviewed in Dobay et al, Haematologica 2017										
PTCL-NOS15	PTCL-GATA3	Agilent SurePrint	HG-U133 Plus2	Fresh Frozen		29.00%	Reviewed in Dobay et al, Haematologica 2017										
PTCL-NOS16	PTCL-GATA3	Agilent SurePrint	HG-U133 Plus2	Fresh Frozen		30.00%	Reviewed in Dobay et al, Haematologica 2017										
PTCL-NOS8	PTCL-GATA3	Agilent SurePrint	HG-U133 Plus2	Fresh Frozen		31.00%	Reviewed in Dobay et al, Haematologica 2017										
PTCL-NOS9	PTCL-GATA3	Agilent SurePrint	HG-U133 Plus2	Fresh Frozen		42.00%	Reviewed in Dobay et al, Haematologica 2017										
PTCL-NOS17*	PTCL-GATA3	*Not Available*	HG-U133 Plus2	Fresh Frozen		*Not Available*											
PTCL-NOS18*	PTCL-GATA3	OncoScan	HG-U133 Plus2	Fresh Frozen	50	32.00%	+	+	-	-	-	-	-	-			
PTCL-NOS19	PTCL-GATA3	OncoScan	HG-U133 Plus2	Fresh Frozen	30	42.00%	+	+	-								
PTCL-NOS20*	PTCL-GATA3	OncoScan	HG-U133 Plus2	Fresh Frozen	20	28.00%	+	|	-	-		-	-	-			
PTCL-NOS21*	PTCL-GATA3	OncoScan	HG-U133 Plus2	Fresh Frozen	70	44.00%	+	+	-	-		-	-	-			
PTCL-NOS22*	PTCL-GATA3	OncoScan	HG-U133 Plus2	Fresh Frozen	60	35.00%	+	+	-	-	-	-	-	-			
PTCL-NOS23*	PTCL-GATA3	OncoScan	HG-U133 Plus2	Fresh Frozen	41.25	46.00%	+	-	-	+							
PTCL-NOS24*	PTCL-GATA3	OncoScan	HG-U133 Plus2	Fresh Frozen	20	23.00%	+	+	-	+							
PTCL-NOS25*	PTCL-GATA3	OncoScan	HG-U133 Plus2	Fresh Frozen	15	32.00%	-	+	-								
PTCL-NOS26	PTCL-GATA3	OncoScan	HG-U133 Plus2	Fresh Frozen		17.00%											
PTCL-NOS27	PTCL-GATA3	OncoScan	HG-U133 Plus2	Fresh Frozen	60	32.00%	+	-	-			-	-	-			
PTCL-NOS28*	PTCL-GATA3	OncoScan	HG-U133 Plus2	FFPE		53.00%						-	-	+			
PTCL-NOS30	PTCL-GATA3	OncoScan	HG-U133 Plus2	FFPE		39.00%						-	-	+			
PTCL-NOS31	PTCL-GATA3	OncoScan	HG-U133 Plus2	Fresh Frozen		29.00%											
PTCL-NOS32*	PTCL-GATA3	OncoScan	HG-U133 Plus2	FFPE		23.00%						-	-	-			
PTCL-NOS29*	PTCL-GATA3	OncoScan	HG-U133 Plus2	Fresh Frozen		23.00%	+	+	-	-							
PTCL-NOS33*	PTCL-NC	OncoScan	DASL Illumina	FFPE		35.00%	+	-	-	-	-	-	-				-
PTCL-NOS34	PTCL-NC	Agilent SurePrint	HG-U133 Plus2	Fresh Frozen		40.00%	Reviewed in Dobay et al, Haematologica 2017										
PTCL-NOS35	PTCL-NC	Agilent SurePrint	HG-U133 Plus2	Fresh Frozen		20.00%	Reviewed in Dobay et al, Haematologica 2017										
PTCL-NOS36*	PTCL-NC	OncoScan	HG-U133 Plus2	Fresh Frozen	7.5	22.00%	+	+	-	-	-		-				
PTCL-NOS37*	PTCL-NC	OncoScan	HG-U133 Plus2	Fresh Frozen	80	22.00%	+	+	-	-		-	-	Partial			
PTCL-NOS38	PTCL-TBX21	OncoScan	DASL Illumina	FFPE		17.00%	+	+	-	-	-	-/+	-/+				-/+
PTCL-NOS39*	PTCL-TBX21	OncoScan	DASL Illumina	FFPE		29.00%	+		-	-/+	-	-	Rare+				-
PTCL-NOS40*	PTCL-TBX21	OncoScan	DASL Illumina	FFPE		27.00%	+	-	-	+	-	-	-				-
PTCL-NOS41*	PTCL-TBX21	OncoScan	DASL Illumina	FFPE		33.00%	+	+	-	-	-	-	-				-
PTCL-NOS42	PTCL-TBX21	OncoScan	DASL Illumina	FFPE		25.00%	+	-	-	-	-	-	-				-
PTCL-NOS43	PTCL-TBX21	OncoScan	DASL Illumina	FFPE		22.00%	+	+	-	-	-	-	-				-
PTCL-NOS44*	PTCL-TBX21	OncoScan	DASL Illumina	FFPE		25.00%	+	+	-	Rare+	-	+	-				-
PTCL-NOS45	PTCL-TBX21	Agilent SurePrint	HG-U133 Plus2	Fresh Frozen		25.00%	Reviewed in Dobay et al, Haematologica 2017										
PTCL-NOS46	PTCL-TBX21	Agilent SurePrint	HG-U133 Plus2	Fresh Frozen		21.00%	Reviewed in Dobay et al, Haematologica 2017										
PTCL-NOS47	PTCL-TBX21	Agilent SurePrint	HG-U133 Plus2	Fresh Frozen		24.00%	Reviewed in Dobay et al, Haematologica 2017										
PTCL-NOS48	PTCL-TBX21	Agilent SurePrint	HG-U133 Plus2	Fresh Frozen		23.00%	Reviewed in Dobay et al, Haematologica 2017										
PTCL-NOS49	PTCL-TBX21	Agilent SurePrint	HG-U133 Plus2	Fresh Frozen		21.00%	Reviewed in Dobay et al, Haematologica 2017										
PTCL-NOS50	PTCL-TBX21	Agilent SurePrint	HG-U133 Plus2	Fresh Frozen		22.00%	Reviewed in Dobay et al, Haematologica 2017										
PTCL-NOS51	PTCL-TBX21	Agilent SurePrint	HG-U133 Plus2	Fresh Frozen		28.00%	Reviewed in Dobay et al, Haematologica 2017										
PTCL-NOS52	PTCL-TBX21	Agilent SurePrint	HG-U133 Plus2	Fresh Frozen		18.00%	Reviewed in Dobay et al, Haematologica 2017										
PTCL-NOS53	PTCL-TBX21	Agilent SurePrint	HG-U133 Plus2	Fresh Frozen		46.00%	Reviewed in Dobay et al, Haematologica 2017										
PTCL-NOS54	PTCL-TBX21	Agilent SurePrint	HG-U133 Plus2	Fresh Frozen		49.00%	Reviewed in Dobay et al, Haematologica 2017										
PTCL-NOS55	PTCL-TBX21	Agilent SurePrint	HG-U133 Plus2	Fresh Frozen		30.00%	Reviewed in Dobay et al, Haematologica 2017										
PTCL-NOS56	PTCL-TBX21	Agilent SurePrint	HG-U133 Plus2	Fresh Frozen		27.00%	Reviewed in Dobay et al, Haematologica 2017										
PTCL-NOS57	PTCL-TBX21	Agilent SurePrint	HG-U133 Plus2	Fresh Frozen		27.00%	Reviewed in Dobay et al, Haematologica 2017										
PTCL-NOS58	PTCL-TBX21	Agilent SurePrint	HG-U133 Plus2	Fresh Frozen		26.00%	Reviewed in Dobay et al, Haematologica 2017										
PTCL-NOS59	PTCL-TBX21	OncoScan	HG-U133 Plus2	FFPE		22.00%						-	-	-			
PTCL-NOS60*	PTCL-TBX21	OncoScan	HG-U133 Plus2	FFPE		60.00%						-	-	+			
PTCL-NOS61*	PTCL-TBX21	OncoScan	HG-U133 Plus2	Fresh Frozen	30	30.00%	+	+	-	+	-	-	-	-			
PTCL-NOS62	PTCL-TBX21	OncoScan	HG-U133 Plus2	Fresh Frozen	60	23.00%	+	-	-	Partial	Partial	-	Partial	Partial			
PTCL-NOS63	PTCL-TBX21	OncoScan	HG-U133 Plus2	Fresh Frozen		21.00%	+	+	-	+	Partial						
PTCL-NOS64*	PTCL-TBX21	OncoScan	HG-U133 Plus2	Fresh Frozen		22.00%											
PTCL-NOS65	PTCL-TBX21	OncoScan	HG-U133 Plus2	FFPE		30.00%						-	-	-			
PTCL-NOS66*	PTCL-TBX21	SNP 250K	HG-U133 Plus2	Fresh Frozen		25.00%	+	+	-	-	-	-	-	-			-
PTCL-NOS67*	PTCL-TBX21	SNP 250K	HG-U133 Plus2	Fresh Frozen	60	24.00%	+	+	+	-		-	-	-			
PTCL-NOS68*	PTCL-TBX21	Not Available	HG-U133 Plus2	FFPE		Not Available	+	+		-		-	Partial				
PTCL-NOS69*	PTCL-TBX21	Not Available	HG-U133 Plus2	FFPE		Not Available	+	+		-		-	-				
PTCL-TFH1*	PTCL-TFH	OncoScan	DASL Illumina	FFPE		20.00%	+	-	-	-	-	+	+				+
PTCL-TFH2*	PTCL-TFH	OncoScan	DASL Illumina	FFPE		28.00%	+	-	+		-	+	-				+
PTCL-TFH3	PTCL-TFH	OncoScan	HG-U133 Plus2	Fresh Frozen		16.00%	+	+	-	+	+	+	+	+			
PTCL-TFH4	PTCL-TFH	OncoScan	HG-U133 Plus2	FFPE		32.00%						-	+	+			
PTCL-TFH5	PTCL-TFH	OncoScan	HG-U133 Plus2	Fresh Frozen	60	20.00%	+			-	+	+	+	+			
PTCL-TFH6	PTCL-TFH	OncoScan	HG-U133 Plus2	Fresh Frozen		22.00%						+	+	+			
PTCL-TFH7	PTCL-TFH	OncoScan	HG-U133 Plus2	Fresh Frozen	60	24.00%	+	-	-		Partial	+	+	+			Partial
PTCL-TFH8*	PTCL-TFH (Expression)	OncoScan	HG-U133 Plus2	FFPE		32.00%						-	Partial	Partial			
PTCL-TFH9	PTCL-TFH (Expression)	OncoScan	HG-U133 Plus2	FFPE		19.00%						-	Partial	Partial			
PTCL-TFH10	PTCL-TFH (Expression)	OncoScan	HG-U133 Plus2	Fresh Frozen		24.00%	+	+	-	Weak	-		Weak				
PTCL-TFH11	PTCL-TFH (Expression)	OncoScan	HG-U133 Plus2	FFPE		29.00%						-	-	Partial			
PTCL-TFH12	PTCL-TFH (Expression)	OncoScan	HG-U133 Plus2	Fresh Frozen		20.00%	+	+	-								
PTCL-TFH13*	PTCL-TFH	SNP 250K	HG-U133 Plus2	Fresh Frozen		33.00%	+	+	-		-	+	Partial	Partial			
PTCL-TFH14*	PTCL-TFH	SNP 250K	HG-U133 Plus2	Fresh Frozen	80	22.00%	+	+	-		+	+	-	+			+
PTCL-TFH15	PTCL-TFH (Expression)	SNP 250K	HG-U133 Plus2	Fresh Frozen	37.5	45.00%	+	|	-								

Table 1: Case IDs and corresponding data. Cases indicated with "*" were sequenced.

T-cell Lines

Four T-cell lines representative of lymphoblastic leukemia (Jurkat), Sezary Syndrome (HuT78), cutaneous T-cell lymphoma (CTCL)/ALCL ALK$^-$ (MAC-1[69,70]) and a mature CD4$^-$CD8$^+$ T-cell lymphoma (T8ML1[71]) were used in the study. These T-cell lines were cultured in 2.05mM L-Glutamine supplemental RPMI 1640 (HyClone) (T8ML1, MAC-1, Jurkat) or IMDM (HuT78), supplemented with 10% or 20% fetal bovine serum (FBS) respectively, penicillin G (199 U/mL) and streptomycin (100 µG/mL). T8ML1 was further supplemented with IL-2 (10 nG/mL). Cell cultures were maintained at 37ºC in 5% CO_2. All cell lines underwent routine mycoplasma testing using the Universal Mycoplasma Detection Kit (ATCC), with the most recent testing completed on August 17, 2017. Approximately, four passages of the cells occurred between thawing and experimental use. The T8ML1 cell line was generously provided from Hiroshi Fujiwara, whom was involved in establishing the cell line[71]. MAC-1 was originally established by Marshall Kadin[72]. Both Jurkat and HuT78 were previously purchased from ATCC. The status of PTEN and TP53 mutation and copy number are indicated in **Table 2**.

Genomic Copy Number Analysis

Genomic deoxyribonucleic acid (DNA) was previously extracted from FF tissues using the AllPrep DNA/RNA kit (Qiagen) and from FFPE samples using AllPrep DNA/RNA FFPE kit (Qiagen). Three different SNP array platforms (Nsp1 SNP 250K, SNP 6.0 and OncoScan, Affymetrix) were used for CN analysis together with previously publish Agilent SurePrint aCGH data[62]. DNA libraries were generated according to the manufacturer's recommendations specific to each platform. Specifically for the OncoScan platform, two raw .CEL files are generated, one for the "AT" array and a second for the "GC" array. The .CEL files are combined in OncoScan Console (Affymetrix) to generate a single .OSCHP file. Briefly, the generation of the .OSCHP file

entails calculating the log2 ratio, allelic difference and B-allele frequency, then identifying normal diploid regions. Based on the normal diploid regions, the log2 ratio, allelic difference and BAF are recomputed if necessary. Visualization of the CNAs was performed with Nexus Copy Number™ software (Bio Discovery, El Segundo, CA, USA) which enables multiple platform analysis using the SNP-FASST2 algorithm. For cases with paired normal (11 AITL on SNP 6.0), Nexus Copy Number enables the combined import of tumor and normal sample. The gain and loss thresholds were set at a log2 ratio of 0.06 and -0.06, respectively. Raw data from deposited CEL files from published studies[66,68] were analyzed using the SNP-FASST2 algorithm with default settings. Segmentation files for the published ALCL study[64] were observed. The percent aberrant genome per case was calculated by taking the total size of the aberrant regions divided by the total size of the genome for chromosomes 1-22. Frequencies of gains and losses along the chromosomes were calculated by Nexus and moving average smoothing at 5 Mb was applied for CNA frequency along the chromosome plots.

Molecular Classification of Peripheral T-cell Lymphomas

Sixty-three cases had previously undergone molecular classification according to the gene signatures previously described[21,55]. The remaining cases were classified using the Affymetrix HG-U133 Plus2 data, RNA-sequencing data (RNA-seq), or Illumina DASL messenger ribonucleic acid (mRNA) expression data and the same gene signatures and Bayesian algorithm described in the previous publications[21,55].

RNA-seq on an additional nine AITL cases classified by morphology and IHC was performed using RNA-TruSeq mRNA Library Preparation Kits (Illumina, San Diego, CA, USA) and an Illumina HiSeq 2000 sequencer. Tophat, Cufflinks and Cuffdiff[73] were used for alignment, read counting and generation of fragments per kilobase million (FPKM) values. We used a pre-defined AITL mRNA signature derived from a well-

characterized histopathological AITL training cohort from earlier studies[21,55] and using the Bayesian algorithm validated eight (of nine) new AITL cases having a high probability (>0.80) with the AITL signature and thus were included in this study.

The Affymetrix HG-U133 Plus2 data from PTCL-GATA3 and PTCL-TBX21 cases from a previous study[21] was imported into BRB array tools (https://brb.nci.nih.gov/BRB-ArrayTools/) and MAS5.0 normalized, as previously described[21]. Data on the Illumina DASL platform from a previous study[61] was separately imported and normalized using BRB ArrayTools. The normalized data from each array platform was exported and the maximally expressed probe set was selected for each gene. The data from the two platforms were merged and the two platforms were cross-platform normalized using the empirical Bayes method (ComBat)[74]. For individual arrays, the correlation between probe set values before and after combat was approximately 0.8-0.98. We re-examined each transcript that was included in the original signature[21] and present in both platforms and selected the transcripts that expressed a positive correlation with the classifier's mean in the FFPE data. The classifier genes were then used for Bayesian classification in FFPE cases, with the Affymetrix HG-U133 Plus2 cases of known classification serving as a training set, as performed in previous studies[21,55]. The cases were classified, if it showed >80% probability of belonging to one subgroup versus other groups as shown in previous studies[21,55]. Additionally, we also performed unsupervised hierarchical clustering using the classifier genes in the cases included in the CNA study and confirmed that there were two main clusters, one dominated by PTCL-GATA3 cases and one dominated by PTCL-TBX21 cases, indicating the magnitude of the differential expression of the classifier genes can tolerate the platform differences.

Integrative Analysis of Copy Number Abnormalities with GEP

Total RNA isolated from FF and FFPE PTCL cases was previously used to obtain GEP data (Affymetrix HG-U133 Plus2 and Illumina DASL) and was included in previous studies[21,55,61,62]. For each gene the probeset with the maximal expression was used. For cases with GEP data on the Affymetrix HG-U133 Plus2, we compared the average mRNA expression level of genes against CN status (gain/amplification, heterozygous/homozygous loss, 2N) using one-sided Student's t-test to determine significance. Ingenuity Pathway Analysis program (Qiagen, Inc) or DAVID v6.8 (https://david.ncifcrf.gov/) was used for the molecular and functional annotation of the genes within aberrant regions, and only pathways with $p<0.05$ and a false discovery rate (FDR) <0.25 were included in the discussion.

Unsupervised Hierarchical Clustering

Unsupervised hierarchical clustering (HC) of molecularly classified PTCL-NOS cases was performed using the CN status of abnormalities identified at a frequency $\geq$10% in either the PTCL-GATA3 or PTCL-TBX21 subgroups. An arm was considered lost or gained accordingly if at least 25% of the arm displayed the aberration. Clustering was performed using Cluster 3.0 (correlation (centered)) similarity metric and average linkage, http://bonsai.hgc.jp/~mdehoon/software/cluster/software.htm). The two validation cohorts were clustered similarly based on the abnormalities identified in the molecularly classified/training series. Correlation of CNAs among cases was performed using Pearson correlation and the R-language "corrplot" package.

NanoString nCounter v2 Cancer CN Assay

The v2 Cancer CN Assay provides analysis of 87 genes commonly found aberrant in cancer and has been optimized for the use of FFPE samples as well. Fifty-four probes targeting invariant regions are also included as controls. DNA (500 nG) was fragmented with AluI restriction enzyme followed by a 24 hour hybridization per the manufacturer. Post-hybridization purification was performed by the nCounter Prep Station followed by image acquirement at maximum sensitivity on the nCounter Digital Analyzer. Subsequent analysis was completed using nSolver Analysis Software 3.0 as suggested per the manufacturer.

Genomic Sequencing and Analysis

A custom panel targeting 334 genes recurrently mutated in NHLs was previously designed using the Agilent SureSelect platform. Fifteen-18 samples were sequenced per lane on an Illumina HiSeq2500 sequencer for an average of 268-fold coverage of targeted regions. Adapter sequences were trimmed using trimmomatic (v0.36). Raw reads were mapped to the human genome (hg19) using the Burrows-Wheeler Aligner-MEM (v0.7.15). Genome Analysis Toolkit (v3.6) was used for local realignment and base quality recalibration. Duplicate marking was done with Picard (v2.4.1). Variant calling and filtering were performed with VarScan 2 (v2.4.0) and Genome Analysis Toolkit UnifiedGenotyper. The variants were annotated using Annovar (http://annovar.openbioinformatics.org). Variant filters applied included requiring that variants should be supported by at least four reads with a minimal VAF of 5% with variant reads on the plus and minus strand. Variants were excluded if they 1) existed in the dbSNP138NotFlagged database (http://annovar.openbioinformatics.org/en/latest/user-guide/filter); 2) were in a regions of segmental duplication (SuperDups, Annovar); 3) did not change protein sequences or

affect splice sites; 4) were recurrent in a set of 92 unrelated normal samples; or 5) were shared by >10 cases unless they are from a gene known to have frequent mutations and thus present in the COSMIC database.

Overall Survival Outcome Analysis

The OS (death from any cause) was estimated using the Kaplan-Meier method, and differences assessed using the Log-rank test. Statistical analyses were performed with the R-language survival package. Differences among groups were considered significant at p-values below 0.05 (*).

PrestoBlue Cell Proliferation Assay

Jurkat, T8ML1, MAC-1 and HuT78 cell lines were treated with different concentrations of Torin 1 (10189-392, BioVision) (100, 200 and 300 nM), Torin 2 (2274-5, BioVision) (10, 20, 40, 60 and 100 nM) and Temsirolimus (TEM) (Chemscene) (1, 2, 3, 4 and 5 µM) for 24 hours. Sensitivity to drug treatment in the four cell lines was assayed in 96 well plates using PrestoBlue™ Cell Viability Reagent (Invitrogen -A13261) per manufacture's protocol and read on a Tecan Infinite M200Pro.

Western Blotting

Jurkat, T8ML1, MAC-1 and HuT78 cell lines were treated with Torin 1 (200 nM), Torin 2 (100 nM), or TEM (2 µM) for 24 hours and then lysed in RIPA buffer (50 mM Tris, pH 7.4, 150 mM NaCl,1% Triton X-100, 0.1% SDS, 1% sodium deoxycholate, 10 mM sodium 2-glycerolphosphate, 1 mM phenylmethylsulfonyl fluoride, 0.4 units/mL aprotinin, 1 mM sodium fluoride and 0.1 mM sodium vanadate). Twenty to 100 µG of whole-cell extracts were separated by sodium dodecyl sulfate-polyacrylamide gel

electrophoresis and transferred to nitrocellulose (Bio-Rad) or polyvinylidene difluoride (Bio-Rad) membranes. Membranes were blocked in Odyssey Blocking Buffer (LI-COR) or Tris buffered saline with 0.1% Tween and 5% milk at room temperature for 30 minutes to 1 hour and then incubated with primary antibody specific to pAKT (S473) (#4060;CST), pAKT (Thr308) (#13038;CST), total AKT (#4691;CST), p4EBP1 (#2855;CST), p-RPS6 (#4858;CST), caspase-3 (#9661;CST) and β-actin (#1616;SC) at 4°C overnight, followed by treatment with secondary antibodies.

Genomic Status of *PTEN* and *TP53*

The genomic DNA from T-cell lines was used to quantify the DNA copy number of PTEN and TP53 in comparison to RPL13A and tonsillar DNA was used as a calibrator (normal). Two Burkitt Lymphoma cell lines (Raji and Namalwa) were included as positive controls. The qPCR experiment was performed using SYBR Green qPCR Kit (Bio Rad. Inc) using primers listed in **Table 2**. The standard ΔΔ CT (CT (PTEN or TP53)–CT (RPL13A) method was used to estimate the status of the genomic locus.

TP53 and PTEN DNA CN status in 4 T-cell lines normalized to the RPL13A housekeeping gene compared to tonsil.

Cell Line	TP53 DNA CN	PTEN DNA CN
Jurkat	2N	2N
T8ML1	2N	Gain
MAC-1	2N	2N
HuT78	Single Loss	2N

Mutation status of 4 T-cell lines as collected from literature.

Cell Line	TP53 Mutation Status	PTEN Mutation Status
Jurkat	Nonsense, Splicing	Frameshift Insertion; Missense
T8ML1	Not Available	Not Available
MAC-1	No Evidence	No Evidence
HuT78	Nonsense	None Reported

Primer sequences used to determine DNA CN status of PTEN and TP53.

Gene	Direction	Sequence
PTEN	Forward	5'-CCACAAAGTGCCTCGTTTAC-3'
PTEN	Reverse	5'-GAAGGCAACTCTGCCAAATAC-3'
TP53	Forward	5'-TGCTGCAAGAGGCAGAAA-3'
TP53	Reverse	5'-GTCAGTCGTGGAAGTGAGAAG-3'

Table 2: Genomic characteristics and primers used to evaluate four T-cell lines.

2.3 RESULTS

Clinical characteristics and molecular classification of PTCL

PTCL cases were classified using our pre-defined GEP signatures[21,55]. These included FF tissues (n=94) profiled by Affymetrix HG-U133 Plus2[21,55,62], FFPE tissues (n=17) profiled using Illumina DASL[61] and eight AITL cases with RNA-seq (**Figure 8**). PTCL-T_{FH} cases (n=15), a provisional entity according to the 2017-WHO classification[17], were identified primarily by morphological assessment and the expression of the WHO-defined IHC markers[17]. However, six cases lacking tissue for IHC were identified based on a recently described PTCL-T_{FH} GEP signature[62], which showed mRNA expression similar to known PTCL-T_{FH} samples (**Figure 9A/B**). When we examined the T_{FH} signature[62] in the entire set, it was found to be enriched in only AITL or PTCL-T_{FH} (**Figure 9B**). After excluding PTCL-T_{FH} cases, PTCL-NOS cases were sub-classified into either the PTCL-GATA3 (n=31) or PTCL-TBX21 (n=30) subgroup using GEP, and five remained unclassifiable (PTCL-NC)[21,55]. PTCL-T_{FH} cases were used only for comparative analysis. There was no significant difference in age between cohorts (**Table-3**). PTCL-GATA3 showed inferior OS compared to other groups (**Figure 9C**) as previously demonstrated[21,60].

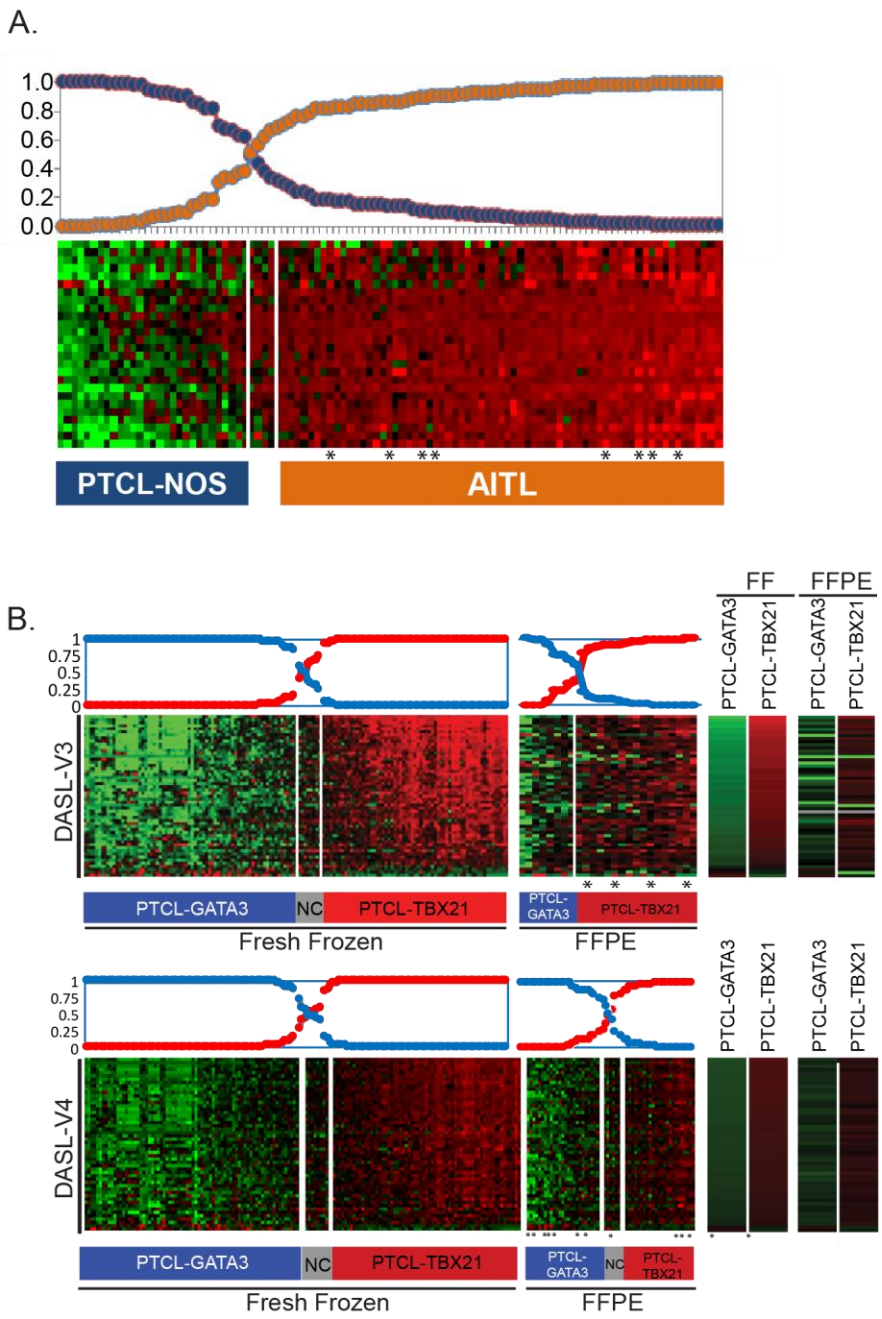

Figure 8: Classification of peripheral T-cell lymphoma entities and subgroups.

A. Analysis of the AITL signature genes identified on the Affymetrix HG-U133 Plus2 platform in RNA-seq data. The Bayesian predictor for AITL (orange) and PTCL-NOS (blue) entities are shown above the heat map and the eight AITL cases included in the study are noted with an asterisk. **B.** PTCL-GATA3/TBX21 subgroup classification using signature genes generated from the Affymetrix HG-U133 Plus2 platform. Robust classifier genes present in both Affymetrix and Illumina DASL V3 or DASL V4 platforms were used to molecularly classify FFPE PTCL-NOS cases. The Bayesian predictor for GATA3 (blue) or TBX21 (red) subgroups are shown below the heat maps and cases included in the study are marked with an asterisk. The Illumina HUMANREF 8_V3_0_R1_11282963_A_WGDASL (DASL V3) or Human HT 12_V4_0_R2_15002873_B_WGDASL (DASL V4) were available from a previously published dataset.

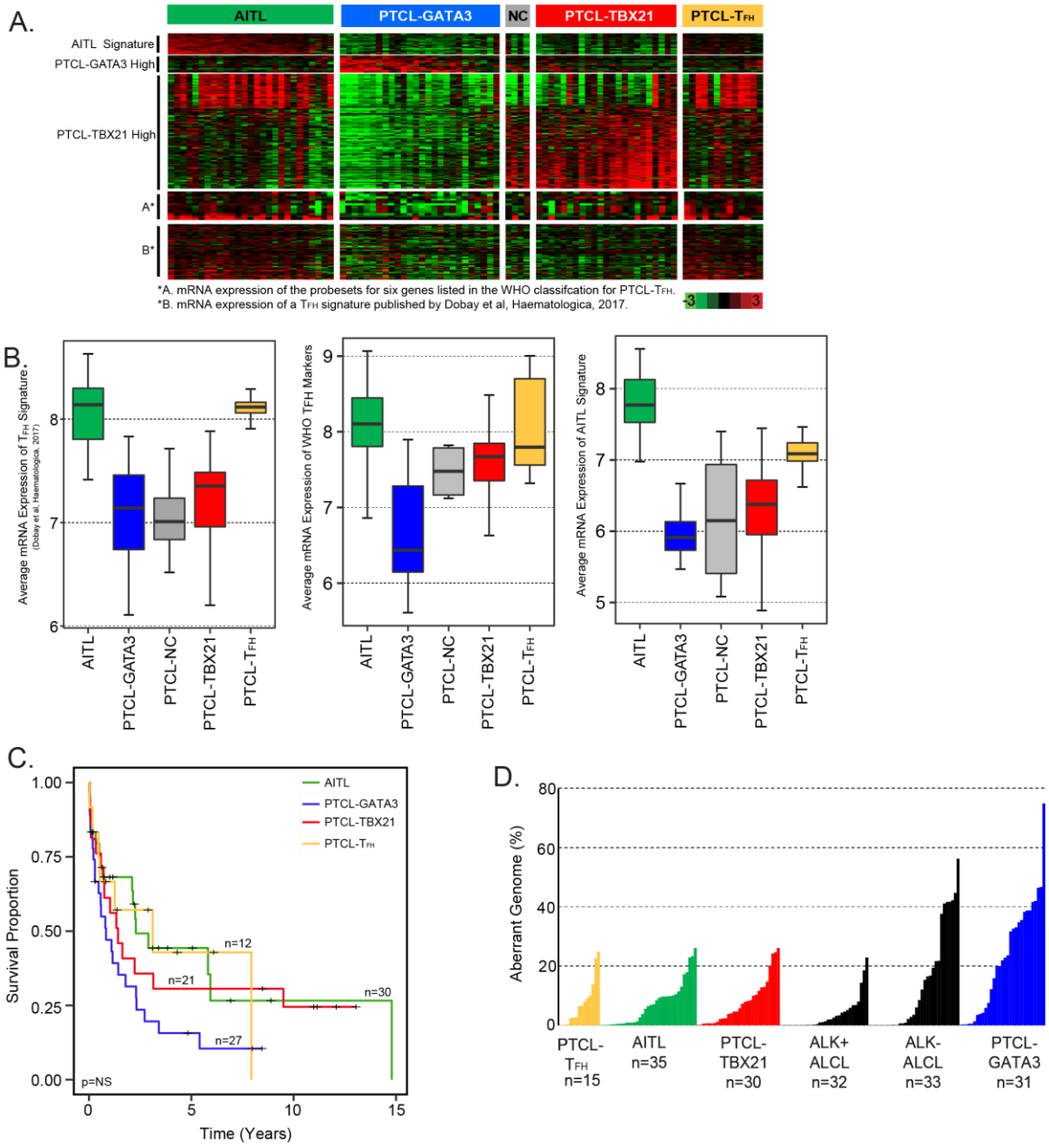

Figure 9: Characteristics of peripheral T-cell lymphoma entities and subgroups.

A. Gene expression data of predefined gene signatures for AITL, the PTCL-GATA3 and PTCL-TBX21 subgroups and PTCL-T_{FH} using FF RNA on the HG-U133 Plus2 platform (Affymetrix). **B.** Average expression of the PTCL-T_{FH} signature in PTCL subgroups (left panel), the probe sets for six genes listed by the WHO to classify PTCL-T_{FH} (middle panel) and the AITL molecular signature (right panel). **C.** Kaplan-Meier curves comparing OS between the PTCL subgroups with available data. **D.** Comparison of percent aberrant genome in PTCL subgroups (PTCL-T_{FH}, AITL, PTCL-TBX21, ALK$^+$ ALCL, ALK$^-$ ALCL and PTCL-GATA3).

				PTCL-NOS Molecular Subgroups			
		AITL	PTCL-NOS	GATA3+	TBX21+	Unclassifiable	PTCL-TFH
	Count	**35**	**66**	**31**	**30**	**5**	**15**
Age at Diagnosis (Years)	**Median**	67	66	67	66	53	61
	Range	45-87	19-97	19-97	26-79	40-69	28-76
	<60	5	11	7	2	2	7
	≥60	30	24	14	9	1	7
Gender	**Male**	18	27	15	9	3	9
	Female	17	11	6	5	0	5
			*Data on 38	*Data on 21	*Data on 14	*Data on 3	*Data on 14

Table 3: Basic clinical characteristics of molecularly classified peripheral T-cell lymphoma cases.

Integrated genomic analysis of molecularly-defined AITL

AITL had the least abnormal genome (mean=7%), with CN gains more frequent than CN losses and a percent aberrant genome comparable to PTCL-T_{FH} and PTCL-TBX21 (**Figure 9D**). Cases with low aberrant genomes showed no significant difference in tumor content compared to highly aberrant cases, as estimated by the ABSOLUTE algorithm based on single nucleotide polymorphism (SNP) hybridization[75] and by morphologic review of the percent of neoplastic T-cells. This suggests that detection of fewer CNAs was not due to low tumor content.

Of the most frequent CNAs (**Figure 10A**), chr5-gain (43%; 15/35) and chr21-gain (23%; 8/35) significantly co-occurred (p=0.01). Gains of chr7/7q, -11, -19 or -22q occurred in at least 10% (4/35) of AITL cases, consistent with a recent study[62]. Integration of CN status and GEP data identified 597 upregulated ($p<0.05$) candidate target genes, which were enriched in biological processes involving RNA/protein metabolism, mitochondrial dysfunction and cell cycle regulation using DAVID analysis.

Chr5-gain in AITL is distinctive, as other hematological malignancies exhibit chr5-loss[76,77]. Examination of chr5 genes in cases with GEP showed that 95 were significantly ($p\leq0.05$) upregulated in the cases with chr5-gain, including IL4, IL13 and MAPK9 which affect cell cycle regulation and T-cell differentiation[78]. Many of these genes showed an expression pattern similar to IL12 activated normal $CD4^+$ T-cells (**Figure 10B**). Genes related to cell cycle (p=0.004, FDR=4.21%) and T-cell activation (p=0.035, FDR=24.0%) were also significantly upregulated in cases with chr5-gain. GSEA indicated marginal enrichment of oxidative phosphorylation-associated genes (p=0.048, FDR=NS). Chr5-gain was significantly associated with $IDH2^{R172}$ mutation (p=0.01), but not with recurrent mutations in DNMT3A, $RHOA^{G17V}$, or TET2. AITL cases without chr5-gain showed enrichments of NF-κB (p=0.009, FDR=11.1%) and PI3K-AKT (p=0.008, FDR=9.47%) pathway signatures according to DAVID, suggesting alternative oncogenic pathways in

these cases. Similar gene-signature association was observed in $IDH2^{WT}$ cases. Interestingly, a marginally higher percent aberrant genome was associated with $IDH2^{R172}$ mutation in AITL (**Figure 10C**).

Compared to the entire chromosome/arm gains, more focal deletions were observed, and included a number of loci located at 1p36.33, 9q34.11, 13q22.3, 16p13.3, 16q24.3, 17p13.1 and 19q13.2-4. We identified frequently deleted genes (≥10%, 4/35) and analyzed only genes expressed (≥1 FPKM) in normal T_{FH} cells[79]. Genes in deleted loci having significant loss of mRNA expression included genes involved with ubiquitylation/proteolysis (FBXO44 and PSMB3), microtubule organization (SLAIN1) and mito-ribosome stability (MRPL28 and MPV17L2). Association with the PI3K-AKT-mTOR pathway was observed in genes lost in ≥4 cases and included negative regulators (STK11, PPP2R2D, PHLPP1, TSC2)[80], PI3K regulatory subunit PIK3R2 (p85β) and genes regulating amino acid-sensing in the mTORC1 signaling pathway (WDR24*)* (**Figure 10D/E**). The positive regulator of PI3K-AKT signaling, PDPK1[80] (16p13.3), which is mutated in 6% of AITL[33], is also deleted in AITL. CN loss of several PI3K-AKT phosphatases (PHLPP1 and/or PPP2R2D) showed a trend of mutual exclusivity with $IDH2^{R172}$ mutations (p=0.057 CoMEt_exact_test[81]). DNMT3A mutations showed a negative correlation with other key regulators of the PI3K-AKT pathway, with some genes showing marginal trend (PIK3R2, PKN3*; p=0.08),* whereas others (STK11, YWHAE, PPP2R2D*;* p=0.12-0.26), did not show statistical significance probably due to low number of cases for analysis. These findings suggest alternative oncogenic mechanisms in mutant cases (**Figure 10F**). Examination of TCR signaling showed that 12% of AITL had *CD28* gain/amplification, in addition to mutations and fusions observed in AITL[33,42,82].

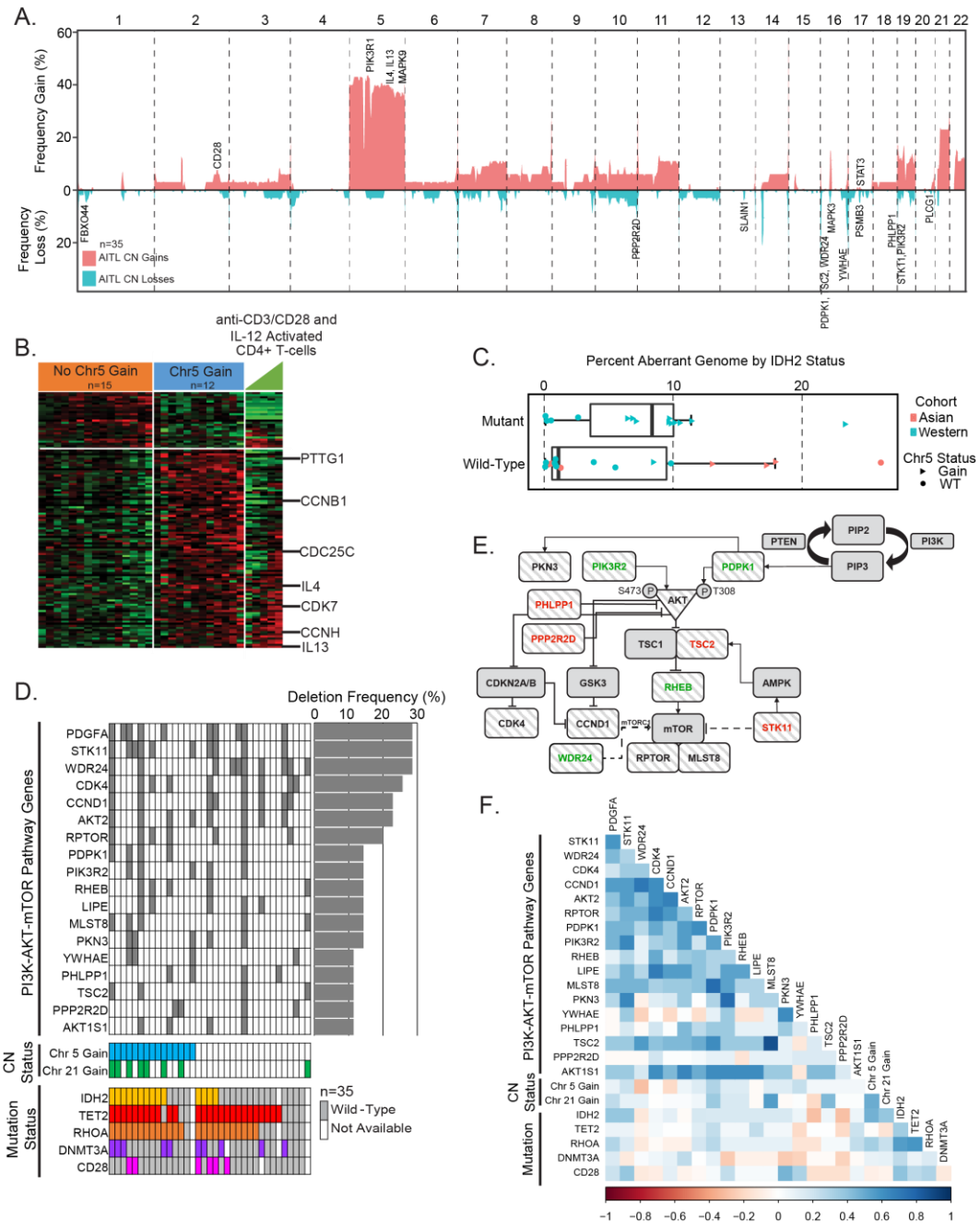

Figure 10: Copy number analysis in angioimmunoblastic T-cell lymphoma.

A. Frequency of chromosomal gains and losses in AITL tumors quantified using Nexus Copy Number. Candidate genes within aberrant loci are indicated. **B.** Heat map of differentially expressed genes (p<0.05) located on chr5 between cases with and without a chr5 gain. **C.** Percent aberrant genome segregated on mutation status of IDH2^{R172} in AITL cases. Asian and Western cohorts are distinguished by color, whereas CN state of chr5 is indicated by shape. **D.** Genes involved in the PI3K–AKT–mTOR pathway that are deleted in ≥10% of AITL cases and their association with frequent CNAs and mutations, which are indicated below. **E.** PI3K–AKT–mTOR schematic diagram with striped patterned genes deleted in AITL at a frequency ≥10%. Genes in red are negative regulators and genes in green are positive regulators. **F.** Matrix of Pearson correlation coefficients for co-occurring genomic abnormalities and mutations in AITL.

Integrated genomic analysis of molecularly-defined PTCL subgroups

PTCL-GATA3 exhibited a more aberrant genome (mean=23%) than PTCL-TBX21 (mean=8%, p<0.001) (**Figure 9D**), with frequent partial/complete chr7-gain (48%; 15/31), partial/complete chr8q gain (45%; 14/31) and chr17q gains (42%; 13/31) (**Figure 11A**). MYC (8q24.21) was gained/amplified in 52% (16/31) with concomitant higher mRNA expression (3.7-fold, p<0.001) (**Figure 11B**) along with an enrichment of MYC target genes (p<0.05, FDR<10%)[21]. Chr17q-gain encompassed STAT3 and was associated with elevated mRNA (2.4-fold, p<0.001) (**Figure 11B**). Focal gain/amplification encompassing REL (2p16.1) was associated with increased mRNA (2.5-fold, p=0.005) (**Figure 11B**).

CN deletions in PTCL-GATA3 included del-17p, del-13q, del-10q, del-9p21.3, del-5q, del-6q21 and del-1q, which affected well-characterized tumor suppressors (TS) [TP53 (58% heterozygous), PTEN (35%; 10 heterozygous, 1 homozygous), FAS (32%; 8 heterozygous, 2 homozygous), CDKN2A/B (45%; 7 heterozygous, 7 homozygous) and PRDM1 (23%; heterozygous)]. Of these, CDKN2A (p=0.03) and FOXO1 (p=0.02) mRNA significantly decreased with CN deletion (**Figure 11B**). Several genes within CNAs were validated using nCounter Cancer CN Assay (**Figure 11C**). CDKN2A loss was associated with poorer OS in PTCL-NOS (p=0.001) and in the PTCL-GATA3 subgroup (p=0.004) (**Figure 11B**). PTEN and TP53 loss and MYC and STAT3 gain demonstrated a trend of inferior OS in PTCL-NOS, but likely reflect the inferior survival of PTCL-GATA3 compared to PTCL-TBX21 since these CNAs are more common in PTCL-GATA3 (**Figure 12)**. We validated OS associations of CDKN2A in combination with an independent series[67] and observed similar survival trends (**Figure 11B**). Furthermore, low CDKN2A mRNA expression associated with poor OS in the series of PTCL-NOS (p=0.007) and a trend in PTCL-GATA3 (**Figure 11D**). Genes within aberrant loci were significantly enriched in biological processes involving splicing, ubiquitination and

signaling pathways (PI3K/mTOR, FAS and TCR). When mRNA expression of these genes was examined, expected changes in expression were observed.

PTCL-TBX21 had fewer CNAs and a less aberrant genome (8%), with 23% of cases having gains along the q-arms of chr1 and chr3. These loci included immune regulatory genes (CD244, CD247 and FASLG) at chr1q23 and cell cycle regulators (TP63 and TPRG1) at chr3q28 with significantly increased mRNA expression ($p<0.05$) in cases with a respective CN gain. Six cases (20%) had a gain encompassing BCL11B (14q32.2, **Figure 11E**), a negative regulator of GATA3 and the TH_2 expression program[83]. Five cases (17%) showed BCL6 gain at 3q27.3, but showed no change in mRNA expression. Recurrent losses were infrequent compared to PTCL-GATA3, but focal deletions were observed on chr6,-10,-16,-17 and -19. Chr6q was affected by deletions in both PTCL-GATA3 and PTCL-TBX21, however the deletions were more telomeric in PTCL-TBX21 (**Figure 11E**) and included newly identified TS (LATS1 and ZC3H12D) or TCR related genes (FYN and IBTK) and TNFAIP3 with concordant low mRNA expression associated with CN deletion. Chr10 deletion included the pro-apoptotic gene BNIP3, TH_2-related gene PRKCQ[84] and cell polarity-related gene PARD3. Genes within CNAs were enriched in cytotoxicity-mediating pathways and processes related to RNA splicing.

Since a cytotoxic CD8+ T-cell group[21,55] was predominantly enriched in PTCL-TBX21[21], we examined a CD8+ cytotoxic GEP signature[85] and corresponding CN data. We observed that cases with a high cytotoxic signature tended to be more aberrant (**Figure 13**).

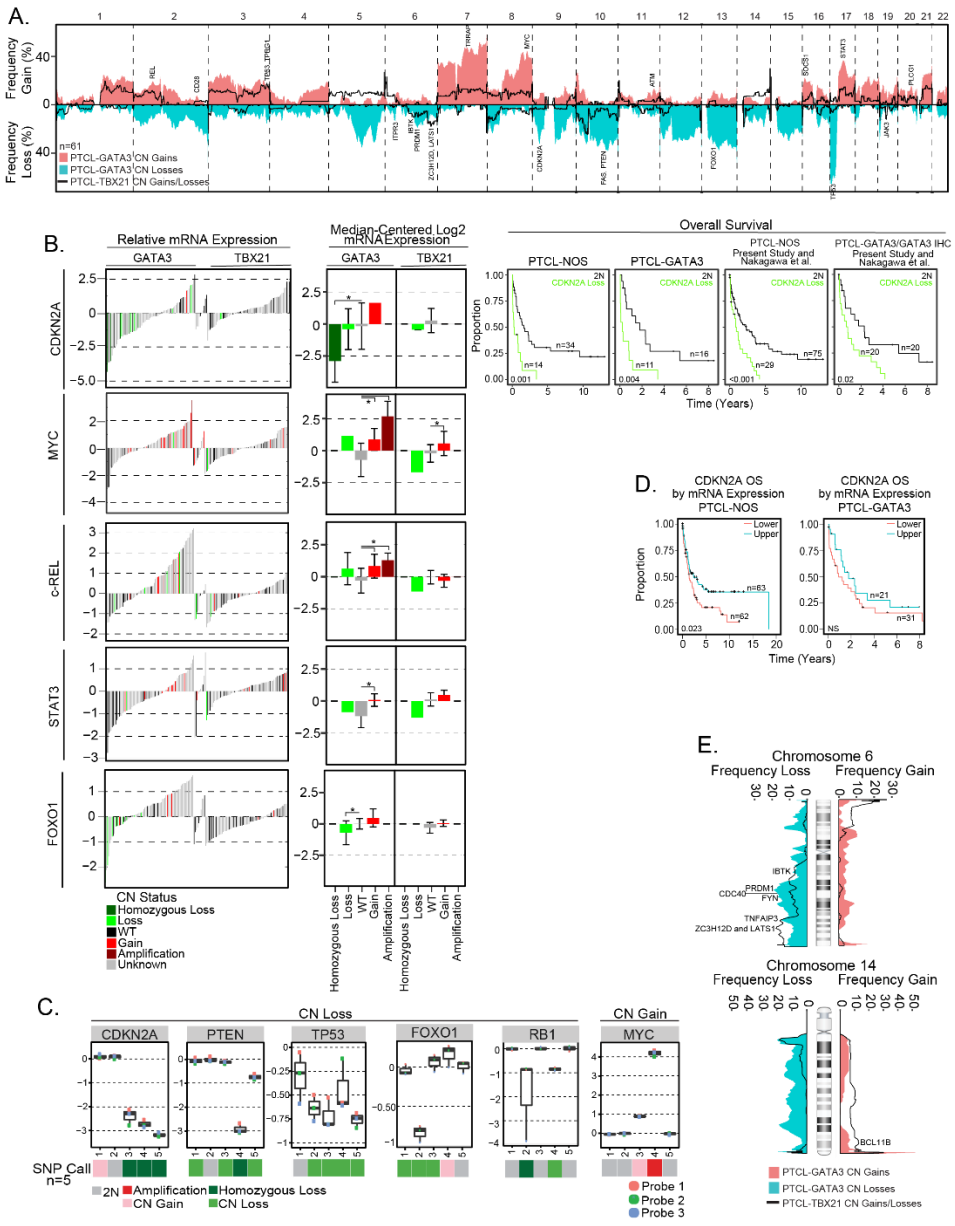

Figure 11: Copy number and expression analysis in molecular subgroups of peripheral T-cell lymphoma.

A. Frequency of chromosomal gains and losses found in PTCL-GATA3 and PTCL-TBX21 tumors. Candidate genes in focal regions are indicated. **B.** The relative mRNA expression (n=157, previously molecularly classified PTCL-NOS) and median-centered log2 mRNA expression (n=47, CN cases with Affymetrix HG-U133 Plus2 gene expression data) of select recurrently aberrant genes with differential gene expression relative to DNA CN status. In the relative mRNA expression plots (left panel), colored bars (except gray) indicate cases included in the present CN analysis. Kaplan-Meier curves comparing specific gene aberrations in the PTCL-NOS entity, PTCL-GATA3 subgroup and combined with a previously published PTCL-NOS series are included for *CDKN2A*, which tended to be associated with poor OS. **C.** Validation of genes within recurrent loci observed in the PTCL-GATA3 subgroup using the NanoString Cancer CNV assay. **D.** Kaplan-Meier curves comparing the upper vs lower halves of *CDKN2A* mRNA expression from all molecular PTCL-NOS cases with GEP and outcome data (n=125) from **B** (left panel) and only in PTCL-GATA3 (n=52; right panel). **E.** Frequency plots of chr6 and chr14 alterations, which have differential regions of abnormality in PTCL-GATA3 and PTCL-TBX21 subgroups. Candidate target genes within the regions are noted.

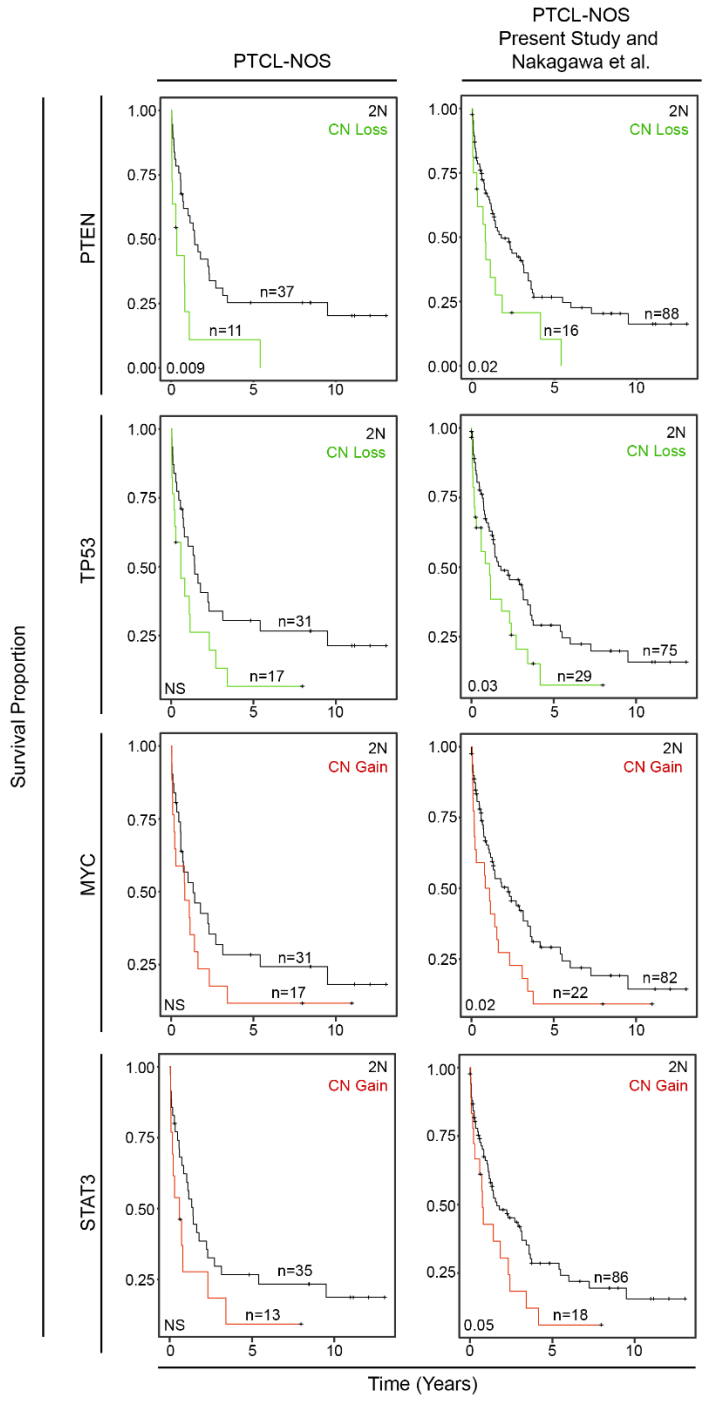

Figure 12: Overall survival associations in peripheral T-cell lymphoma-not otherwise specified.

Kaplan-Meier curves comparing OS between cases with or without PTEN loss, TP53 loss, MYC gain or STAT3 gain as indicated. The left column is comparing overall survival from the present PTCL-NOS cohort and the right column is comparing overall survival from the present PTCL-NOS cohort combined with a previously published PTCL-NOS cohort.

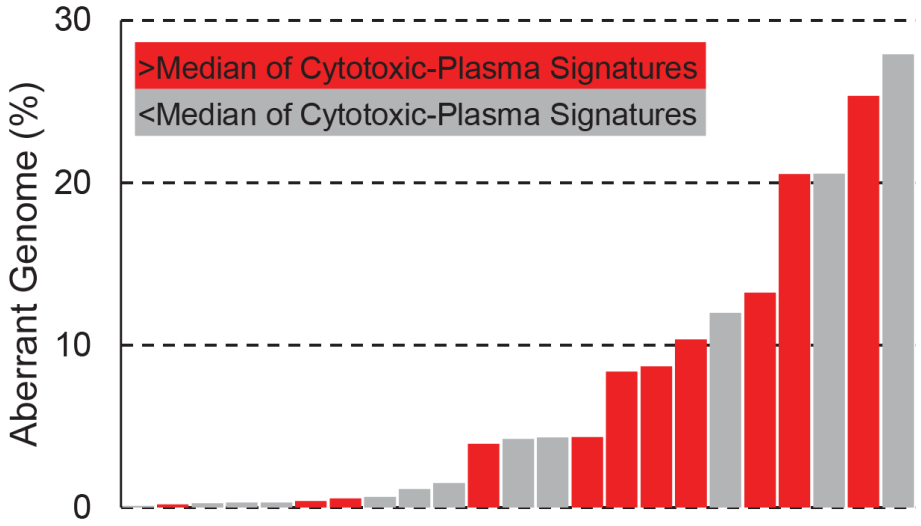

Figure 13: Percent aberrant genome distribution of PTCL-TBX21 cases with increased expression of a cytotoxic signature.

The cytotoxic signature was calculated by finding the difference between the $CD8^+$ cytotoxic and plasma cell signatures. Red indicates cases with a cytotoxic signature greater than the median and gray represents cases with a cytotoxic signature lower than the median.

Validation of subgroup specific CNAs and comparative analysis with other major PTCL entities

Since genomic profiles were distinct between PTCL-GATA3 and PTCL-TBX21, we examined whether CNAs could delineate these two subgroups. Using unsupervised HC of CNAs present in ≥10% of either PTCL-GATA3 or PTCL-TBX21, we observed two distinct clusters enriched in either PTCL-GATA3 or PTCL-TBX21 cases. Analysis of genomic CN profiles from two available PTCL-NOS cohorts[65,67] showed similar abnormalities with two major HC clusters of cases characterized by similar CNAs. Expression of CCR4 (GATA3 target gene) and CXCR3 (TBX21 target gene)[86] was available in one series[67] and was used as surrogate markers for the two subgroups, as GATA3/CCR4 and TBX21/CXCR3 showed a positive correlation at protein and mRNA levels (**Figure 14A/B**)[87]. The CCR4-positive group had a higher average aberrant genome compared to CXCR3/CCR3-positive cases, an observation concordant with PTCL-GATA3 versus PTCL-TBX21 (**Figure 14C**). Meta-analysis of all series (n=159) showed distinct clusters with comparable percent aberrant genome distributions and enrichment in either of the molecular subgroups with significant differences in CNAs (**Figure 14D**). This large cohort allowed for correlative association of CNAs. TP53 loss significantly (Fisher's exact test) co-occurred with losses of PTEN ($p<0.001$), PRDM1 (0.002) and CDKN2A ($p<0.001$), but had either no or a negative correlation with CNAs present in PTCL-TBX21 (**Figure 14E**).

We compared the AITL, PTCL-TBX21 and PTCL-GATA3 genomic profiles with other PTCL entities (**Figure 15A/B**), including ALCL[64], ATLL[68] and systemic CTCL[66]. PTCL-TBX21 has a low-complexity genome similar to AITL; whereas, PTCL-GATA3 showed a highly aberrant genome more comparable to ATLL and ALK^- ALCL (**Figure 15C**). Several CNAs were distinct among entities (**Figure 15D**). Co-occurring gains of chr5 and chr21 were unique to AITL. CDKN2A, PRDM1 and TP53 deletions were

comparable between PTCL-GATA3 and ATLL, but PTEN deletions were uncommon in ATLL[68]. Del-5q, del-9, del-12, del-13q, del-15q and chr7-gain were more frequently associated with PTCL-GATA3. PTCL-TBX21 had few CNAs, the most recurrent being del-10p and chr1q-gain the latter of which was also observed in ATLL, ALCL and PTCL-GATA3, but not in AITL or CTCL[64,66,68].

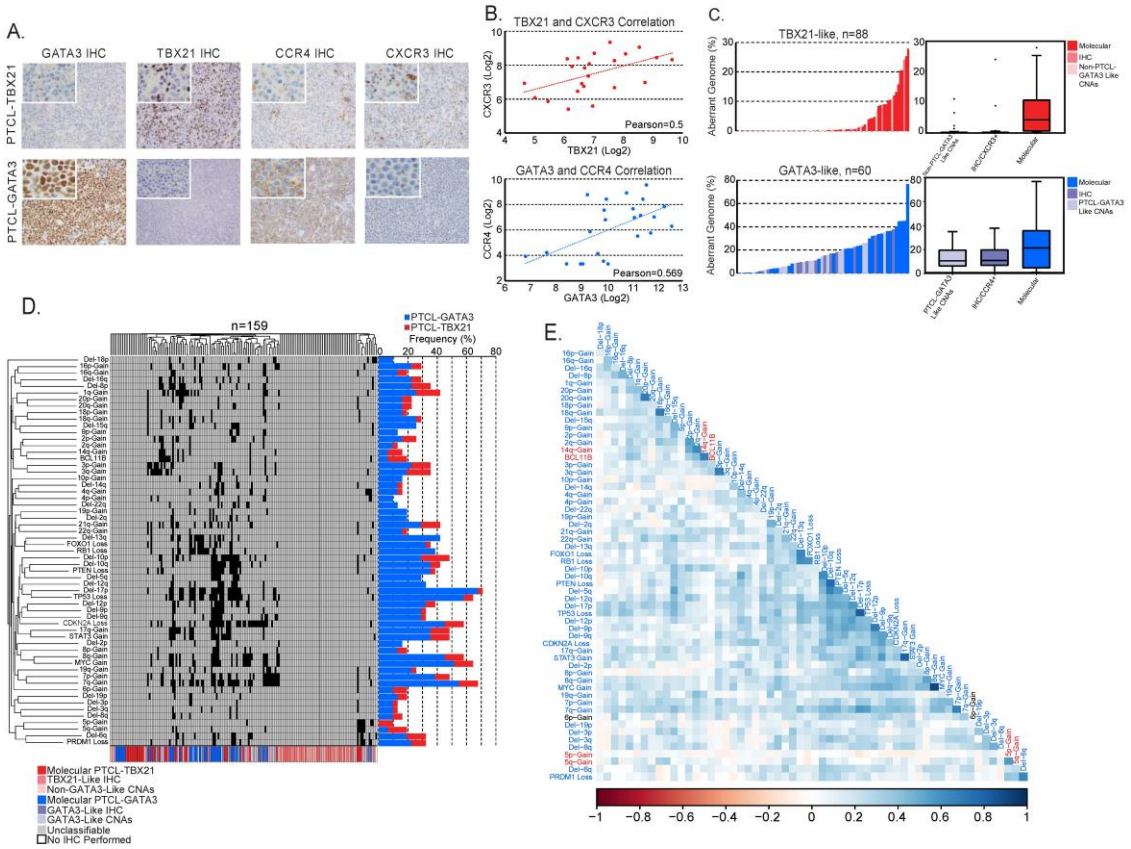

Figure 14: Unsupervised hierarchical clustering of copy number abnormalities in peripheral T-cell lymphoma.

A. IHC staining of GATA3, TBX21, CCR4 and CXCR3 in a molecularly classified case of PTCL-TBX21 (upper panels) or PTCL-GATA3 (lower panels). Original magnification of ×200 with an inset magnification of ×400. **B.** Positive correlation of TBX21 and CXCR3 mRNA expression in the PTCL-TBX21 subgroup (upper panel) and GATA3 and CCR4 mRNA expression in the PTCL-GATA3 subgroup (lower panel). **C.** Histograms (left panels) and boxplots (right panels) of the percent aberrant genome of PTCL-GATA3 and PTCL-TBX21 molecularly classified cases, along with PTCL-GATA3–like and PTCL-TBX21–like cases, from two published series. **D.** Unsupervised HC of three PTCL-NOS series by recurrent CNAs observed in the PTCL-GATA3 or PTCL-TBX21 molecular subgroups at a frequency ≥10%. The molecular PTCL-GATA3/GATA3–like cases (blue shades) dominate the central clusters, whereas the outside clusters, which tend to lack frequent CNAs, are predominately molecular PTCL-TBX21/TBX21–like cases (red shades). The frequency of these aberrations in the molecularly classified PTCL-NOS subgroups from the present study are depicted to the right of the cluster. **E.** Matrix of Pearson correlation coefficients for co-occurring CNAs. Abnormalities depicted in blue type are more frequent in PTCL-GATA3, whereas abnormalities depicted in red type are more frequent in PTCL-TBX21. The black type (6p-Gain) represents a CNA that was observed at near-equal frequencies in the two molecular subgroups.

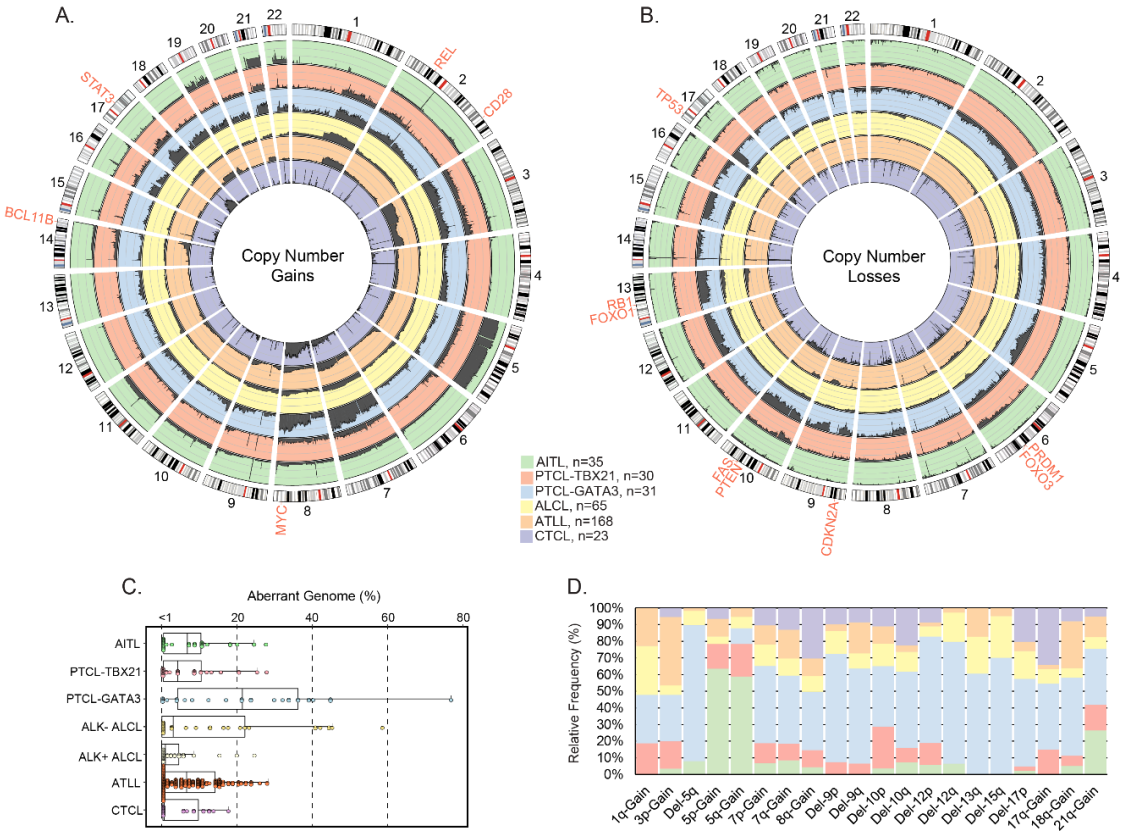

Figure 15: Comparison of copy number abnormalities found in peripheral T-cell lymphoma entities/subgroups.

Circos plots comparing the frequency of gains **(A.)** and losses **(B.)** found in PTCL entities/subgroups (AITL, PTCL-TBX21, PTCL-GATA3, ALCL, ATLL and CTCL). The dark gray shading denotes aberrant regions. The scale lines represent 20% increments. **C.** Boxplot of the aberrant genome in PTCL entities/subgroups. The dot plot overlay represents the aberrant genome of individual samples separated into 1% bins. **D.** Relative frequency distribution of CNAs presenting at a frequency ≥25% in ≥1 PTCL entity or subgroup.

Mutational analysis of PTCL subgroups

Mutation analysis of genes within aberrant loci was performed in 31 PTCL molecular-subgroup cases and five PTCL-T_{FH} cases (**Figure 16A**). Amplicon-sequencing data of four genes (CD28, DNMT3A, RHOA and TET2) from a previous study[88] was available in nine cases. 100% concordance in variant-calls was observed with the custom-capture platform, demonstrating adequate coverage and robustness in variant calling.

TP53 mutations were associated with PTCL-GATA3 (5/17) and co-occurred with CN loss (**Figure 16A**); thus, aberrant TP53 signaling due to mutation and CN deletion was significantly associated with PTCL-GATA3 (Fisher's exact test, $p<0.001$). TP53 mutations occurred in the DNA binding and tetramerization domains, including the hotspot $TP53^{R175H}$ (n=2) (**Figure 16B**). These aberrations did not show association with mRNA expression. Other DNA repair or TP53 signaling genes (ATM and TRRAP) were mutated in both subgroups. PRDM1 mutations identified in the PTCL-GATA3 subgroup co-occurred with CN deletion. Despite recurrent deletions in other TS (FOXO1 and PTEN), mutations were infrequent or absent, and expectedly no mutation in CDKN2A was observed due to bi-allelic deletions. Other genes with CNAs were involved in JAK-STAT (SOCS1 and JAK3), PI3K-AKT (ITPR3 and ITPKB) and T-cell activation (PLCG1, PTPRC, FYN and VAV1) and were mutated with no significant difference between the subgroups (**Figure 16A**).

Mutations in the DNA methylation regulator TET2 were observed at near equal frequencies in PTCL-GATA3 (4/17) and PTCL-TBX21 (3/11), but TET1, TET3 and DNMT3A mutations were enriched in PTCL-TBX21 (4/11 versus 2/17). Histone-methyltransferases showed a similar mutation frequency (**Figure 16A**). An uncommon $IDH2^{R172W}$ variant was observed in one PTCL-TBX21 case, which harbored a $RHOA^{G17V}$

and a DNMT3A mutation, but lacked a PTCL-T_{FH} immunophenotype upon IHC examination. Interestingly, DNMT3A mutations in PTCL-TBX21 were restricted to the MTase motif of the catalytic domain and affected DNMT3A^{R882} (2/2), which was also observed in our larger cohort[88] in contrast to AITL, where only 1/22 cases showed DNMT3A^{R882} mutation (**Figure 16C**). PTCL-T_{FH} cases showed a mutation profile closer to AITL cases[33,89], but without *IDH2* mutation. A mutation of TET3 co-occurring with TET2 and BCL11B gain was present in one case; however, too few cases were studied for a definitive assessment (**Figure 16A**).

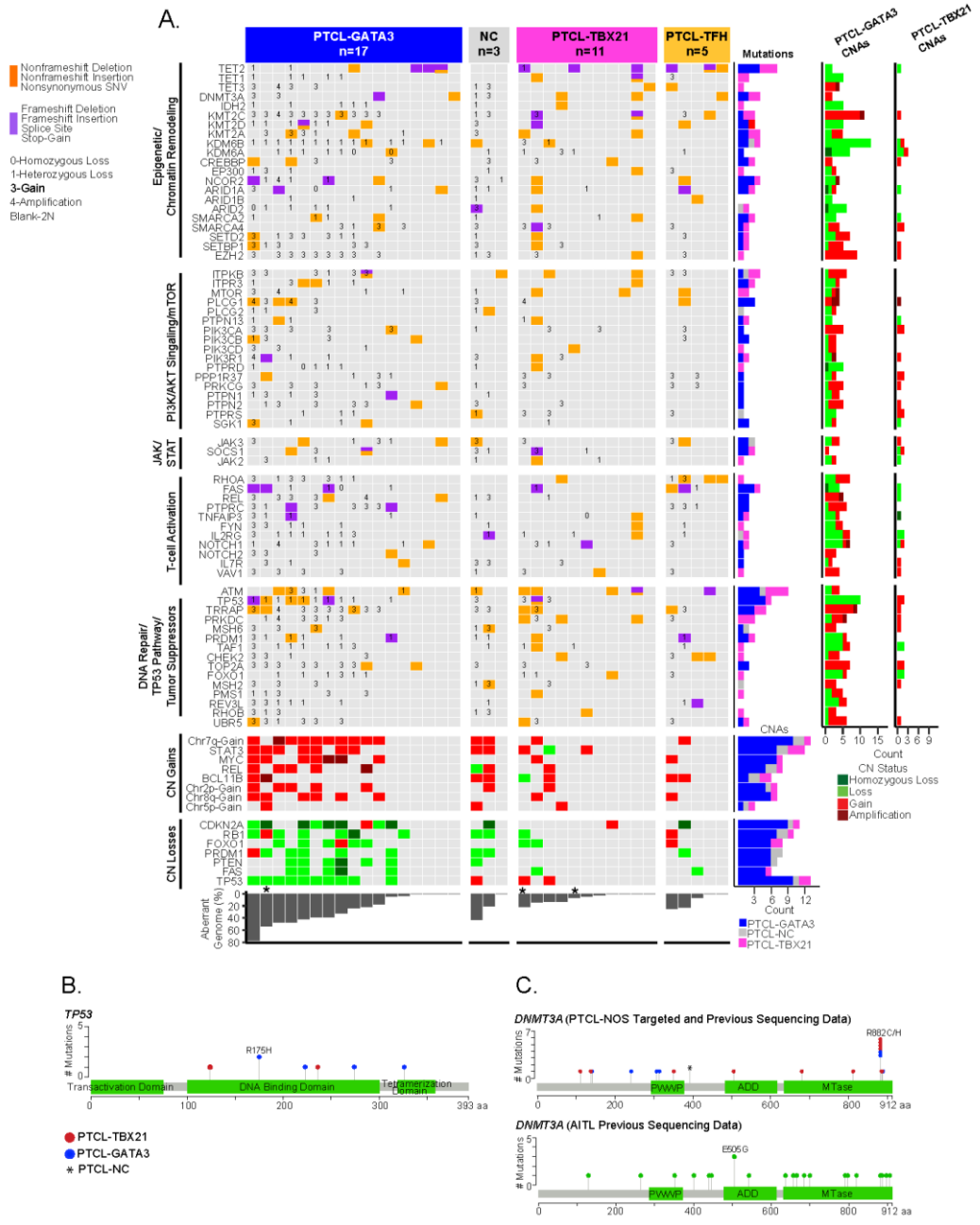

Figure 16: Select copy number abnormalities or genes found to be recurrently mutated in molecular peripheral T-cell lymphoma subgroups.

A. The block color represents the type of mutation. Blocks with two colors indicate that >1 type of mutation was observed in the case. CN status of the mutated genes are noted (3=copy gain, 4=amplification, 1=copy loss, 0=homozygous copy loss). The bar graphs to the right of the plot indicate the number of cases with the denoted mutation or CNA. The total percent aberrant genome is indicated below the plot. *Denotes three cases that were only included for mutation analysis and CN status was determined by CopywriteR. Schematic diagrams of the location of coding mutations identified in TP53 **(B.)** and DNMT3A **(C.)**. The DNMT3A schematic diagram combines targeted sequencing results from this study with previous amplicon sequencing data. The figures were generated using MutationMapper. Mtase=methyltransferase.

2.4 DISCUSSION

Comprehensive genetic characterization of AITL and newly defined PTCL-NOS molecular subgroups validated their distinct genetic evolution and identified potential therapeutic targets. Though, we used well characterized cases supported by GEP and pathology review, there is still the possibility that the frequency of aberrations of some of the molecular entities may be underestimated due to low tumor content cases, which is commonly observed in many PTCLs. However, major CNAs in AITL were consistent with previous cytogenetic and aCGH studies[62,90,91]. However, integrative analysis with GEP revealed that genetic changes targeted oncogenic pathways not previously identified[90-93]. Comparative analysis with other major WHO-defined PTCL entities showed that AITL harbors a minimally aberrant genome. Chr5-gain (43%) co-occurring with chr21-gain and $IDH2^{R172}$ mutation were specifically associated with AITL. Contrary to previous studies[90,91], trisomy-3 was infrequent (1/35). This discrepancy in chr3-gain was noted in an earlier cytogenetic study (interphase 78% versus metaphase 41%)[94] and was also not observed in a recent aCGH study[62] although it is possible that trisomy-3 may be present in sub-clones and not detected by hybridization-based platforms[93]. Chr13q22 loss was observed in 14% (5/35), in agreement with previous findings[93], and may target SLAIN1 (13q22.3), involved in microtubule re-organization. Chr5-gain significantly co-occurred with chr21-gain, but the cooperative roles of these abnormalities are challenging to decipher, as they harbor epigenetic mutations and pleiotropic effects due to $IDH2^{R172}$ mutation induced increased 2-hydroxyglutarate (2-HG). 2-HG inhibits α-KG-dependent dioxygenases (histone-demethylases and the TET family of 5mC hydroxylases)[95] and can also promote the Warburg effect by directly competing with α-KG in the Krebs cycle, thus altering the epigenetic and metabolic programs in T-cells. IDH2 mutation is associated with a more pronounced T_{FH}-signature and T-cell activation

via epigenetic modification[88] and tends to have a more aberrant genome compared to WT cases, possibly due to an inhibitory effect of 2-HG on DNA repair enzymes[96]. In contrast, $IDH2^{WT}$ cases showed significant enrichment of PI3K-AKT activation pathways, and had focal losses of negative regulators (phosphatases) of the PI3K-AKT pathway. Thus, constitutive activation of the PI3K-AKT pathway or impairment of the DNA repair pathway and disturbed metabolic pathways may be unique vulnerabilities that can be exploited in AITL depending on the mutational status of IDH2. WT cells may show a more sensitive response to PI3K-mTOR inhibitors, whereas IDH2-mutant cells may be particularly sensitive to alkylating agents[96] and PARP inhibitors may have synergistic effects.

According to the recent WHO classification of lymphoid tumors[17], PTCL-T_{FH} is now included as a provisional entity of T-cell lymphoid neoplasms. In concordance with a previous study[62], we observed differences in the CN profiles of PTCL-T_{FH} and AITL, specifically chr5-gain is infrequent in PTCL-T_{FH} while loss of chr6q and chr1q-gain is more common. The mutation profile of PTCL-T_{FH} identified mutations in TET2, DNMT3A and RHOA, which are also common in AITL; however, we did not observe $IDH2^{R172}$ mutations consistent with previous reports[33,97]. Although the number of PTCL-T_{FH} cases studied to date is small, the data suggests that PTCL-T_{FH} may be a genetically distinct entity from AITL.

We provided evidence that novel molecular subgroups[21] evolve by distinct genetic pathways and are characterized by distinct genomic complexity. By GEP, PTCL-GATA3 represents a subgroup distinct from PTCL-TBX21, which may contain a non-cytotoxic and a cytotoxic subgroup characterized by CD8+ T-cells[21]. CNAs support the GEP classification, as PTCL-GATA3 showed high genomic complexity with frequent CNAs of well-known TS and oncogenes, some with functional consequences observed at the mRNA level and inferior survival, which is in agreement with earlier studies[21,60]. A

recent paper demonstrated that PTCL-NOS cases classified as GATA3-expressing on a different platform trended towards poorer overall survival[98]. In contrast, PTCL-TBX21 had low genomic complexity and did not show prominent TS deletions and mutations. *TP53* signaling was a primary target in more than 50% of PTCL-GATA3 cases by bi-allelic deletion/mutation of TP53, CDKN2A/2B ($p14^{ARF}$/$p16^{INK4A}$) or RB1. $P14^{ARF}$ is a negative regulator of TP53 signaling and $p16^{INK4A}$ regulates the RB-mediated G_1 checkpoint. CDKN2A showed prognostic significance in PTCL-GATA3, but validation with additional cases is required. PRDM1, important in the homeostatic control of T-cell activation and proliferation, is likely the driver of del-6q21. PRDM1 loss may promote the development of PTCL-GATA3. Remarkably, del-5q was exclusive to PTCL-GATA3; whereas chr5-gain and a focal 14q32-gain encompassing BCL11B were noted more frequently in PTCL-TBX21. BCL11B is critical in T-cell differentiation at the DN3/4 stage by preventing differentiation of early T-cells into NK-cells and other innate immune cell lineages in part by repressing GATA*3* expression[83]. However, its role in the lymphomagenesis of PTCL-TBX21 is unclear. Genes regulating NF-κB signaling (ZC3H12DC/p34[99] and TNFAIP3) and TS kinase (LATS1) were more frequently lost in PTCL-TBX21. Genomic losses observed in PTCL-TBX21 targeted genes associated with cell-mediated cytotoxicity and cellular processes involving metabolic reprogramming[100]. A meta-analysis of two additional PTCL-NOS cohorts[65,67] demonstrated that subgroup associated CNA profiles can be validated and delineated independently, evident by the clustering of percent aberrant genome, specific CNA association with clinical outcome data and/or expression of GATA3 and TBX21 target genes (CCR4 and CXCR3*,* respectively). Although many of the CNAs are significantly associated with a specific subgroup as shown in **Figure 15**, with the exception of TP53 loss (~50%), the majority of these CNAs do not exceed 25-30% and thus may not be

usable per se as molecular subgroup classifiers, but rather may aid in the molecular diagnosis in challenging PTCL-NOS cases.

Although MYC-CDKN2A-TP53 signaling axis deregulation is often observed in NHLs, co-occurrence of impaired TP53 signaling and PTEN loss is uncommon in neoplasms, as studies have shown functional interdependence and mutations are often mutually exclusive[101]. TP53 directly regulates PTEN mRNA expression[102] and PTEN stabilizes TP53 by inhibiting MDM2 translocation to the nucleus[103] and can directly bind and stabilize TP53 in the nucleus[104]. TP53 and PTEN co-deletions are significantly associated with PTCL-GATA3 but not PTCL-TBX21 or other T-NHLs. Thus, their cooperative role in T-cell lymphomagenesis warrants further investigation. We noted mutual exclusivity of TP53 loss and TET1/2/3 mutations, suggesting that epigenetic alterations due to TET deficiency and TP53 functional impairment may lead to distinct clonal evolution.

Recently, Horwitz *et al* showed clinical efficacy of a PI3K-δ,γ inhibitor (duvelisib) in a phase I trial of PTCL-NOS patients[105]. Because the promising response in this clinical trial and pre-clinical models[105], it would be essential to precisely classify PTCL cases and their genomic abnormalities for correlative studies for future multi-institutional clinical trials. Many of the CNAs (deletions of PTEN, STK11 and TSC2 and/or MYC amplification) likely converge to constitutively activate PI3K-AKT-mTOR signaling[80]. The mTOR pathway is critical for the integration of costimulatory, cytokine, environmental and metabolic cues necessary for T-cell differentiation[106], T-helper cell polarization[107] and proliferation[108]. TP53 negatively regulates mTOR pathways via PTEN-AKT and the TSC2-AMPK β1 axis[109]. Though preliminary, we observed that mTOR signaling pathways can be a promising target for therapeutic intervention using a number of T-cell lines (**Figure 17**). Since these T-cell lines are not derived from AITL or PTCL-

GATA3/TBX21, the findings will need to be validated and more specifically defined using authentic PTCL cell lines or xenograft models when available.

In summary, the complexity of PTCL can be addressed with greater clarity with the integration of global genomic analyses. This study provides further evidence of the existence of the two separate subgroups (PTCL-GATA3 and PTCL-TBX21) previously identified[21] within the PTCL-NOS group, and it has identified genetic features that are distinct between the two. AITL cases showed a CN profile different from these two subgroups and the IDH2-mutated group exhibited unique features, which may indicate exploitable therapeutic vulnerabilities.

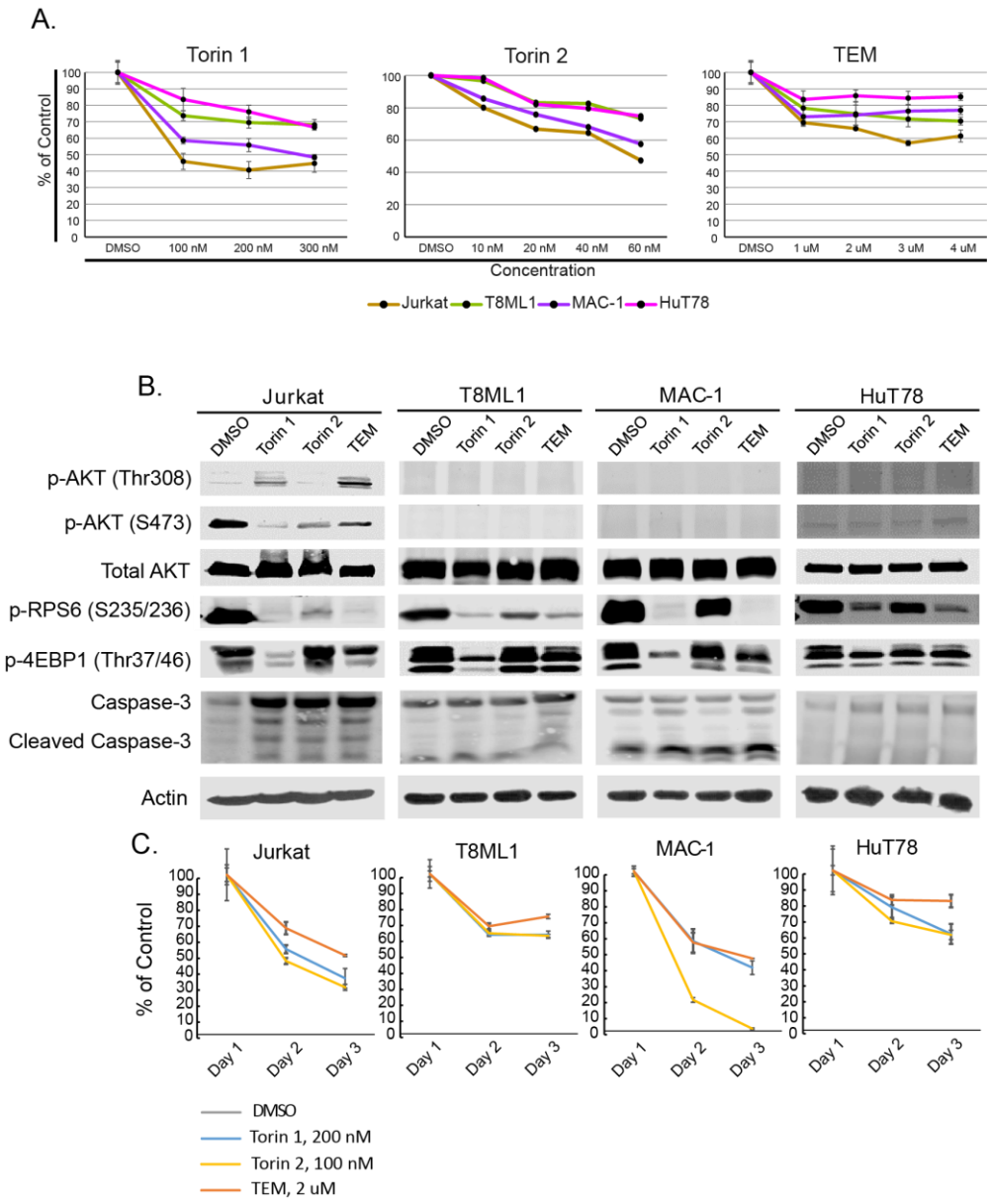

Figure 17: mTOR inhibition in T-cell lines.

A. Drug dose response curve for four T-cell lines (Jurkat, T8ML1, MAC-1, and HuT78) following 24 hours of mTOR inhibitor treatment at the indicated concentrations. **B.** Western blots of Jurkat, T8ML1, MAC-1 and HuT78 cells after treatment with control (DMSO), Torin 1 (200 nM), Torin 2 (100 nM), or TEM (2 μM) for 48 hours. The inhibitors target core components of mTOR signaling and resulted in reduced phosphorylation of rapamycin-sensitive (RPS6S235) and insensitive (4EBP1T37/46) substrates of mTORC1 and mTORC2. A complex effect on AKT phosphorylation was observed in Jurkat with inhibition of AKTS473 phosphorylation, but increased AKTThr308 phosphorylation, an effect observed with TEM and Torin1, but not with dual inhibitor Torin2. Increased cleavage of Caspase-3 upon drug treatment was prominent in Jurkat cells, indicating activation of the apoptotic pathway. **C.** PrestoBlue proliferation assay of Jurkat, T8ML1, MAC-1 and HuT78 after treatment with DMSO, Torin 1, Torin 2, or TEM at the doses depicted in the legend. Values were normalized to the control (DMSO). Jurkat cells were more sensitive to Torin1/2 compared to TEM, whereas MAC-1 was most sensitive to Torin2; T8ML1 and HuT78 were >50% viable at 48 hours. Cell lines were less sensitive to the FDA-approved mTOR inhibitor TEM, even at 2μM. Data presented represents one representative experiment of three independent experiments.

CHAPTER 3: LONG-TERM DEFICIENCY OF TET2 IN CD4$^+$ T-CELLS PROMOTES T-CELL LYMPHOMA WITH A T_{FH} CELL IMMUNOPHENOTYPE

3.1 INTRODUCTION

AITL is the most common PTCL entity in North America and Europe, where it accounts for up to 35% of non-cutaneous PTCLs. AITL is defined as a neoplasm of mature T_{FH} cells characterized by prominent proliferation of vessels and follicular dendritic cells in affected LNs[18,23,110]. AITL exhibits an aggressive clinical course, and unfortunately no major improvement in patient outcome has been achieved over the last three decades[54]. We have performed genome-wide GEP, high-resolution DNA CN analysis and NGS, thus defining robust biological molecular classifiers reflecting cellular-origin, prognosis and dysregulated oncogenic pathways in AITL[21,24,34,111]. We and others identified frequent mutations in genes that regulate the epigenome (TET2, DNMT3A and IDH2) and in genes encoding proximal TCR signaling molecules and key intracellular effectors[32,34,62]. Further, we identified CNAs targeting the PI3K/AKT/mTOR pathway[111]. Taken together, these genomic analyses suggest two major cooperative oncogenic mechanisms in AITL, initial epigenomic dysregulation in CD4$^+$ T-cells, followed by aberrant activation of TCR signaling.

TET2 mutations are present in >70% of AITL cases[32,34-36,112], unlike other TET members (TET1 or TET3), which are either infrequent or not mutated in AITL, but are more commonly observed in AML and acute lymphocytic leukemia (ALL). These findings suggest that the three TETs have non-overlapping activities and loss of the TET2 enzyme is particularly critical for T_{FH}-derived tumors. TET2 is an α-KG dependent enzyme that catalyzes the oxidation of 5-mC to 5-hmC as the first oxidative step toward cytosine demethylation[113]. Therefore, loss of TET2 leads to aberrant hypermethylation of the genome, but how the epigenetic alterations predispose the T-cells to neoplastic transformation is not clear.

AITL is a challenging disease to investigate due to the absence of cell lines or genetically faithful animal models, which has greatly impacted pre-clinical investigations of novel therapeutic interventions for these patients. Despite TET2 being the most recurrent mutation in AITL, little has been done to explore the role of TET2 in a more mature T-cell lymphoma model. Several previous models evaluated the result of TET2 loss at earlier stages, such as in the hematopoietic stem cells, often resulting in an array of diseases mostly effecting the myeloid lineages, and less frequently T and B-cell lineages[38,114-117]. The early loss of TET2 resulted in increased stem cell self-renewal, mutagenicity and competitive advantage, with the small proportion of mice that did develop a T-cell lymphoma having increased T_{FH} populations and marked splenomegaly. These earlier studies suggested that TET2 deficiency alone may not be sufficient to generate a lymphoma; therefore, others have generated murine models with additional alterations including DNMT3A^{R882H} and RHOA^{G17V}[40,41,118,119]. When TET2 loss was combined with RHOA^{G17V}, an AITL-like disease was achieved with increased expression of PI3K/MAPK and mTOR signaling[40,41] and dysregulated Foxo1 expression[41,119]. The DNMT3A^{R882H} model was combined with an early loss of TET2, but only achieved an AITL-like disease following serial transplantations, as the primary recipients more commonly developed AML and ATLL[118]. More recently, loss of TET2 was investigated in development of B-cell lymphoma and the GC reaction[38]. Loss of TET2 resulted in GC hyperplasia, impaired class switch recombination and inhibited plasma cell differentiation by interfering with B-cell transit through the GC[38]. Therefore, we generated a conditional knockout model of Tet2 loss in CD4^{+} T-cells (Tet2$^{-/-}$) and demonstrated development of T-cell tumors with a T_{FH} phenotype. We also performed system analyses of Tet2-deficiency in T-cells and identified oncogenic pathways mediated by loss of Tet2.

3.2 MATERIALS AND METHODS

Generation of Murine Model

The transgenic $Tet2^{Flox/Flox}$ mouse[114] was kindly provided by Dr. Ross Levine, and the transgenic CD4-Cre mouse was purchased from Jackson Laboratory (#017336). The $Tet2^{Flox/Flox}$ mouse harbors alleles with loxP sites on either side of Tet2 exon 3. The crossed progeny were on a mixed C57BL/6 x 129 background and referred to hereafter as $Tet2^{-/-}$, resulted in Cre-mediated deletion of the third exon of Tet2 in $CD4^{+}$ T-cells, leading to the nonsense-mediated decay of Tet2. Where indicated, mice were injected intraperitoneal with $2X10^{8}$ sheep red blood cells (SRBCs, Rockland R405-0050) in 200 µL of phosphate-buffered saline (PBS) to induce a GC reaction. Control recipient mice received intraperitoneal injections of 200 µL of PBS alone.

All animals were housed at the University of Nebraska Medical Center or City of Hope National Medical Center. All animal procedures were conducted in accordance with the Guidelines for the Care and Use of Laboratory Animals and were approved by the Institutional Animal Care and Use Committees at the University of Nebraska Medical Center and City of Hope National Medical Center.

Genotyping and Rearrangement Confirmation

The Mouse Direct PCR Kit (B4001) was used for rapid tissue digestion (30 minutes) followed by standard PCR amplification with supplied reagents for murine genotyping. Cell-specific rearrangement of Tet2 was also confirmed by standard PCR. The primers used to detect the Tet2 and CD4-Cre and corresponding thermal cycler programs are detailed below:

Tet2:

LoxP3R Rearrangement: 5’-TAGAGGGAGGGGGCATAAGT-3’

Flox Forward: 5'-AAGAATTGCTACAGGCCTGC-3'

Flox Reverse: 5'-TTCTTTAGCCCTTGCTGAGC-3'

Genotyping: 95°-5 minutes; 40 cycles of 95°-30 seconds → 64°-30 seconds → 72°-1 minute; 72°-5 minutes; 4°-hold

Rearrangement: 95°-5 minutes; 30 cycles of 95°-30 seconds → 55°-30 seconds → 72°-30 seconds; 72°-2 minutes; 12°-hold

CD4-Cre:

Forward: 5'-GCGGTCTGGCAGTAAAAACTATC-3'

Reverse: 5'-GTGAAACAGCATTGCTGTCACTT-3'

94°-3 minutes; 35 cycles of 94°-30 seconds → 51.7°-1 minute → 72°-1 minute; 72°-2 minutes; 10°-hold

$CD4^+$ T-cell Isolation and Cell Culture Technique

Spleens were dissected from $Tet2^{-/-}$ or WT mice and made into single-cell suspensions. $CD4^+$ T-cells were isolated from the total splenocytes using the negative selection EasySep™ Mouse $CD4^+$ T Cell Isolation Kit (Stemcell Technologies). $CD4^+$ T-cells were maintained in culture at 1,000,000 cells/mL in RPMI 1640 containing glutamine, 20% FBS, 1% penicillin streptomycin, 1x 2-mercaptoethanol, 20 nG/mL recombinant mouse IL-2 and 25 µL/mL Dynabeads Mouse T-Activator CD3/CD28.

Cellular Proliferation Assays

Cellular proliferation assays were performed using the PrestoBlue™ Cell Viability Reagent (Invitrogen-A13261) per manufacturer's protocol. For our assays, 4 µL of the PrestoBlue reagent was incubated with 36 µL of cells in a 96-well plate for 1 hour and then read on a Tecan Infinite M200Pro.

Cellular Apoptosis

The percentage of apoptosis was calculated using an ACEA NovoCyte flow cytometer after dual Annexin-V and 7-AAD staining per manufacturer's instruction using 100,000 cells (BD Biosciences).

Flow Cytometry

Flow cytometry data was acquired on an ACEA NovoCyte flow cytometer. Subsequent data analysis was performed with NovoExpress software and standard flow gating of forward and side-scatter to ensure only single cells were evaluated. A list of antibodies used is included in **Table 4**.

$CD4^+$ T-cells were stained with a T-cell panel to determine isolation purity. The panel consisted of CD3 molecular complex, CD4 and CD8a. This panel was also completed on single-cell splenocyte suspensions. Splenocytes were stained for major lymphoid populations including again the CD3 molecular complex (T-cell), CD45R/B220 (B-cell) and CD335 (NK cell). A third panel consisting of GR-1 and CD11B (MAC-1) was performed to identify monocytes, neutrophils, eosinophils and granulocytes. CD69 was used to detect T-cell activation. A Ghost Dye viability stain was included in the staining protocol to distinguish dead versus alive cells. All of these panels only require extracellular staining and those the same protocol was followed. In brief, 200,000 cells per panel were re-suspended in staining buffer (1x PBS + 0.5% BSA + 2mM EDTA). Cells were incubated with the primary antibodies for 30 minutes at 4° followed by two washes before analysis.

The T_{FH} staining protocol including CD4, PD1 and CXCR5 required a 3-step staining protocol for CXCR5. First, 200,000 cells were re-suspended in staining buffer in the presence of mouse Fc block at a 1:200 dilution for 30 minutes at 4°. The cells were then washed and incubated with CXCR5 for 30 minutes at 4°. Following a wash, the

cells were incubated with biotin-labeled IgG for 30 minutes at 4°. Another wash was performed and the cells were incubated with APC-labeled streptavidin and antibodies for CD4 and PD1 for 30 minutes at 4°. Following two washes, the cells were analyzed. Examples of the gating strategies used are included in **Figure 18 A-D**.

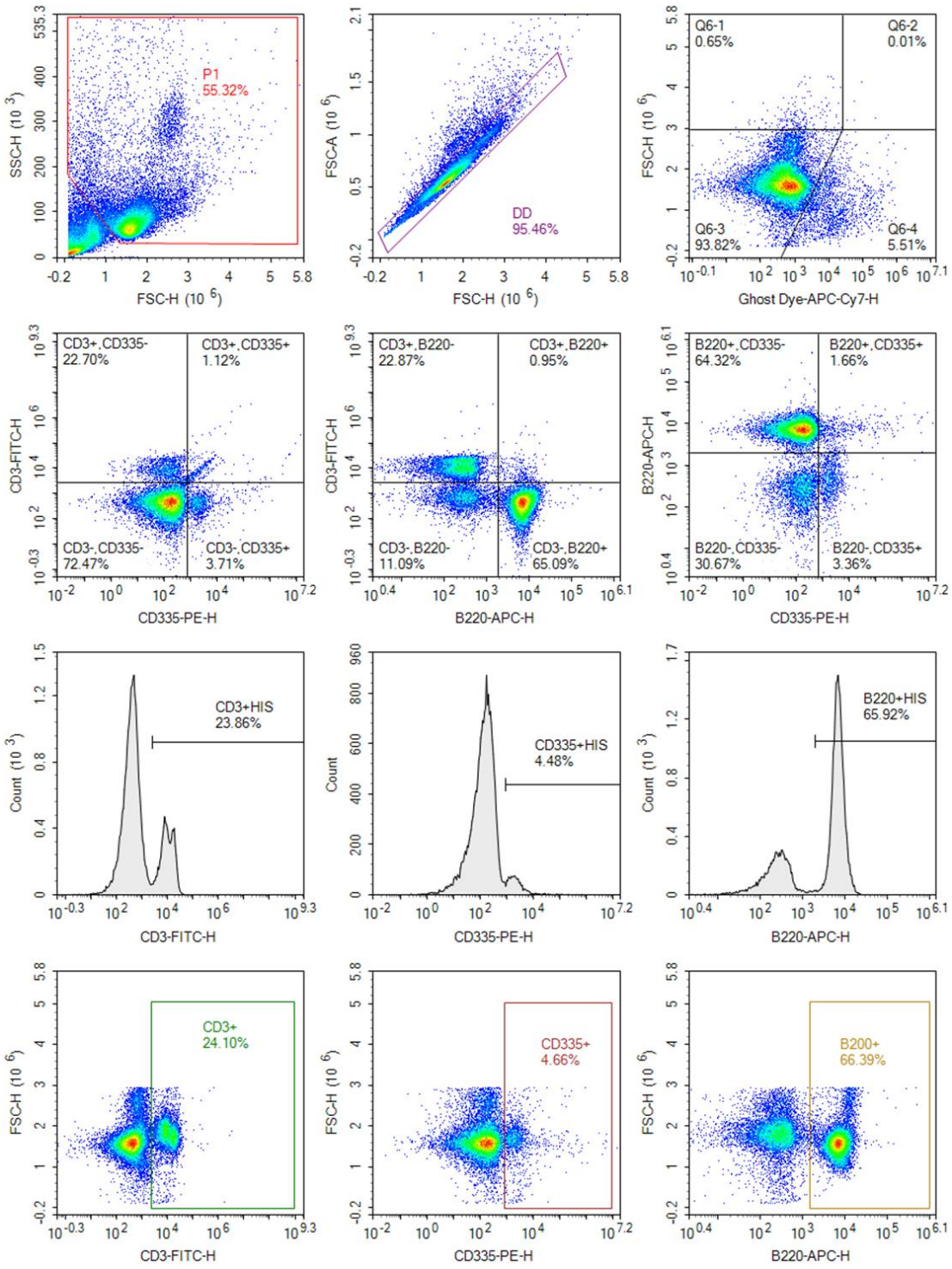

Figure 18: Flow cytometry gating strategy.

A. Gating strategy for the T (CD3-FITC), NK (CD335-PE) and B (B220-APC) cell panel. Ghost Dye was used as a viability marker.

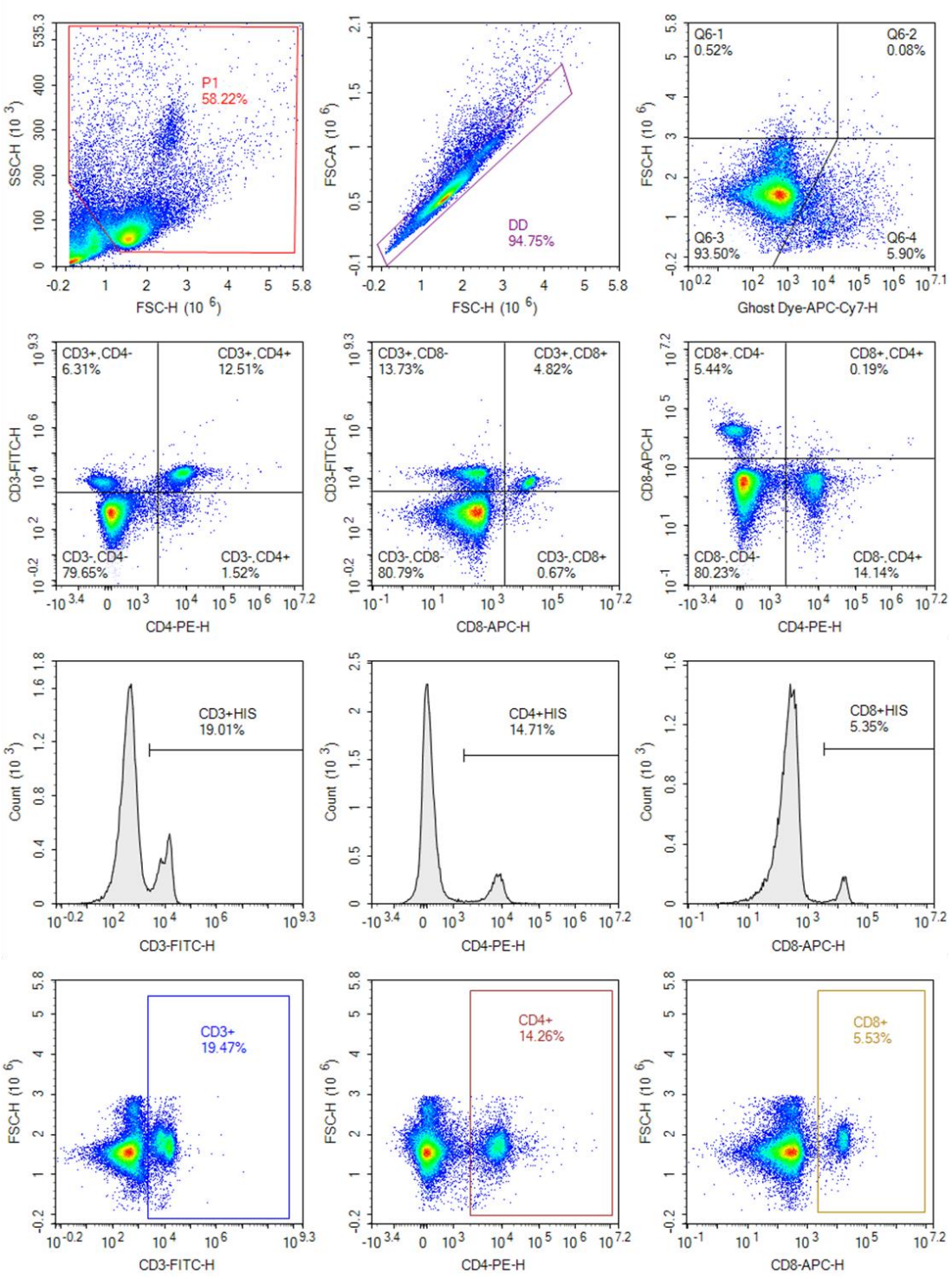

B. Gating strategy for the major T-cell subsets (CD3-FITC, CD4-PE and CD8-APC). Ghost Dye was used as a viability marker.

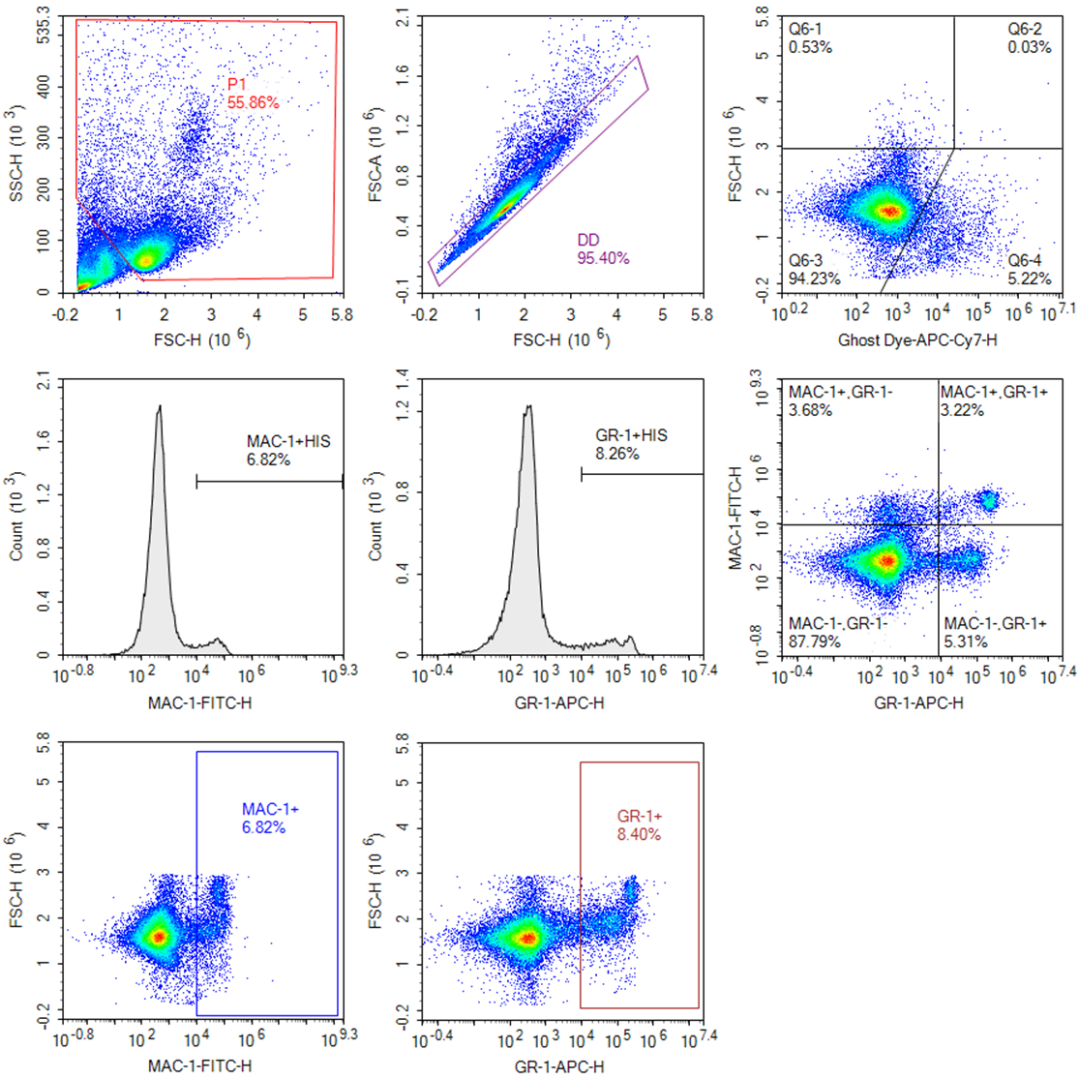

C. Gating strategy for the myeloid MAC-1 (FITC) and GR-1 (APC) cells. Ghost Dye was used as a viability marker.

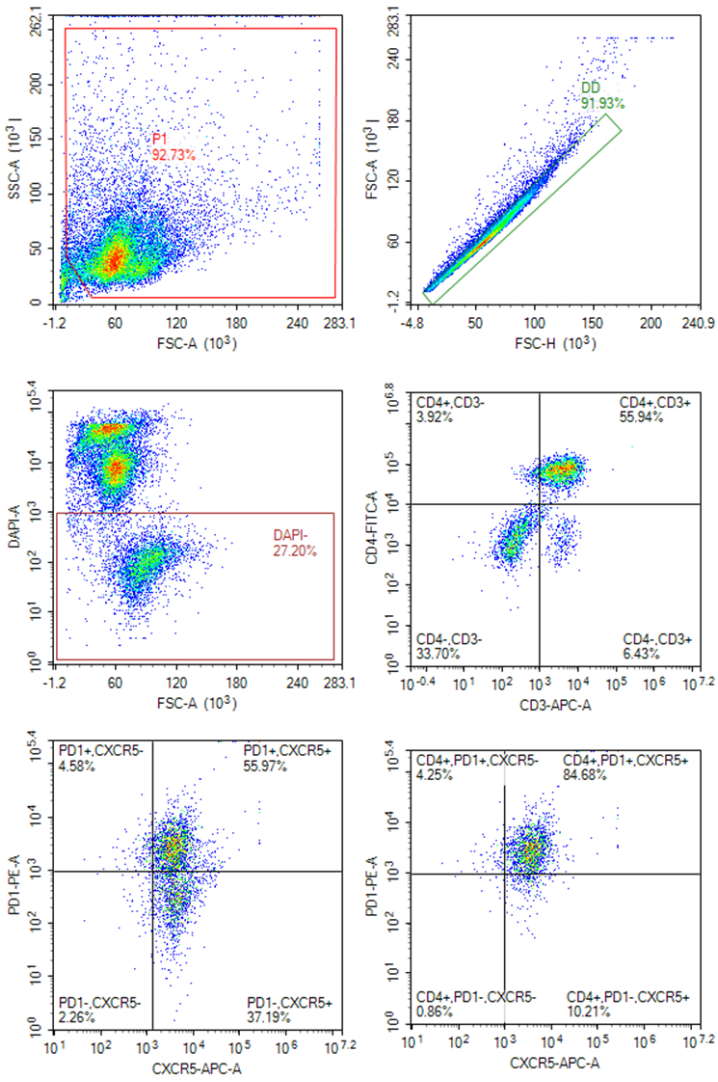

D. Gating strategy for the TFH cell panel (CD4-FITC, PD1-PE and CXCR5-APC). DAPI was used as a viability marker.

Marker	Clone	Source	Catalog
CD3 Molecular Complex	17A2	BD	561798
CD45R	RA3-6B2	BD	553092
CD335	29A1.4	BD	560757
CD4	GK1.5	BD	557308
CD8a	53-6.7	BD	553035
GR-1	RB6-8C5	Biolegend	108412
CD11B	M1/70	Biolegend	101205
CD279	J43	eBioscience	12-9985
CXCR5	2G8	BD	551961
Goat Anti-Rat IgG (H+L)	Polyclonal	Jackson Immuno Research Labs	112-065-062
APC Streptavidin	NA	BD	554067
CD69	H1.2F3	BD	553236

Table 4: Flow cytometry antibodies for detection of murine cells.

Histopathology and Immunohistochemistry

Mouse tissues were harvested and fixed in 10% buffered formalin for 24 hours prior to being paraffin-embedded in the Tissue Science Facility at the University of Nebraska Medical Center. Tissue sections underwent H&E staining using standard procedures. IHC was performed on tissue sections with antibodies targeting CD3, CD4, CD8, CD19 and Ki-67 in the Tissue Science Facility at the University of Nebraska Medical Center or CD20 at the City of Hope National Medical Center. A detailed list of antibodies is included in **Table 5**. Ki-67 staining was analyzed using the pathology softare QuPath (https://qupath.github.io/).

Marker	Source	Catalog	Dilution
CD3e (SP7)	Invitrogen	MA1-90582	1:100
CD4 (EPR19514)	Abcam	ab183685	1:800
CD8a (4SM15)	eBioscience	14-0808-80	1:100
CD19 (D4V4B)	Cell Signaling Technologies	90176	1:800
Ki-67 (SP6)	Abcam	ab16667	NA
CD20 (SP32)	Abcam	ab64088	NA

Table 5: Murine immunohistochemistry antibodies.

RNA and DNA Extraction

Total DNA and RNA was isolated and purified using the AllPrep DNA/RNA Kit (QIAGEN) per manufacturer's protocol and eluted in nuclease-free water. The concentrations of total DNA and RNA were determined by Quibit fluorometric quantification (Invitrogen). Initial RNA quality was determined by fragment analysis on the Agilent 2200 TapeStation (Agilent Technologies). The minimum RINe value sequenced was seven, with the majority greater than nine.

RNA-Sequencing and Analysis

RNA-seq libraries were prepared with 175 nG of RNA extracted from either $CD4^+$ T-cells or tumor tissue following the Illumina TruSeq RNA Sample Preparation v2 protocol (Illumina). The samples were sequenced on a NextSeq500 instrument to obtain 20 million, 75 base pair paired-end reads. The sequencing reads were aligned to mm10 using the STAR aligner (v2.5.3)[120]. Counts per gene were assessed using HTSeq (v0.9.1)[121]. TCR and B-cell receptor clonotypes were analyzed using MiXCR (v3.0.7)[122]. HTSeq counts were imported into BRB ArrayTools for analysis with DESeq. Cluster 3.0 and Java TreeViewer were used for generation of heat maps.

Polarizing Cell Culture Conditions

Unless otherwise noted, cells were kept in polarizing culture conditions for 96 hours. **Table 6** contains a list of cytokines and monoclonal antibodies that were supplemented into media containing RPMI 1640, 20% FBS, 1% penicillin streptomycin and 1x 2-mercaptoethanol with 25 µL/mL Dynabeads Mouse T-Activator CD3/CD28. The polarizing medias consisted of: TH_1 (IL12, IL2 and αIL4), TH_2 (IL4, IL2 and αIFNγ) and T_{FH} (IL6, IL21, αIFNγ and αTGFβ).

Interleukin	Concentration	Source	Catalog	Polarization
Mouse Recombinant IL6	100 nG/mL	Stemcell Technologies	78052.1	T_{FH}
Mouse Recombinant IL21	50 nG/mL	Stemcell Technologies	78116	T_{FH}
α-TGF-β	20 μG/mL	Biolegend	521703	T_{FH}
α-IFNγ	40 μG/mL	Biolegend	505834	T_{FH}
α-IL4	40 μG/mL	Biolegend	504122	T_{FH}
Mouse Recombinant IL12	20 nG/mL	Stemcell Technologies	78028.1	TH_1
Mouse Recombinant IL2	20 nG/mL	Stemcell Technologies	78081	TH_1
α-IL4	10 μG/mL	Biolegend	504122	TH_1
Mouse Recombinant IL2	20 nG/mL	Stemcell Technologies	78081	TH_2
Mouse Recombinant IL4	20 nG/mL	Stemcell Technologies	78047	TH_2
α-IFNγ	10 μG/mL	Biolegend	505834	TH_2

Table 6: Polarizing cytokines and monoclonal antibodies.

Murine Tumor Transplantation

Primary tumor tissue or cells from $Tet2^{-/-}$ mice were injected subcutaneously into NOD *scid* gamma (NSG) mice. The injected cells were live frozen single-cell suspensions from either neoplastic LNs or spleens. The injected amounts ranged from 5-15 million cells and an earlier disease onset was observed in mice receiving more cells, 132 and 86 days, respectively. NSG mice receiving tumor tissue (chopped or not chopped) reached lethal disease earlier than the single-cell suspensions and were used for secondary and tertiary transplants.

DNA Immunoblot for 5-hydroxymethylcytosine Detection

500 nG of $CD4^+$ T-cell DNA was added to 200 µL of nuclease-free water. The DNA was denatured by incubating at 95°C for 10 minutes. 200 µL of 20X SSC buffer was added immediately and the sample was chilled on ice for 5 minutes. 100 µL of nuclease free water was added to the DNA solution to achieve a final volume of 500 µL and a concentration of 1 nG/µL. A series of two 2-fold dilutions was set up. The Amersham Hybond-N^+ membrane was pre-wet in 10X SSC buffer and then dried by applying vacuum pressure. We then applied 250 µL of DNA solutions and controls to the membrane and allowed them to incubate on the membrane for 10 minutes. Light vacuum pressure was applied to draw the solutions through the membrane. The membrane will be mostly dry. Allow the membrane to air dry completely and UV cross-link at 120,000 micro-J/cm^2. The membrane was then incubated with MethyleneBlue for 10 minutes while shaking at room temperature to detect bound DNA. After imaging, the blue stain was removed by a 1% SDS wash and three subsequent water washes. Next, the membrane was placed in blocking buffer for 1 hour at room temperature and washed 3 times for 5 minutes each with 1X TBST. The membrane was incubated with the primary antibody (5-hydroxymethylcytosine, clone 59.1, Active Motif 40900) with

agitation overnight at 4°C. The membrane was washed three times with 1X TBST. The membrane was incubated with the HRP-conjugated secondary antibody in blocking buffer with agitation for 1 hour at room temperature. The membrane was washed three times with 1X TBST. The membrane was developed with Clarity ECL and exposed to x-ray film.

Statistical Analysis

Statistical analyses were performed in Microsoft Excel 2016 and GraphPad Prism 8. Results were reported as mean ± standard deviation unless otherwise indicated. Student's t-test was performed assuming equal variance. A p-value <0.05 was considered statistically significant. Survival is represented as Kaplan-Meier curves and Log-rank was used to determine the significance. For experiments with animals, "n" represents the number of animals included. All experiments represented by images have been repeated at least twice and a representative image was shown.

3.3 RESULTS

Frequent mutation of TET2, but not TET1 or TET3 in AITL

Our genetic analysis in AITL indicated that TET2 mutations were observed in 73% (99/135) of AITL cases, whereas mutations in either TET1 or TET3 were infrequent. Consistent with earlier observations, TET2 mutations were identified at varying VAFs, with a subset of cases showing higher than expected relative to neoplastic T-cells estimated from the VAF of tumor-specific mutations in corresponding cases ($RHOA^{G17V}$ and $IDH2^{R172}$), suggesting pre-neoplastic lesions. Though TET2 mutations were observed throughout the gene body, mutations in the catalytic domain were more frequent in cases with comparatively higher VAF, 48% and 31%, respectively (**Figure 19**). RHOA mutations are heterozygous and tumor-specific, so we calculated a higher than expected VAF for TET2 to be greater than twice the RHOA VAF. When we examined the mRNA expression level of TET family members using RNA-seq, TET1 was minimally expressed. In contrast, TET2 and TET3 expression showed comparable expression levels with normal naïve T-cells or T_{FH} cells (**Figure 20A/B**). In AITL, no significant difference in TET2 mRNA expression was noted in cases carrying a TET2 mutation (**Figure 20C**). Further, TET2 mutation status did not predict inferior OS, but a trend towards poorer outcome was observed in cases with a TET2 VAF more than twice that of its corresponding RHOA VAF, however it was not significant (**Figure 21A/B**).

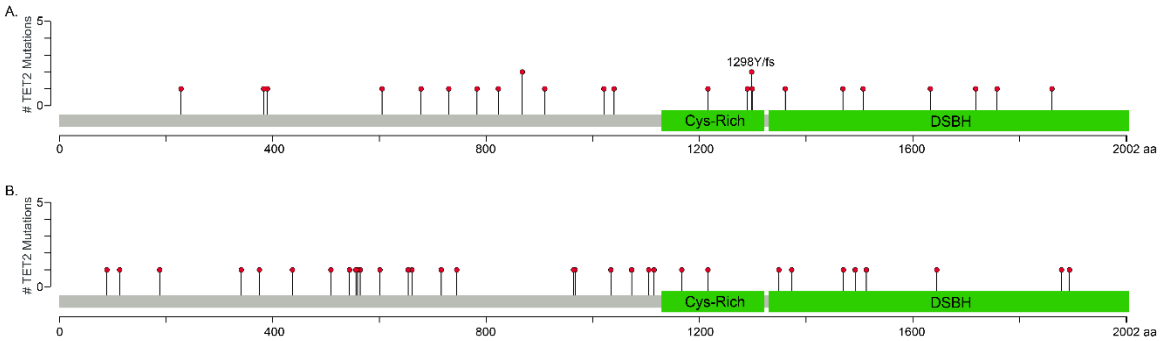

Figure 19: Mutation spectrum of TET2 in AITL.

A. TET2 mutations with a VAF greater than twice the RHOA VAF in cases with mutations of both genes. Only the highest TET2 VAF for each AITL specimen was plotted if more than one TET2 mutation was detected. **B.** TET2 mutations with a VAF less than twice the RHOA VAF in cases with mutations of both genes. Only the highest TET2 VAF for each AITL specimen was plotted if more than one TET2 mutation was detected.

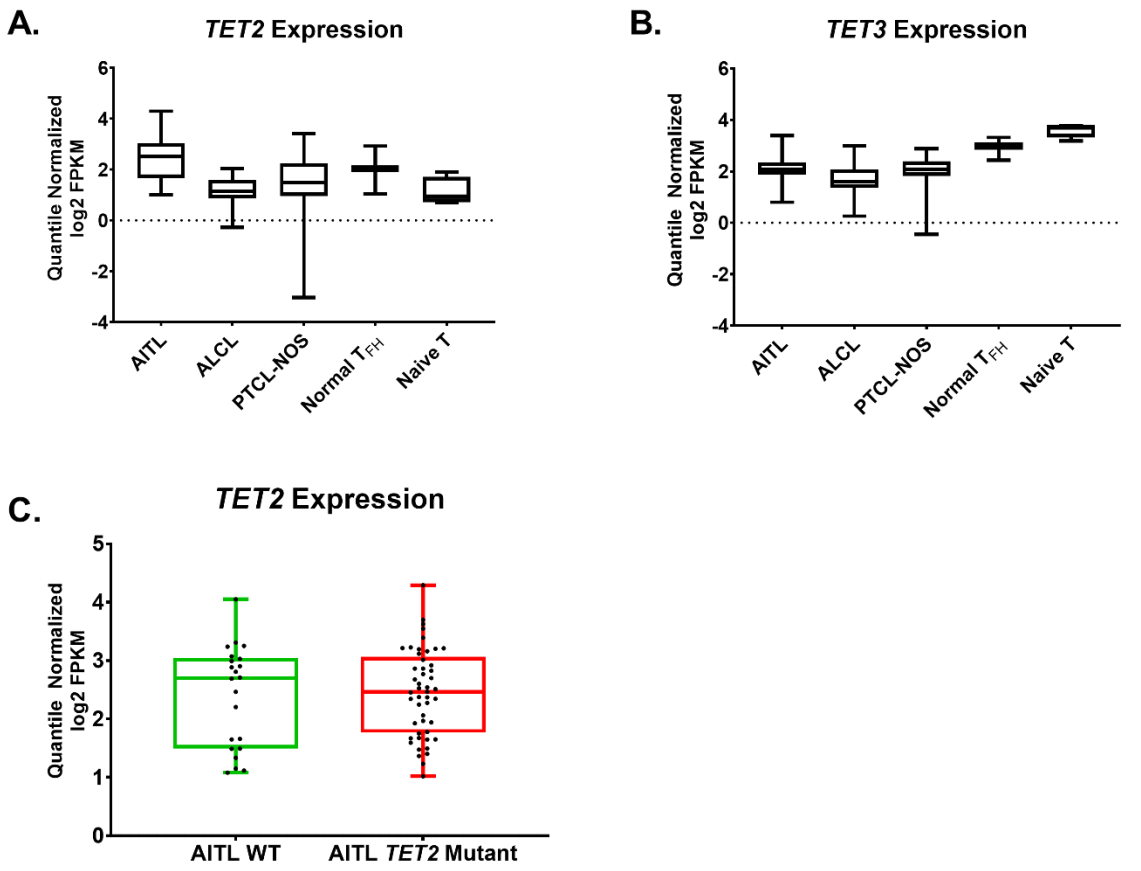

Figure 20: TET2 mRNA expression detected by RNA-sequencing in peripheral T-cell lymphoma.

A. TET2 expression in major peripheral T-cell lymphoma entities including AITL (n=71), ALCL (n=36), PTCL-NOS (n=26), normal T_{FH} cells (n=3) and Naïve T-cells (n=4). **B.** TET3 expression in major peripheral T-cell lymphoma entities including AITL (n=71), ALCL (n=36), PTCL-NOS (n=26), normal T_{FH} cells (n=3) and Naïve T-cells (n=4). **C.** TET2 expression in AITL delineated by wild-type TET2 (n=22) or TET2 mutant (n=49).

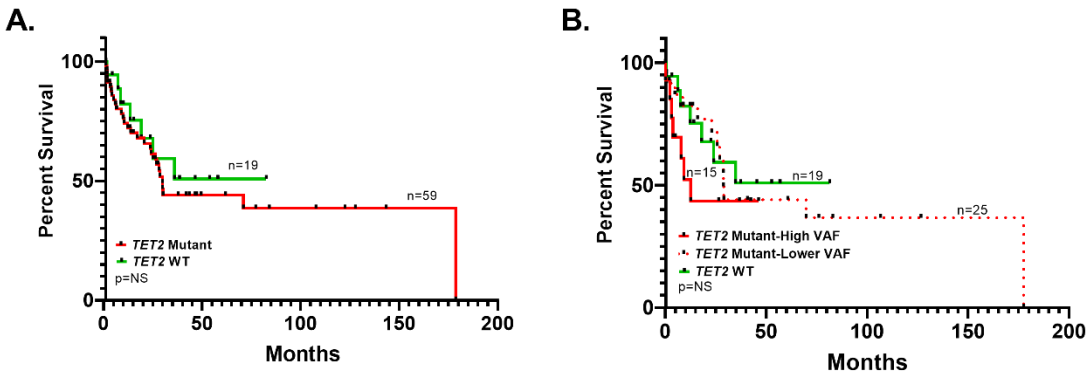

Figure 21: Overall survival in angioimmunoblastic T-cell lymphoma by TET2 mutation status.

A. The presence of a TET2 mutation does not result in significantly worse overall survival in AITL patients.
B. Although not significant, AITL patients harboring a TET2 mutation having a VAF more than twice the VAF of RHOA have a trend towards inferior survival.

Generation of a conditional murine model with Tet2 loss in CD4$^+$ T-cells

Due to the high prevalence of TET2 mutations in AITL and the current limited understanding of the underlying pathobiology of TET2 in AITL lymphomagenesis, we generated a murine model with conditional loss of Tet2 in CD4$^+$ T-cells. To obtain a T-cell specific knockout of Tet2, we generated Tet2$^{-/-}$ mice as described in the methods and validated the genotype by standard PCR (**Figure 22A**). The cell-specific rearrangement of Tet2 was confirmed in CD4$^+$ T-cells using standard PCR with primers spanning the loxP sites surrounding exon three (**Figure 22B/C**). RNA-seq further validated the loss of Tet2 with no exon three mapped reads in Tet2$^{-/-}$ CD4$^+$ T-cells compared to WT (**Figure 22D**). Tet2 and Tet3 mRNA expression by RNA-sequencing was detected in the CD4$^+$ T-cells at near equal frequencies between Tet2$^{-/-}$ and WT mice, however the Tet2 transcript is non-functional. Overall, Tet3 had the highest expression with Tet2 detected at lower levels, and no to very minimal expression of Tet1 (**Figure 23A**). The neoplastic Tet2$^{-/-}$ CD4$^+$ T-cells did have a significant reduction of both Tet1 ($p=0.009$ versus Cre$^-$ and 0.008 versus Cre$^+$) and Tet3 ($p=0.004$ versus Cre$^-$ and 0.009 versus Cre$^+$) (**Figure 23A**). However, when looking at neoplastic splenocytes, rather than only CD4$^+$ T-cells, compared to WT splenocytes, no changes were observed in expression of Tet1, 2 or 3 (**Figure 23B**). Of note, the two older time points (48 and 60 weeks) tended to have lower expression of all Tet members in both the Cre$^-$ and Cre$^+$ CD4$^+$ T-cells (**Figure 23A**), suggesting expression may decrease with age and the reason for why decreased expression is seen in the neoplastic T-cells as these mice are significantly older.

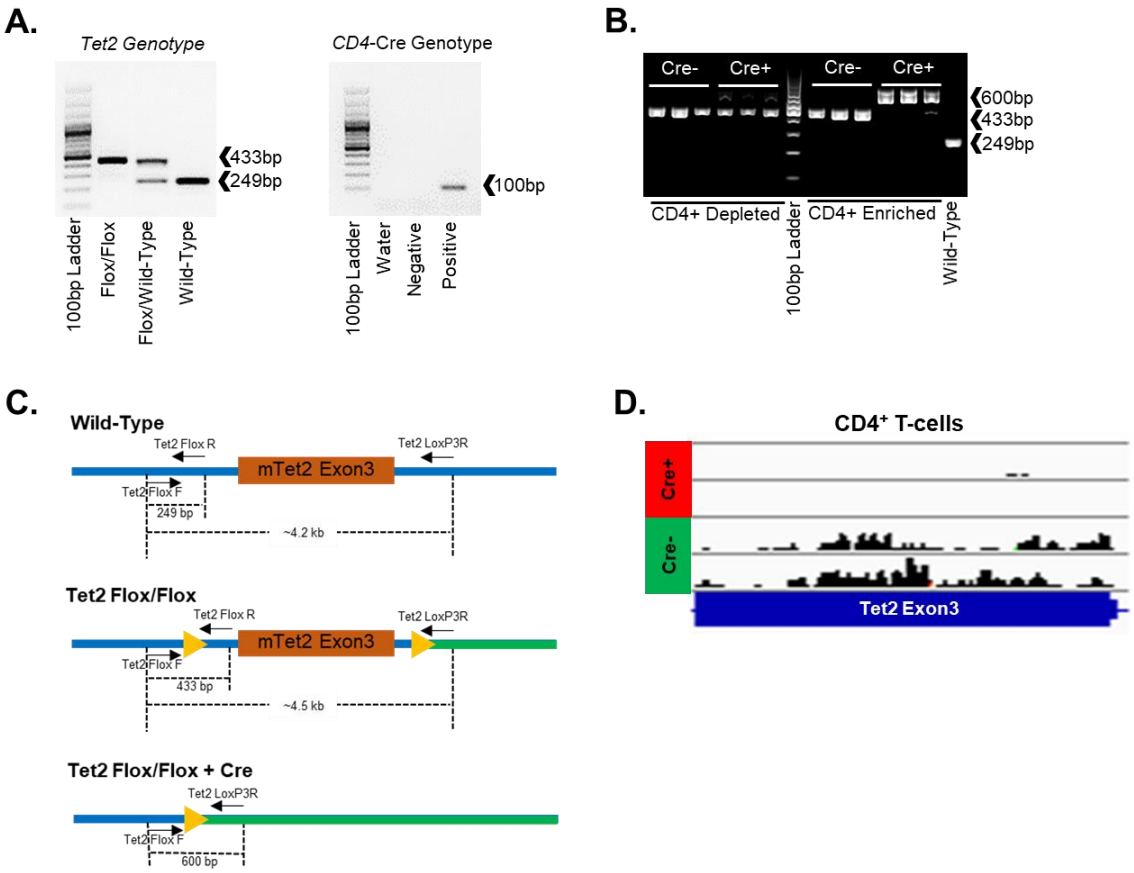

Figure 22: Murine model genotyping and confirmation of Tet2 rearrangement in CD4⁺ T-cells.

A. Gel imaging demonstrating Tet2 and CD4-Cre genotyping by standard PCR. If both Tet2 alleles are floxed, a product appears at 433 base pairs compared to a heterozygous floxed allele, which shows bands at both 433 base pairs and the wild-type length of 249 base pairs. The Cre-transgene results in a positive band at 100 base pairs or no product band if Cre⁻. **B.** The Tet2 rearrangement was cell-specific as the band at 600 base pairs, which indicates removal of exon 3, was only observed in the CD4⁺ T-cells of mice that were Cre⁺. **C.** Schematic of the primer locations for detecting floxed Tet2 alleles and Tet2 rearrangement. **D.** RNA-sequencing confirms removal of Tet2 exon 3 in the CD4⁺ T-cells of Cre⁺ mice by the lack of mapped reads compared to Cre⁻ mice. Shown are only two representative samples.

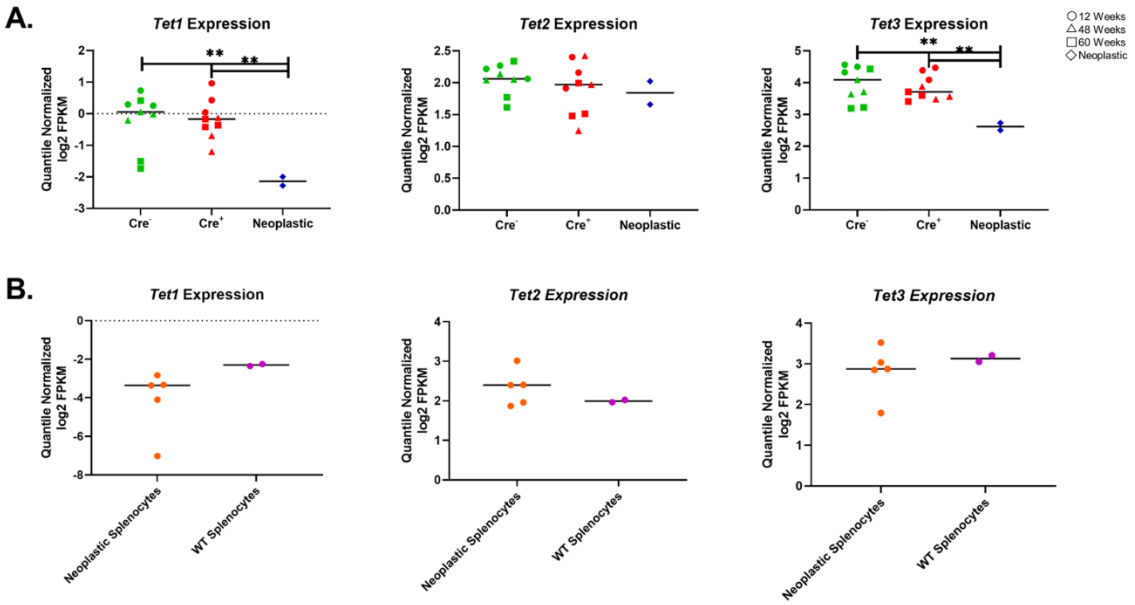

Figure 23: mRNA expression of the Tet family in murine cells detected by RNA-sequencing.

A. mRNA expression of Tet1, Tet2 and Tet3 in 12 week, 48 week, 60 week and neoplastic $CD4^+$ T-cells. The green color indicates wild-type, the red color indicates $Tet2^{-/-}$ pre-neoplasm and the blue color indicates neoplastic $Tet2^{-/-}$. As indicated in the legend, the different shapes indicate different ages. **B.** mRNA expression of Tet1, Tet2 and Tet3 in neoplastic $Tet2^{-/-}$ splenocytes (orange color) and age-matched wild-type control splenocytes (purple color).

Loss of Tet2 in CD4$^+$ T-cells does not alter major lymphoid populations pre-neoplasm

To investigate the role of Tet2 loss in cellular development and differentiation, we evaluated major lymphoid subpopulations by flow cytometry in the spleen of Tet2$^{-/-}$ mice at 12, 48 and 60 weeks of age prior to lymphoma development. No major change in either B220$^+$ B-cells, CD3$^+$ T-cells or CD335$^+$ NK cells was observed at any of the ages (**Figure 24A-C**). As anticipated, there was a significant decrease in the B220$^+$ B-cell population ($p<0.01$) and a significant increase in the CD3$^+$ T-cell population ($p=0.04$-0.002) with age, 48 and 60 weeks compared to 12 weeks, in both the WT and Tet2$^{-/-}$ mice at equal frequencies. There was a reduced ratio of Mac-1$^+$/Gr-1$^+$ associated with Tet2$^{-/-}$ mice compared to age-matched WT at 48 (not significant) and 60 weeks ($p=0.03$) (**Figure 24D**). No major change was observed in the total CD3$^+$/CD4$^+$ or CD3$^+$/CD8$^+$ T-cell subpopulations (**Figure 24E/F**).

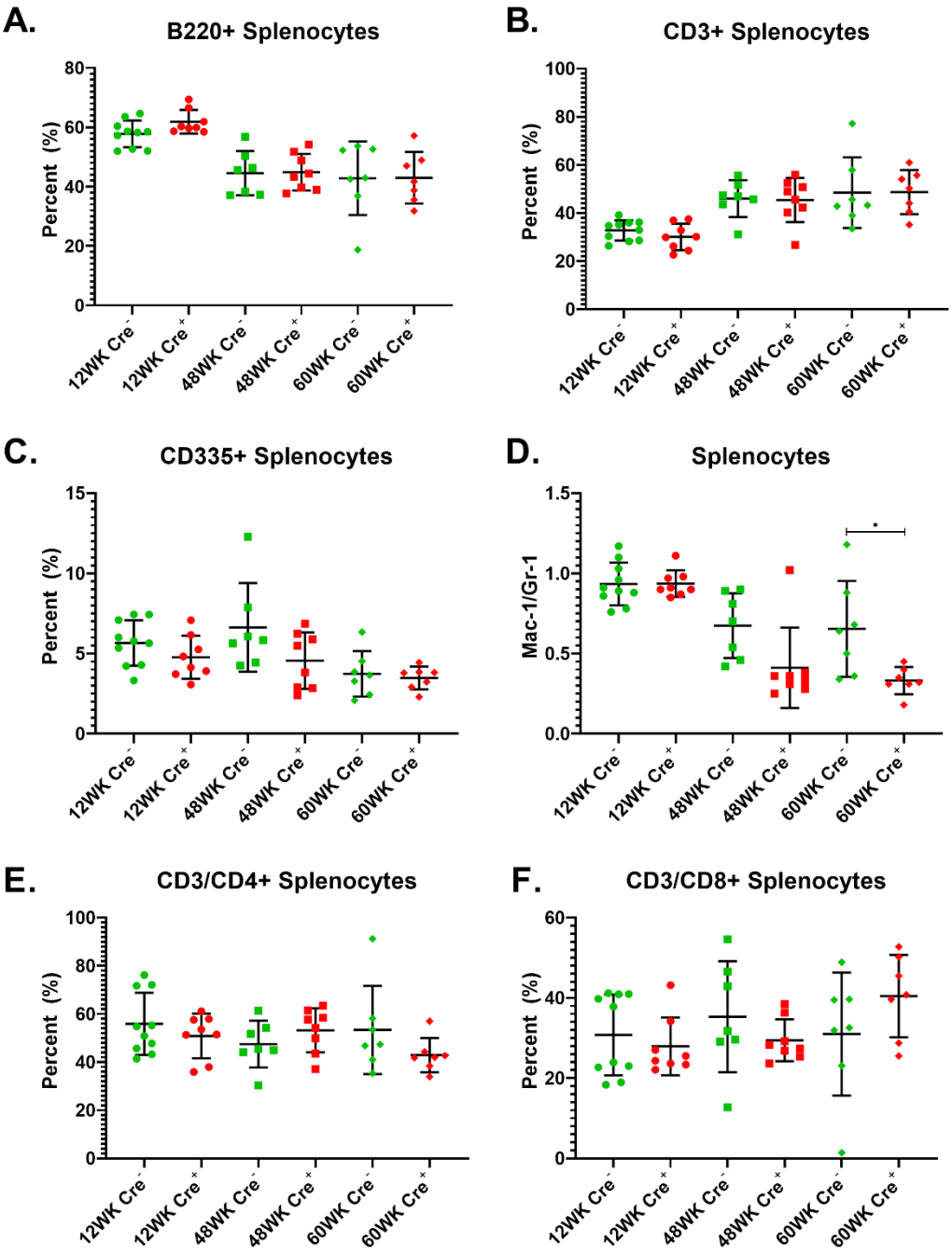

Figure 24: Flow cytometry analysis of major lymphoid and myeloid populations in murine splenocytes.

A. B220^{+} B-cells decreased with age, but remained consistent between WT and Tet2$^{-/-}$ mice. **B.** CD3^{+} T-cells increased with age, but remained consistent between WT and Tet2$^{-/-}$ mice. **C.** No change in CD335^{+} natural killer cells was observed with age or genotype. **D.** Mac-1/Gr-1 ratio decreased with age, with a more pronounced decrease in Tet2$^{-/-}$ mice. At 60 weeks, the difference was statistically significant (p=0.03). **E.** No change in CD3^{+}/CD4^{+} T-cells was observed with age or genotype. **F.** No change in CD3^{+}/CD8^{+} T-cells was observed with age or genotype.

Histopathological and immunophenotypic characteristics of Tet2-deficient $CD4^+$ T-cells reveal T_{FH} cell-derived lymphoma

The long-term loss of Tet2 in $CD4^+$ T-cells led to development of lymphoma in 12 of 26 mice evaluated. These tumors were characterized by massive splenomegaly, marked generalized lymphadenopathy, hepatomegaly and occasional involvement of other parenchymal organs as observed by histopathological examination (**Figure 25A-C**) with disease characteristics indicated in **Table 7.** Flow cytometry showed an increase of $CD3^+/CD4^+$ splenocytes (56% in $Tet2^{-/-}$ versus 8% in WT), with the $CD4^+$ T-cell population expressing high $PD1^+$ and $CXCR5^+$ (65% in $Tet2^{-/-}$ versus 5% in WT), characteristic of T_{FH} cells (**Figure 25C/D**). The traditional architecture of the spleen was effaced (**Figure 26**) with large nodular clusters of neoplastic cells that were variable in size from small to intermediate to large. Immunostains showed the neoplastic cells to be $CD3^+$ T-cells with atypical $CD19^+$ B-cells. The T-cells are predominately $CD4^+$ and show significant cytologic atypia. $CD8^+$ T-cells highlight scattered background cytotoxic T-cells. The $CD19^+$ B-cells formed large clusters, and on average appear to be larger in size than the $CD3^+$ T-cells (**Figure 26**)**.** Tet2 rearrangement in $CD4^+$ T-cells was confirmed by PCR. $CD19^+$ cells were isolated from two neoplastic splenocytes samples and checked for Tet2 rearrangement. Interestingly, we observed that one tumor out of eight examined, which had aberrant $CD19^+$ expression (~50%) compared to $CD20^+$ expression (~10%), had Tet2 rearrangement in a portion of the cells. The $CD20^+$ population observed by IHC matched the frequency that was observed by flow cytometry; suggesting that the neoplastic cells may be aberrantly expressing CD19 and thus showed the rearrangement. A second neoplastic sample which had equal/overlapping $CD19^+$ and $CD20^+$ expression showed a predominant band indicating homozygous Tet2 floxed alleles as expected; however, a faint band can be observed at the re-arranged size as the magnetic cell isolations are not 100% pure (**Figure 27**).

Tumor clonality was determined using MiXCR and RNA-seq data from neoplastic splenocytes. Looking at TCR α and β, all tumors appeared to have a clonal T-cell fraction. A sample was considered clonal if the two most frequent clones were ten times higher than the third most frequent clone, as used previously for human AITL[123]; whereas, WT splenocytes have a more equal distribution of clone fraction (**Figure 28A**). When evaluating a primary tumor and its corresponding first passage tumor, we observed one of the two most frequent α and β clones from the primary tumor to be dominant in the generated recipient tumor (**Figure 28B**). Further, B-cell clonality was of interest as tumor evaluation by IHC revealed atypical $CD19^+$ B-cells in the spleen. Similar to T-cells, we observed dominant B-cell clones in the lymphoma-bearing mice and the NSG transplant tumor revealed a dominant B-cell clone corresponding to the donor (**Figure 28C/D**).

As expected, $Tet2^{-/-}$ mice had significantly poorer OS ($p=0.01$) with a median survival of 1.74 years compared to 2.31 years in WT (**Figure 29A**). To determine if Tet2 loss in $CD4^+$ T-cells could manifest effects in mature B-cells undergoing the GC reaction, we induced T cell–dependent antigen response with SRBCs in a cohort of WT and $Tet2^{-/-}$ mice. We observed that SRBC stimulation led to a slightly earlier disease onset as compared to $Tet2^{-/-}$ mice receiving control PBS injections, with a median survival of 1.42 years and 1.93 years respectively (**Figure 29B**). Further, the overall survival between WT and $Tet2^{-/-}$ lymphoma-bearing mice specifically was also significant ($p<0.0001$) (**Figure 29C**). We sacrificed a cohort of animals 10-14 days after a single SRBC injection, and spleens were examined by IHC for Ki-67. This staining revealed a slight increase in the area of GCs in $Tet2^{-/-}$ mice, but was significant at 12 weeks ($p<0.001$) (**Figure 30**). No difference in the total number of GCs was observed between genotypes.

To determine the malignant character of the tumor cells, we transplanted single-cell suspensions of neoplastic cells or tumor tissue into three-month-old NSG recipient

mice. NSG mice receiving chopped tumor tissue reached a lethal disease as early as 40 days, compared to mice receiving not chopped tumor tissue, which reached a lethal disease as early as 14 days. Both of these are earlier than the NSG mice that received live frozen single-cells suspensions, which took between 86 and 132 days to have a disease phenotype. The time period before disease onset in mice receiving live frozen single-cell suspensions corresponded to the number of cells injected. The tumor tissue transplants were successfully transplanted for three passages, at which time we stopped further passages. Histopathological analysis of the recipient-derived tumors revealed similar architecture and immunophenotype to that of the initial donor tumor. For example, in the liver we observed abnormal lymphoid infiltrate in the sinusoids forming nodules with neoplastic cells large in size with irregular nuclear borders in both the primary and transplant (**Figure 31**). We completed RNA-seq on the primary and first passage neoplastic splenocytes and observed high concordance between the two (0.97), demonstrating that the T_{FH} cell-derived lymphoma cells are transplantable and aggressive.

ID	Gender	*Tet2*	CD4-Cre	Overall Survival	Notes	RNA-Sequencing	Injection
Mouse 1	Male	Flox/Flox	Positive	2.51	$CD8^+$ Proliferation		
Mouse 2	Female	Flox/Flox	Positive	2.19	Cervical Mass		SRBC
Mouse 3	Female	Flox/Flox	Positive	1.44	FD, Lymphoma		
Mouse 4	Male	Flox/Flox	Positive	1.36	FD, Lymphoma		
Mouse 5	Male	Flox/Flox	Positive	1.46	FD, Unknown Disease		
Mouse 6	Female	Flox/Flox	Positive	1.32	Liposarcoma		SRBC
Mouse 7	Male	Flox/Flox	Positive	2.29	Lung Cancer		PBS
Mouse 8	Female	Flox/Flox	Positive	1.31	Lymphoma		
Mouse 9	Male	Flox/Flox	Positive	1.74	Lymphoma		
Mouse 10	Male	Flox/Flox	Positive	1.71	Lymphoma	Yes-Splenocytes	
Mouse 11	Female	Flox/Flox	Positive	1.78	Lymphoma	Yes-Splenocytes and $CD4^+$	
Mouse 12	Female	Flox/Flox	Positive	0.49	Lymphoma	Yes-Splenocytes and $CD4^+$	
Mouse 13	Male	Flox/Flox	Positive	1.42	Lymphoma	Yes-Splenocytes	SRBC
Mouse 14	Female	Flox/Flox	Positive	1.39	Lymphoma	Yes-Splenocytes	PBS
Mouse 15	Male	Flox/Flox	Positive	1.56	Lymphoma		PBS
Mouse 16	Male	Flox/Flox	Positive	1.30	Lymphoma		
Mouse 17	Female	Flox/Flox	Positive	2.39	Lymphoma		PBS
Mouse 18	Female	Flox/Flox	Positive	0.89	Myeloid		
Mouse 19	Female	Flox/Flox	Positive	1.96	Natural Death		
Mouse 20	Male	Flox/Flox	Positive	1.71	Natural Death		
Mouse 21	Female	Flox/Flox	Positive	2.53	Natural Death		SRBC
Mouse 22	Female	Flox/Flox	Positive	2.71	Rectal Prolapse		
Mouse 23	Male	Flox/Flox	Positive	1.31	Sarcoma		SRBC
Mouse 24	Male	Flox/Flox	Positive	1.93	Splenomegaly		PBS
Mouse 25	Male	Flox/Flox	Positive	2.17	Splenomegaly		PBS
Mouse 26	Male	Flox/Flox	Positive	1.69	Unknown Disease		PBS

Table 7: Disease characteristics of $Tet2^{-/-}$ mice evaluated for long-term survival.

OS (years) and observed disease in $Tet2^{-/-}$ mice evaluated for long-term survival. The mice used for profiling by RNA-sequencing are indicated. It is also indicated if the mouse received an injection of SRBCs or control PBS every three weeks.

*FD=Found Dead

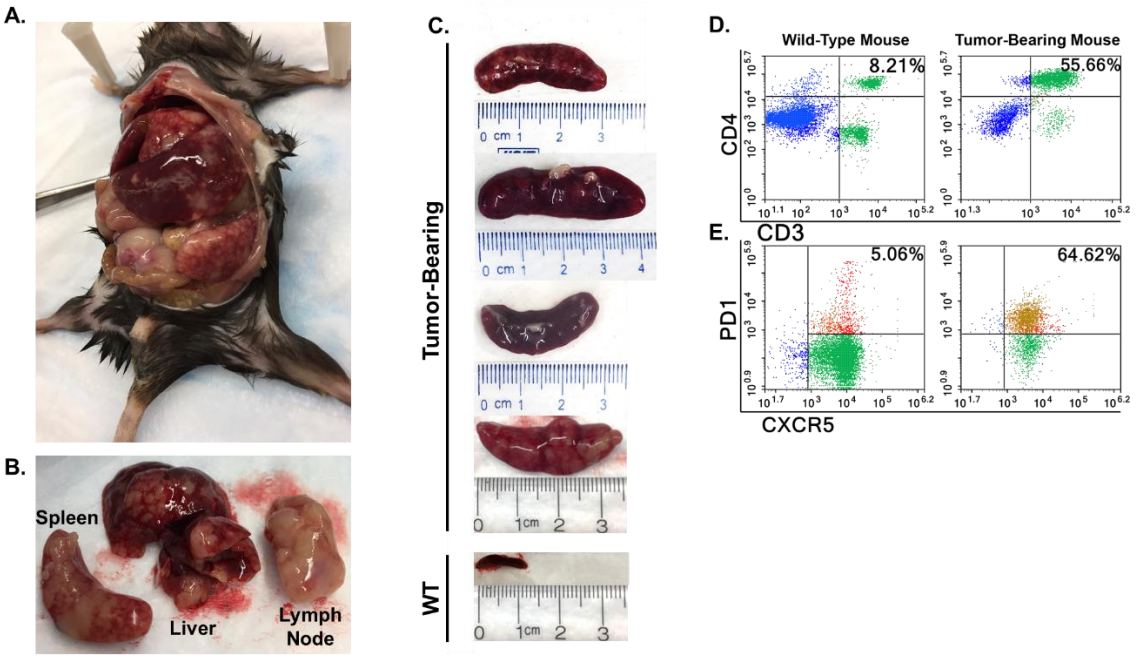

Figure 25: Physical and phenotypic characterization of Tet2$^{-/-}$ tumor-bearing mice.

A. Necropsy of a tumor-bearing Tet2$^{-/-}$ mice. Enlargement of the spleen and liver are evident with obvious infiltration. **B.** Neoplastic infiltration of the spleen, liver and lymph node was common in lymphoma tumor-bearing Tet2$^{-/-}$ mice. **C.** Significant splenomegaly was observed in Tet2$^{-/-}$ mice compared to age-matched WT mice. **D.** Increased percentage of CD3^{+}/CD4^{+} splenocytes in a representative lymphoma tumor-bearing Tet2$^{-/-}$ mouse compared to an age-matched WT control. **E.** Increased percentage of T_{FH}^{+} splenocytes (CD4^{+} and PD1/CXCR5^{High}) in a representative lymphoma tumor-bearing Tet2$^{-/-}$ mouse compared to an age-matched WT control.

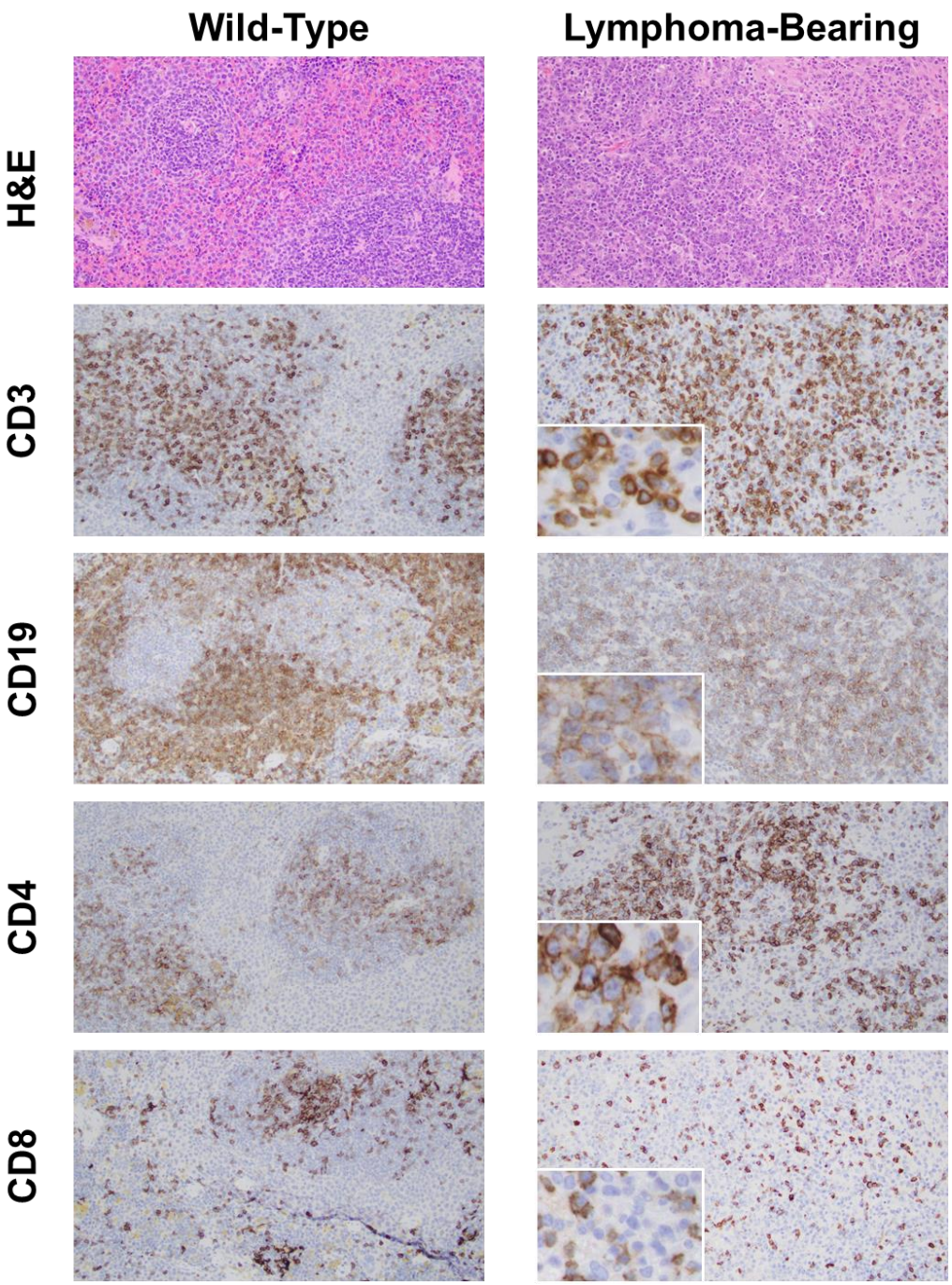

Figure 26: Morphologic and immunohistochemical characteristics of Tet2$^{-/-}$ tumor-bearing mice.

All images are of spleen sections from a WT age-matched control mouse (left) or a representative Tet2$^{-/-}$ tumor-bearing mouse (right). The WT spleen shows a maintained architecture with well-defined white and red pulp areas. The white pulp contains a reactive follicle highlighted by CD19 and a T-cell zone highlighted by CD3. The T-cell zone contains a mixture of CD4 and CD8-positive T-cells. The tumor-infiltrated spleen shows effacement of the traditional architecture with large nodular clusters of variable sized cells. Neoplastic cells are CD3^{+} and predominantly CD4^{+} with significant cytologic atypia. CD8^{+} T-cells are rare and highlight background cytotoxic T-cells. The CD19^{+} cells formed large clusters and appear to be larger in size than the CD3^{+} T-cells. Images were taken at a 20x magnification with insets at 40x.

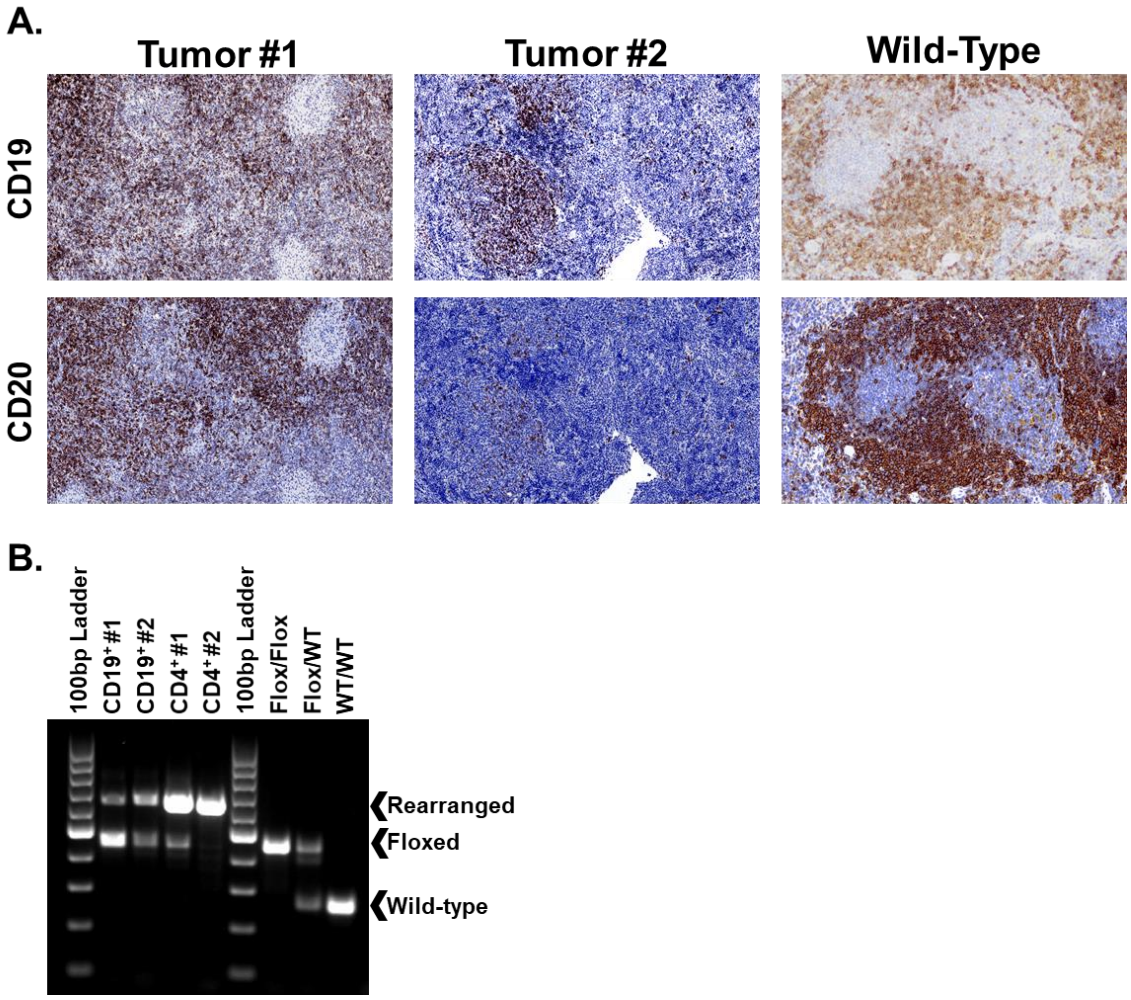

Figure 27: Tet2 rearrangement in neoplastic cells by standard PCR.

A. IHC of CD19 and CD20 in two neoplastic spleens and one age-matched WT control. We see in #1 equal staining of CD19 and CD20. In Tumor #2, aberrant CD19 expression was observed with rare focal CD20 staining. The WT sample indicated typical B-cell staining with overlapping CD19 and CD20 expression. **B.** $CD19^+$ #1 and $CD4^+$ #1 correspond to cells isolated from the same neoplastic splenocytes shown as Tumor #1 in panel A. Accordingly, $CD19^+$ #2 and $CD4^+$ #2 correspond to cells isolated from the same neoplastic splenocytes shown as Tumor #2 in panel A. $CD19^+$ #2 is the sample that by IHC demonstrated aberrant CD19 expression, likely suggesting why we see the two bands. In $CD19^+$ #1 a faint band is observed at the rearranged size (>600 base pairs) compared to the homozygous floxed size (433 base pairs), suggesting amplification of other cells types as magnetic cell isolation kits are not 100% pure. The same can be seen in $CD4^+$ #1 where the predominant band is at the rearrangement size as expected, with a faint band at the homozygous floxed size.

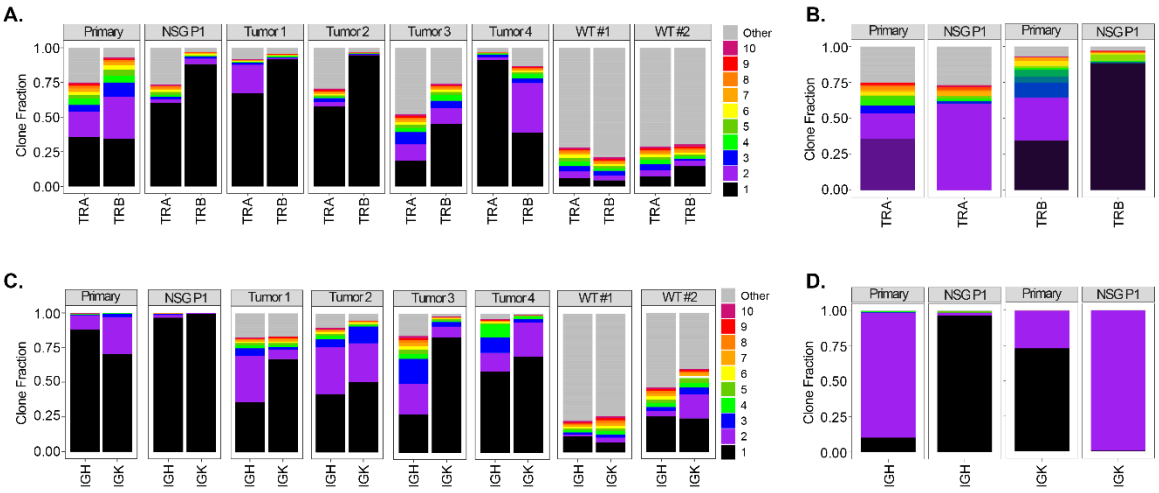

Figure 28: Neoplastic splenocytes from Tet2$^{-/-}$ mice have clonal T and B-cell populations.

A. Contribution of CDR3α and CDR3β sequences to the T-cell receptor repertoire in five primary tumor samples, one tumor from the first passage of an NSG recipient and two wild-type mice. Each bar represents an individual clonotype, with black to magenta showing the first to tenth ranked predominant clonotypes. Grey represents the rest of the identified clonotypes in the sample. The colors between samples do not indicate the same clone. **B.** CDR3α (left) and CDR3β (right) sequences indicated that one of the top two clones in the primary tumor sample was the dominate clone in the corresponding NSG passage 1 tumor. The colors between samples represent the same clone. **C.** Contribution of IgH and Igκ sequences to the B-cell receptor repertoire in five primary tumor samples, one tumor from the first passage of an NSG recipient and two wild-type mice. Each bar represents an individual clonotype, with black to magenta showing the first to tenth ranked predominant clonotypes. Grey represents the rest of the identified clonotypes in the sample. The colors between samples do not indicate the same clone. **D.** IgH (left) and Igκ (right) sequences indicated that one of the top two clones in the primary tumor sample was the dominate clone in the corresponding NSG passage 1 tumor. The colors between samples represent the same clone.

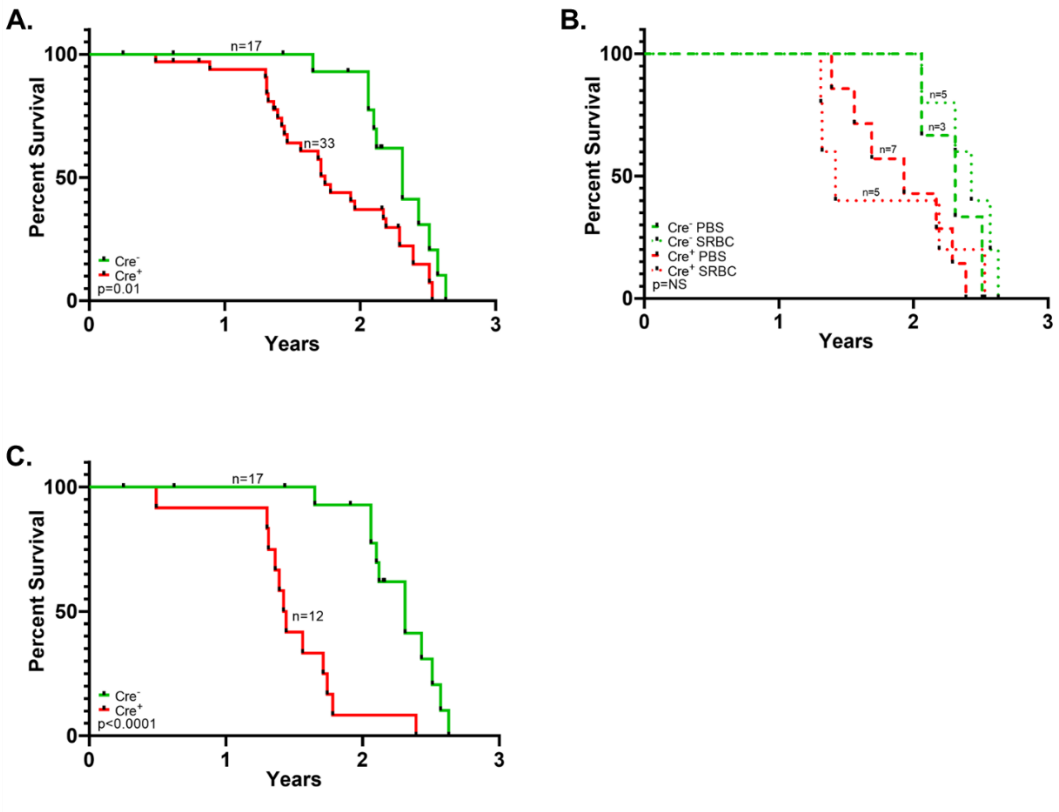

Figure 29: Tet2$^{-/-}$ mice have inferior survival.

A. Kaplan-Meier plot of the overall survival between Tet2$^{-/-}$ and WT mice demonstrated that Tet2$^{-/-}$ mice have significantly worse overall survival (p=0.01). The median overall survival of Tet2$^{-/-}$ mice was 1.74 years. **B.** Kaplan-Meier plot of a small cohort of Tet2$^{-/-}$ and wild-type mice injected with SRBCs or PBS (control) every three weeks. Consistent with **A**, Tet2$^{-/-}$ mice had inferior outcome, with earlier death observed in Tet2$^{-/-}$ mice receiving the SRBCs. **C.** Kaplan-Meier plot of the overall survival between Tet2$^{-/-}$ which developed lymphoma or are still alive and WT mice demonstrated Tet2$^{-/-}$ lymphoma-bearing mice have significantly worse overall survival (p=0.02).

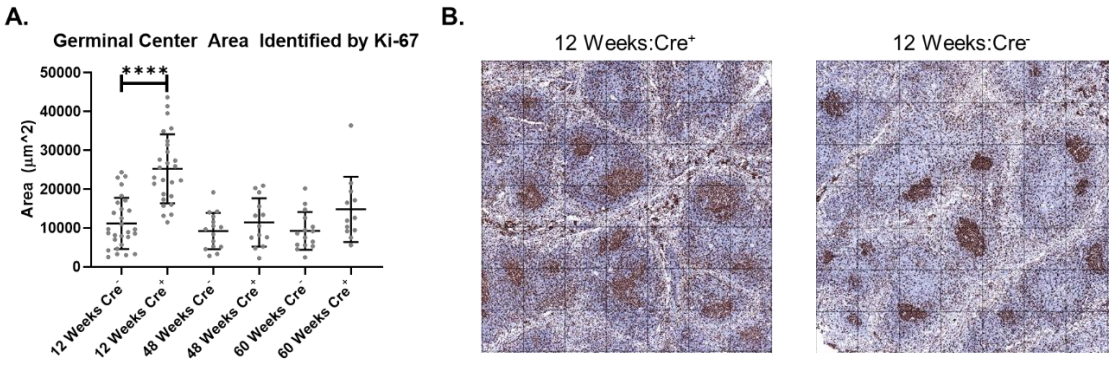

Figure 30: Ki-67 staining in mice injected with sheep red blood cells to stimulate a germinal center reaction.

QuPath was used to identify and measure the area of GCs in Ki-67 IHC scanned at 20x. All mice were injected one time with SRBCs 10-14 days prior to collection. **A.** At 12 weeks of age, Tet2$^{-/-}$ mice showed a significant increase in the area of GCs compared to WT mice. Although not significant, the average area of GCs was larger in Tet2$^{-/-}$ mice compared to WT at later time points (48 and 60 weeks). **B.** A representative image of the Ki-67 staining from a Cre^{+} mice showing larger GCs (left) compared to a WT mouse showing smaller GCs (right).

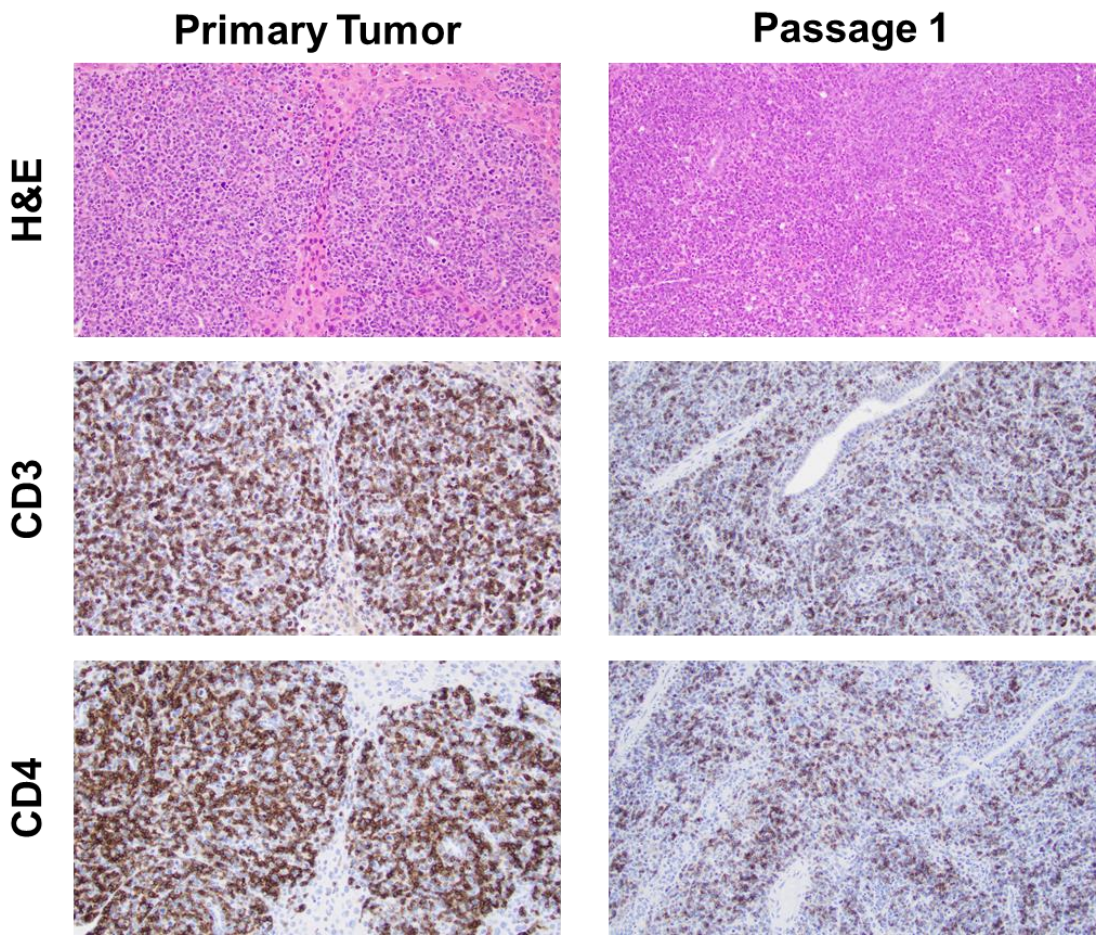

Figure 31: Morphologic and immunohistochemical features of a primary murine lymphoma tumor and the first NSG passage.

All images are of liver sections from a primary lymphoma tumor (left) or the first passage of the same tumor in a NSG recipient mouse (right). Consistent in both, the liver shows an abnormal lymphoid infiltrate in the sinusoids forming nodules. The neoplastic cells are large in size and show irregular nuclear borders. The neoplastic cells are primarily $CD3^+/CD4^+$ T-cells.

Loss of Tet2 resulted in altered gene expression of oncogenic pathways and increased T_{FH} expression

To delineate the genes dysregulated by Tet2 loss leading to lymphomagenesis, we analyzed the transcriptional signatures of $Tet2^{-/-}$ $CD4^+$ T-cells using RNA-seq. $CD4^+$ T-cells were collected at three pre-neoplastic time points (12, 48 and 60 weeks) and at the lethal state in lymphoma-bearing mice. A correlation analysis was performed between time point biological replicates and a range 0.96-1 was observed, suggesting high correlation and appropriate biological replicates. Unsupervised hierarchical clustering unveiled three major clusters (**Figure 32**). Cluster 1 consisted primarily of the early 12-week time point which had the fewest differential genes between $Tet2^{-/-}$ and WT. Cluster 2 was composed of the later time points (48 and 60 weeks) with the $Tet2^{-/-}$ $CD4^+$ T-cells forming smaller sub-clusters. Cluster 3 was composed of the neoplastic cells, with the neoplastic CD4+ T-cells clustering with their corresponding neoplastic splenocytes.

Since T_{FH} cells are the cells of interest, we observed a T_{FH} gene expression signature (Icos, Cxcr5, Pdcd1, Bcl6, Il21 and CXCL13) and found a gradual increase over time in $Tet2^{-/-}$ $CD4^+$ T-cells (**Figure 33**). Interestingly, although we see the increased T_{FH} phenotype by RNA-seq, we did not observe an increase in total number of $CD4^+$ T-cells by flow cytometry. This suggests that Tet2 loss resulted in skewed T_{FH} differentiation of $CD4^+$ T-cells without effecting major lymphoid populations. Although the WT $CD4^+$ T-cells also demonstrate an increase in expression of the T_{FH}-related genes to an extent, the highest expression was observed in $CD4^+$ T-cells isolated from neoplastic splenocytes with all T_{FH} markers except CXCL13 significantly increased compared to all pre-neoplastic $CD4^+$ T-cells (FDR<0.1, >1 log2 fold-change), further suggestive of a T_{FH} cell-derived lymphoma.

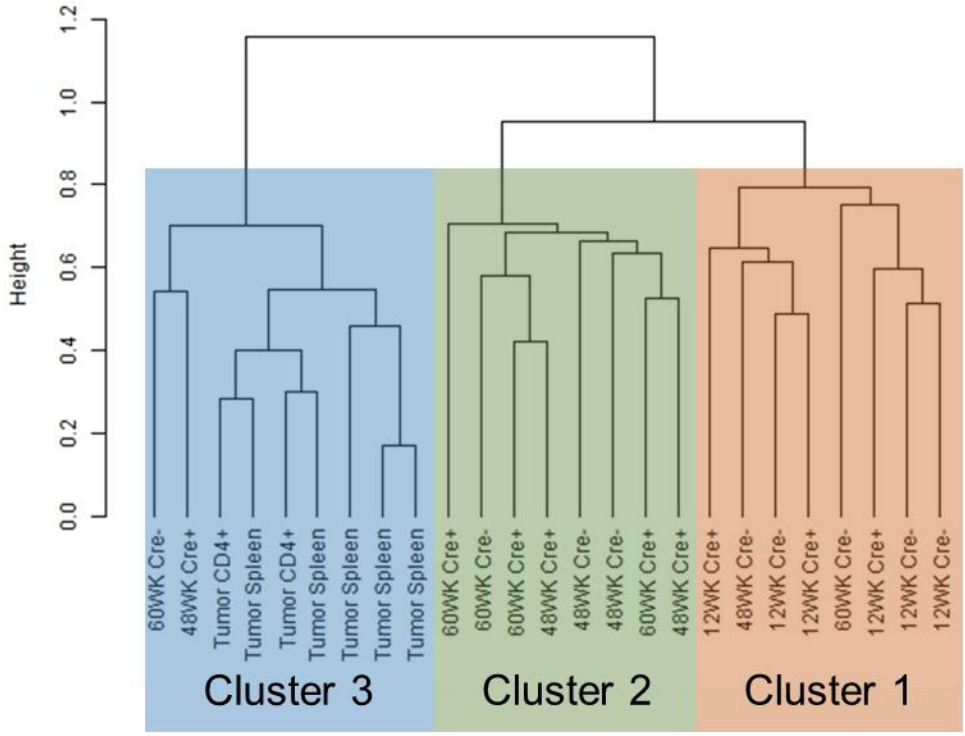

Figure 32: Unsupervised hierarchical clustering of RNA-sequencing expression data.

Unsupervised hierarchical clustering of $CD4^+$ T-cells from three pre-neoplastic time points (12, 48 and 60 weeks) and five neoplastic splenocyte samples with two corresponding neoplastic $CD4^+$ T-cells. Cluster 1 consists primarily of the youngest 12-week time point, which demonstrated minimal changes. Cluster 2 is composed of the 48 and 60 week time points with $Tet2^{-/-}$ (Cre+) samples forming smaller sub-clusters. Cluster 3 is comprised of the neoplastic cells, with corresponding $CD4^+$ T-cells and splenocytes clustering together. The cluster was performing using centered correlation and average linkage.

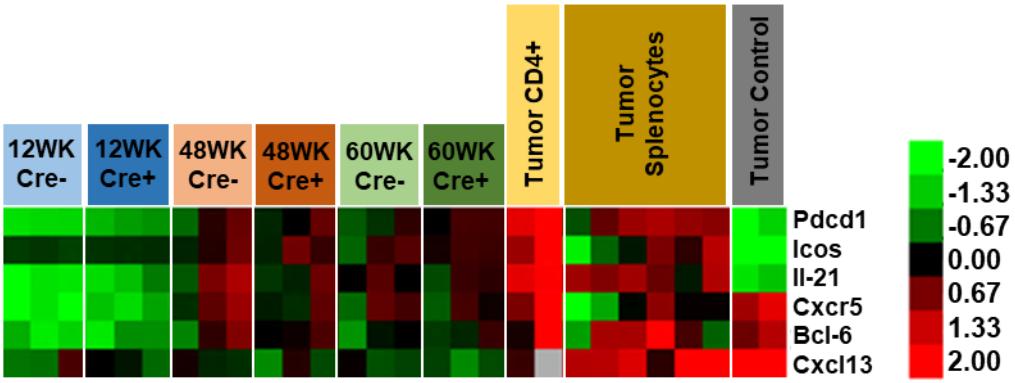

Figure 33: T_{FH} gene signature expression increased with age, with highest expression in the neoplastic cells.

Key genes expressed in T_{FH} cells were examined in RNA-sequencing data. All samples are purified $CD4^+$ T-cells, except for five tumor splenocyte samples indicated in the mustard color. At 12 weeks, minimal changes in expression are observed; however, the expression of the T_{FH} genes increased with age. The highest expression was observed in the neoplastic $CD4^+$ T-cells, and consistently seen in the neoplastic splenocytes. *Tumor control (gray) represents two age-matched WT control splenocyte samples.

DESeq was used to determine the differentially expressed genes (DEG) between WT and Tet2$^{-/-}$ CD4^{+} T-cells at the pre-neoplastic time points with a FDR ≤0.1 and a fold-change of ≥1.2. At 12 weeks, no DEGs were significant between WT and Tet2$^{-/-}$ CD4^{+} T-cells. The 48 week Tet2$^{-/-}$ CD4^{+} T-cell sample that clustered with the tumors and showed a clonal T-cell population was removed for determining the DEGs; thus, at 48 weeks only three DEGs were observed with Eif2s3y increased in Tet2$^{-/-}$ CD4^{+} T-cells and Prg4 and Clec4n decreased compared to WT. The 60-week time point had the most DEGs, with 123 having decreased expression and only nine with increased expression. Further, Clec4n overlapped between the 48 and 60-week time points as being significantly decreased in the Tet2$^{-/-}$ CD4^{+} T-cells. Thus, we observed that as cells were Tet2-deficient longer, more DEGs were identified with the majority of them having reduced expression. When comparing all WT versus all pre-neoplastic Tet2$^{-/-}$ CD4^{+} T-cells, we again observed Prg4 to be significantly decreased in Tet2$^{-/-}$ CD4^{+} T-cells; in addition to E330021D16Rik, Popdc2 and Actg2, all of which were also significantly decreased in Tet2$^{-/-}$ CD4^{+} T-cells.

Next, the two neoplastic CD4^{+} T-cell samples were compared against all 17 WT and TET2$^{-/-}$ CD4^{+} T-cell samples (excluding the 48-week sample with clonality). This comparison identified 3,047 DEGs, 816 having decreased expression and 2,231 having increased expression. DAVID was applied to the list of DEGs to identify pathway enrichments. Pathways of interest that were enriched amongst the DEGs included cytokine-cytokine receptor interaction (p≤0.001, FDR≤0.001), hematopoietic cell lineage (p≤0.001, FDR≤0.001), cell cycle (p≤0.001, FDR≤0.003), chemokine (p≤0.001, FDR=0.007), HIF-1 (p≤0.001, FDR=0.014), PI3K-AKT (p=0.004, FDR=0.05), JAK-STAT (p=0.04, FDR=0.40), NF-κB (p=0.04, FDR=0.41) and Foxo (p=0.04, FDR=0.43) signaling pathways. We have listed some pathways with higher FDR values than ideal

as they have been implicated in T-cell lymphoma previously and showed a consistent trend. We then used GSEA Preranked analysis on the list of DEG (n=6,620) disregarding the fold-change cutoff of 1.2, but maintaining the FDR requirement of ≤0.1. In doing so, we observed that the neoplastic Tet2$^{-/-}$ CD4^{+} T-cells were enriched in the PICCALUGA_ANGIOIMMUNOBLASTIC_LYMPHOMA_UP signature (p=0.001, FDR=0.041) (**Figure 34A**). Piccaluga *et al* previously published differential gene expression data between AITL and normal T-lymphocytes identified by the Affymetrix HG-U133 Plus2 platform[23]. We compared the DEGs they identified to what we observed in our neoplastic CD4^{+} T-cells compared to all pre-neoplastic CD4^{+} T-cells (WT and Tet2$^{-/-}$) . In this comparison, of the 251 genes that had a corresponding murine transcript in our data, we observed 116 genes to overlap between the two lists of DEGs. Of the 116 overlapping genes, 82 of them corresponded in either decreased or increased expression between the human and murine data, with 29 having decreased expression and 53 having increased expression. Interestingly, the 48 week Tet2$^{-/-}$ CD4^{+} T-cell sample that showed a clonal T-cell population by RNA-seq, had corresponding expression patterns to the neoplastic CD4^{+} T-cells for the genes overlapping with the human AITL, further suggesting that particular mouse had begun the malignant transformation (**Figure 34B**). Further, we profiled two age-matched WT splenocytes samples to compare against the five neoplastic splenocytes samples, identifying 1,228 DEGs between the two groups, with increased expression of 694 genes and decreased expression of 534 genes in the neoplastic splenocytes. After applying DAVID to the genes upregulated, pathways including cytokine-cytokine interaction (p≤0.001, FDR≤0.001), cell cycle (p≤0.001, FDR≤0.001), DNA replication (p≤0.001, FDR=0.004), TCR activation (p=0.005, FDR=0.063) and TCR signaling (p=0.006, FDR=0.07) were enriched.

In collaboration with the Chan Laboratory at City of Hope National Medical Center, CRISPR constructs targeting exon three or exon six of TET2 were designed. These constructs, in addition to a control construct, were used in primary human $CD3^+$ T-cells, followed by $CD4^+$ T-cell selection and maintenance in culture. RNA-seq was performed on an early time point, ~30 days in culture, and a late time point, ~100 days in culture. Using the same cut-offs as for the murine RNA-seq data, FDR <0.1 and fold-change of 1.2, we identified DEGs using DESeq. At the early time point only five DEGs were observed, of which only one had increased expression (ITGAX) in the TET2-deficient cells. Similar to the murine model, the later time point resulted in more DEGs, 639, of which 351 were increased and 288 were decreased in the TET2-deficient cells. Interestingly, a few pathways overlapped between comparison of the long-term cultured TET2-deficient human cells and control and what was observed in the murine model comparison between neoplastic $Tet2^{-/-}$ $CD4^+$ T-cells and pre-neoplastic $CD4^+$ T-cells. These overlapping pathways included cytokine-cytokine receptor interaction ($p \leq 0.001$, $FDR \leq 0.001$), chemokine signaling ($p \leq 0.001$, $FDR \leq 0.001$), hematopoietic cell lineage ($p \leq 0.001$, $FDR = 0.013$) and PI3K-AKT signaling ($p = 0.06$, $FDR = 0.525$) (**Figure 35**). Although the p-value for PI3K-AKT and the FDR is higher than ideal, we have included the PI3K-AKT pathway as it was highly significant in our murine model analysis and we have observed increased expression in a previous subset of human AITL[111].

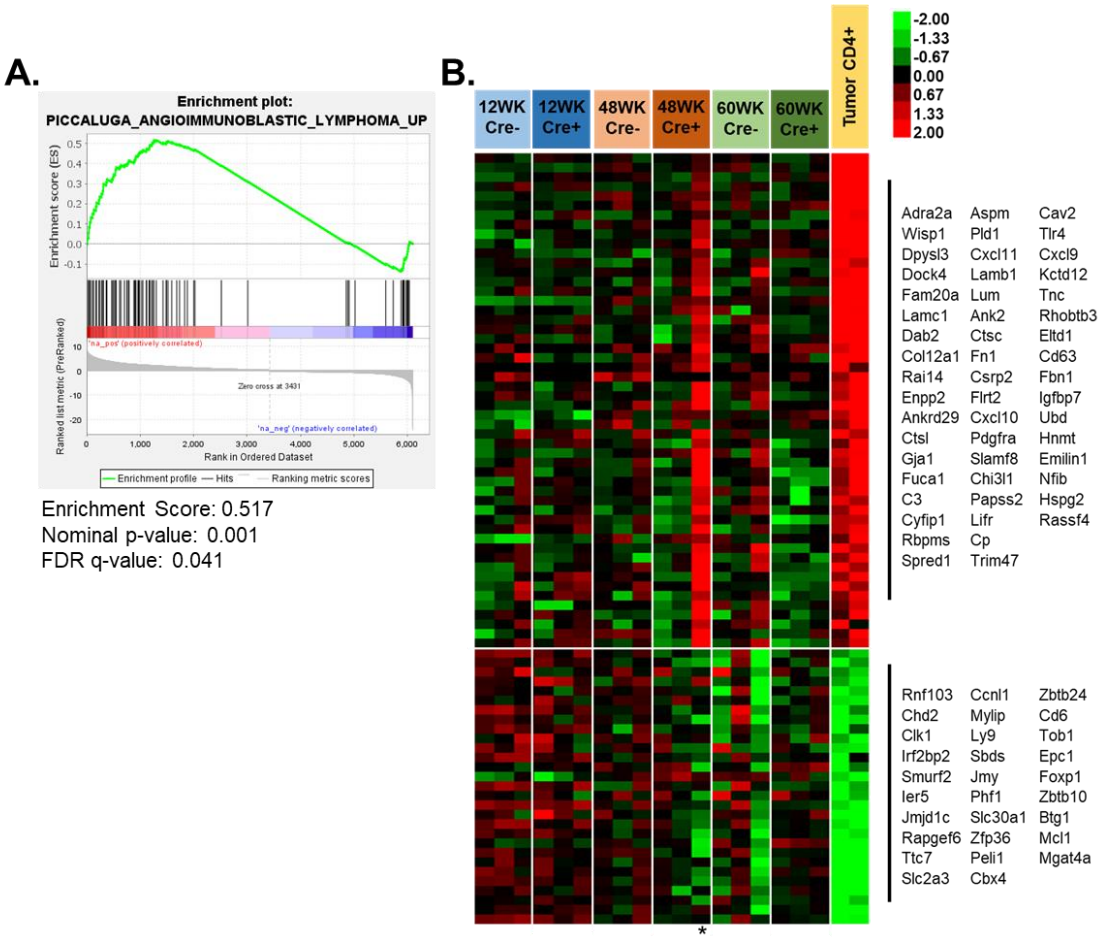

Figure 34: Enrichment of genes associated with angioimmunoblastic T-cell lymphoma in humans detected in neoplastic Tet2$^{-/-}$ CD4^{+} T-cells.

A. GSEA enrichment plot demonstrating an enrichment of the PICCALUGA_ANGIOIMMUNOBLASTIC_ LYMPHOMA_UP signature in neoplastic Tet2$^{-/-}$ CD4^{+} T-cells against all pre-neoplastic CD4^{+} T-cells in a pre-ranked differentially expressed gene list. **B.** Piccaluga *et al* previously published a list of differentially expressed genes between human AITL and normal T lymphocytes[23]. That gene list was examined against the differentially expressed genes identified from comparing neoplastic CD4^{+} T-cells against all pre-neoplastic CD4^{+} T-cells (WT and Tet2$^{-/-}$). Shown are the 82 genes that had concordant gene expression patterns in both AITL and neoplastic murine CD4^{+} T-cells. The 48 week Cre^{+} sample indicated with an "*" represents one sample which indicated clonal T-cell expansion by RNA-sequencing, suggesting it had already began malignant transformation.

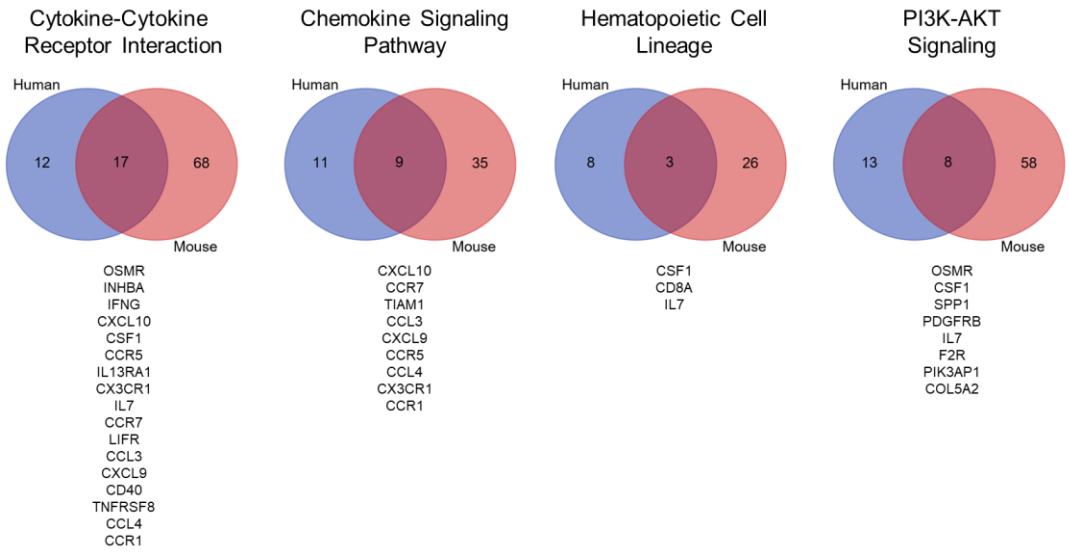

Figure 35: Overlapping gene signatures identified in human and murine cells.

Shown are four pathways of interest with overlapping differentially expressed genes between human TET2-deficient $CD4^+$ T-cells versus a wild-type controls after ~100 days in culture and murine neoplastic $Tet2^{-/-}$ $CD4^+$ T-cells versus pre-neoplastic wild-type and $Tet2^{-/-}$ $CD4^+$ T-cells.

Tet2 loss results in repression of Foxo1 and its downstream targets likely through upregulation of Icos, in turn promoting T_{FH} differentiation

As mentioned earlier, down regulation of the Foxo1 itself ($p \leq 0.001$, FDR≤0.001, log2 fold-change=-1.846) and its downstream targets was identified by DAVID in the neoplastic Tet2$^{-/-}$ CD4^{+} T-cells compared to all pre-neoplastic CD4^{+} T-cells. Foxo1 has been shown to inhibit T_{FH} cell differentiation and thus was of interest. Klf2 ($p \leq 0.001$, FDR≤0.001, log2 fold-change=-2.6), a downstream target of Foxo1, has also been implemented in regulation of T_{FH} cell differentiation. Klf2 regulates expression of Cxcr5 ($p=0.01$, FDR=0.034, log2 fold-change=1.1), Ccr7 ($p \leq 0.001$, FDR≤0.001, log2 fold-change=-3.39), Sell ($p \leq 0.001$, FDR≤0.001, log2 fold-change=-2.0), Selplg ($p \leq 0.001$, FDR≤0.001, log2 fold-change=-1.13) and S1pr1 ($p \leq 0.001$, FDR≤0.001, log2 fold-change=-2.29) as shown in **Figure 36A** and we observed significant differences in the genes between neoplastic Tet2$^{-/-}$ CD4^{+} T-cells and all pre-neoplastic CD4^{+} T-cells. Therefore, a Foxo1 signaling pathway directed towards T_{FH} differentiation was compiled from literature and viewed in the murine RNA-seq data, revealing a gradual increase in the genes expected to be overexpressed and a gradual decrease in the genes expected to decrease with the most drastic changes in the neoplastic Tet2$^{-/-}$ CD4^{+} T-cells (**Figure 36B**). We observed increased PI3K-AKT activation in the neoplastic T-cells compared to pre-neoplastic CD4^{+} T-cells ($p=0.004$, FDR=0.05). As ICOS and CD28 are both TCR co-stimulators and known to activate PI3K, we looked at changes in expression with neoplastic development. We observed no changes in CD28, but rather a significant increase of Icos in the neoplastic Tet2$^{-/-}$ CD4^{+} T-cells ($p<0.05$ for all comparisons) (**Figure 36C**). Icos has been shown to be more effective at activating PI3K and downstream AKT[15], and thus in turn inhibiting Foxo1[124]. In addition, we observe a significant enrichment of AKT in the 12 weeks and 60 weeks Tet2$^{-/-}$ CD4^{+} T-cells

compared to WT and a non-significant but positive enrichment of PI3K-AKT in the neoplastic Tet2$^{-/-}$ CD4^{+} T-cells by GSEA (**Figure 36D/E**). Unfortunately the reduced number of samples at 48 weeks limited our GSEA analysis. Although more investigation is required and we feel warranted, these observations suggest that Icos overexpression may lead to the inactivation of Foxo1 and downstream targets likely through PI3K-AKT signaling resulting in preferential T_{FH} differentiation.

Further, we have optimized the *in vitro* culture conditions for the murine CD4^{+} T-cells to allow for future investigations into PI3K-AKT and Foxo1 signaling and other oncogenic pathways. Although we used cells from 12 week old mice and saw no difference between WT and Tet2-deficienct cells, we were able to generate a prolife of proliferation, activation and apoptosis (**Figure 37**). We did observe that the cells adjusted to the change in environment, from *in vivo* to *in vitro*, after approximately 48 hours. This is seen by the increased cell counts at 48 hours and a decrease from the initial heightened levels of apoptosis. However not performed yet, we hypothesize that more drastic changes would be observed between the two genotypes at later ages as we observed that long-term loss of Tet2 was needed to see significant changes in gene expression levels. Further, we have optimized culture conditions in order to polarize to TH_1, TH_2 and T_{FH} T-cell subsets (**Table 6**). These have been validated by concordant increase of TBX21^{+} under TH_1 conditions, GATA3^{+} under TH_2 conditions and PD1^{+}/CXCR5^{+} under T_{FH} conditions detected by flow cytometry (**Figure 38**). These conditions will also be valuable for seeing if the skewing capacity of cells is different between genotypes and will allow us to look more closely at Foxo1 under T_{FH} conditions.

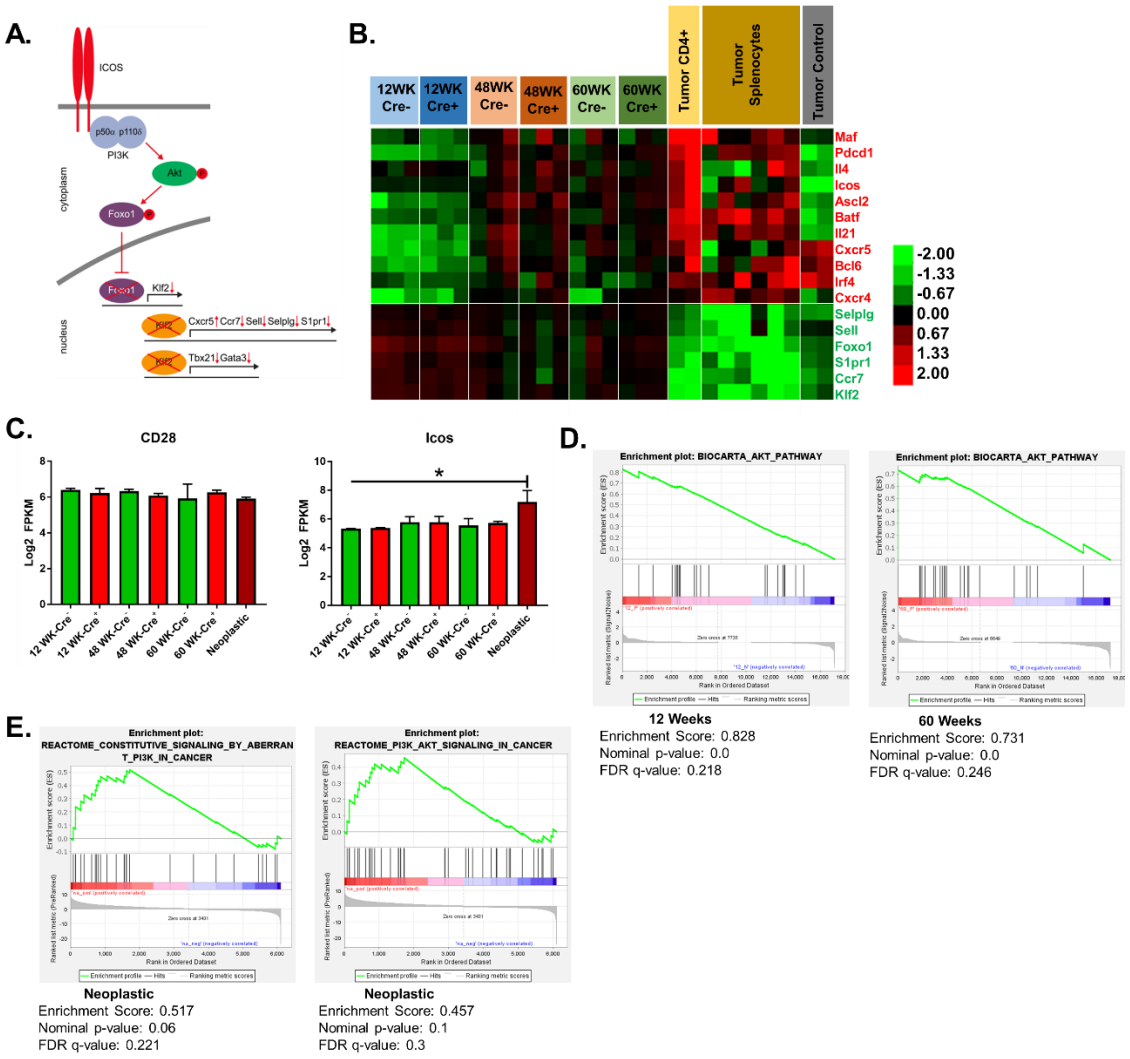

Figure 36: Increased PI3K-AKT expression and decreased expression of Foxo1 and downstream targets was observed in neoplastic Tet2$^{-/-}$ CD4^{+} T-cells.

A. Schematic of Icos signaling repressing Foxo1 and downstream target Klf2 promoting T_{FH} differentiation through upregulating Cxcr5 and downregulating Ccr7, Sell, Selplg and S1pr1. **B.** Heat map of Foxo1-related genes implicated in T_{FH} differentiation. The genes labeled in red are expected to be increased in T_{FH} differentiation as compared to the genes listed in green, which are expected to be decreased. An increase in the T_{FH} signature and decrease in Foxo1 and its downstream targets is observed in the neoplastic (tumor) cells. *Tumor control (gray) represents two age-matched wild-type control splenocyte samples. **C.** Log2 FPKM values of CD28 and Icos in CD4^{+} T-cells. Neoplastic Tet2$^{-/-}$ CD4^{+} T-cells had significantly higher expression of Icos compared to all others. **D.** GSEA enrichment plots of the BIOCARTA_AKT_PATHWAY in Tet2$^{-/-}$ CD4^{+} T-cells at 12 (left) and 60 (right) weeks compared to WT. **E.** Although not statistically significant, likely due to only have two neoplastic samples, we see enrichments in the REACTOME_CONSTITUTIVE_SIGNALING_BY_ABERRANT_PI3K_IN_CANCER (left) and REACTOME_PI3K_AKT_SIGNALING_IN_CANCER (right) by the GSEA Preranked analysis of DEGs with increased expression in neoplastic Tet2$^{-/-}$ CD4^{+} T-cells. *Panel A has been modified with permission from: Hutloff A. Regulation of T follicular helper cells by ICOS. Oncotarget. 2015;6(26):21785-21786. Creative Commons Attribution 3.0 License (https://creativecommons.org/licenses/by/3.0/)*

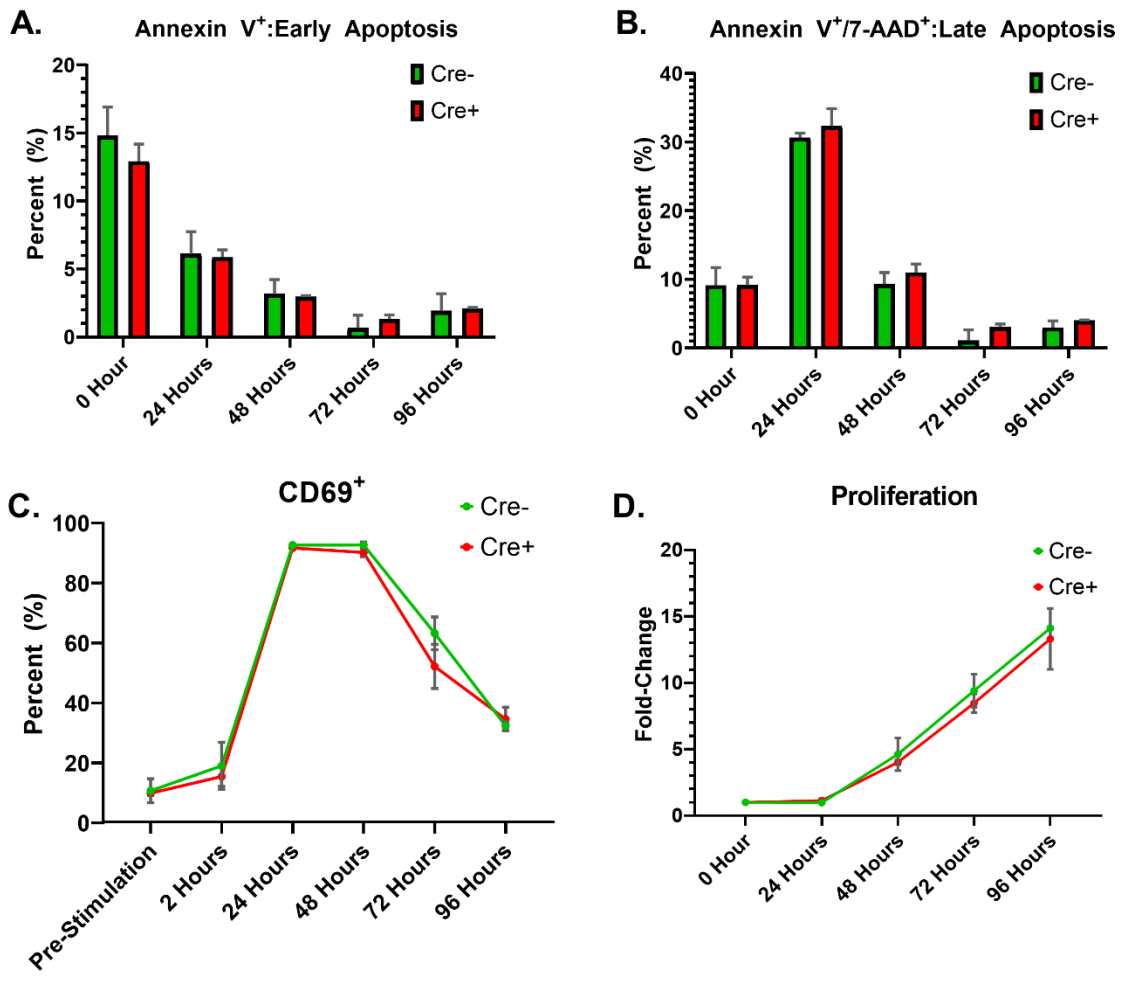

Figure 37: *In vitro* characterization of Tet2$^{-/-}$ CD4^{+} T-cells.

A and B. Apoptosis analyzed by flow cytometry determined by expression of Annexin V and 7-AAD. Comparable levels were seen between genotypes at each time point, with heightened levels during the first 24 hours *in vitro*. **C.** Flow cytometry detection of CD69 following anti-CD3/CD28 stimulation *in vitro*. This trend is commonly observed in literature, with maximal expression between 24 and 48 hours. **D.** Proliferation was detected with PrestoBlue. Similar fold-change was observed between genotypes. All experiments were performed on freshly isolated CD4+ T-cells. WT/Cre^{-}=2, Tet2$^{-/-}$/Cre^{+}=3.

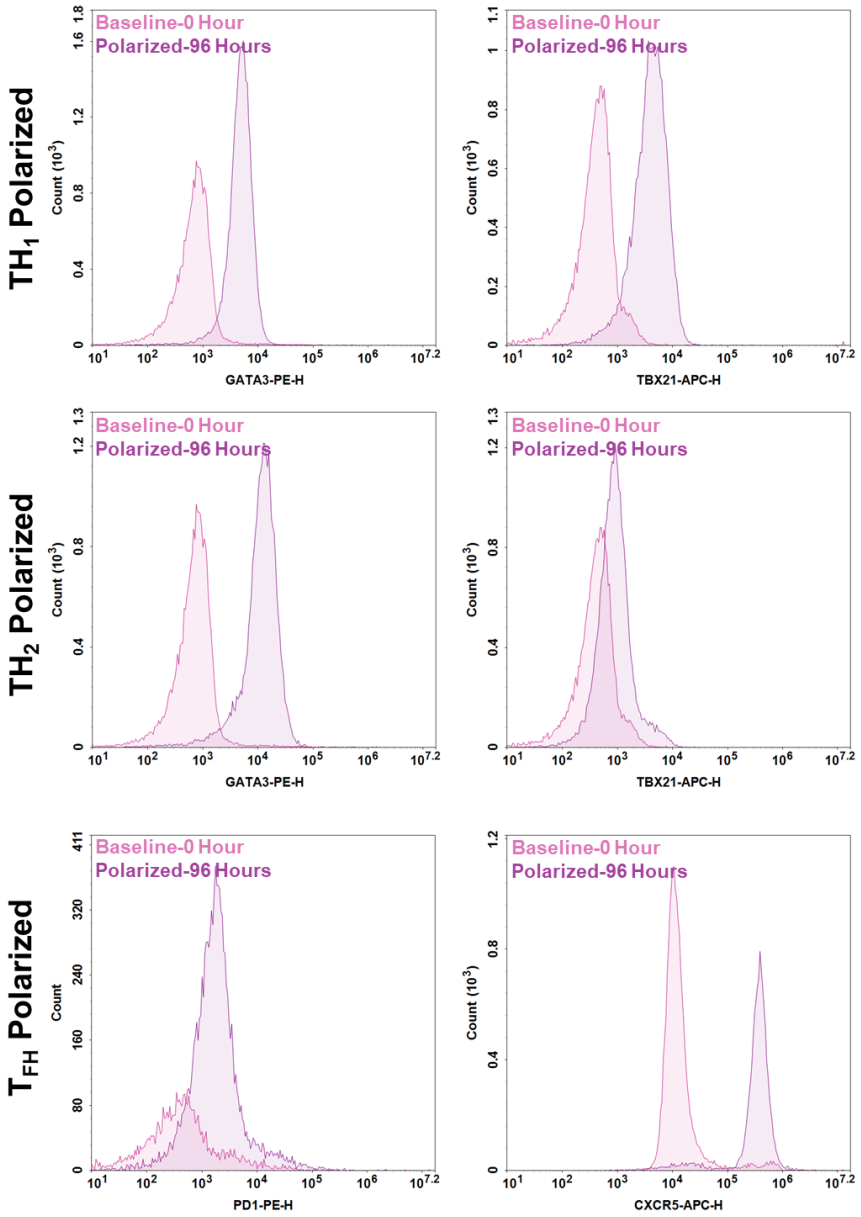

Figure 38: Flow cytometry analysis to determine TH_1, TH_2 and T_{FH} *in vitro* polarization.

Flow cytometry was performed to check key markers of TH_1, TH_2 and T_{FH} cell phenotypes. All cells were first stained for CD4 to ensure a pure culture was maintained. TH_1 polarization was detected by increased TBX21 expression. TH_2 polarization was confirmed by increased GATA3 expression. T_{FH} polarization was confirmed by increased expression of PD1 and CXCR5. The baseline expression was determined immediately after plating. Cells were maintained in polarizing conditions for 96 hours.

3.4 DISCUSSION

TET2 is critical in hematopoiesis, including regulation of the self-renewal capacity of stem cells and lineage commitment[125]. Genetic analyses of AITL revealed recurrent loss-of-function mutations of TET2 in upwards of 80% of patients. Besides AITL, TET2 is commonly mutated in a number of hematological diseases, including chronic myelomonocytic leukemia, myelodysplastic syndrome, AML, and B-cell lymphoma[125]. Heterozygous loss of TET2 due to mutation is much more frequent than homozygous loss, although both have been observed in hematological malignancies. In AITL, TET2 mutations are observed at variable VAFs, often higher than expected relative to estimated tumor content. With these observations, and the frequent observation of TET2 mutations in the HSC of the healthy elderly population with clonal hematopoiesis[126,127], TET2 is assumed to be an early arising mutation, likely requiring the accumulation of additional mutations to determine myeloid or lymphoid lineage commitment. For AITL, these additional mutations are likely RHOA and IDH2, as DNMT3A is also frequently observed in myeloid neoplasms and patients with clonal hematopoiesis[126,127].

Although we broadly know that TET2 is an epigenetic regulator modulating DNA hydroxymethylation, as we have also demonstrated with a decrease in global 5-hmC in $Tet2^{-/-}$ $CD4^+$ T-cells (**Figure 39**), the long-term loss in $CD4^+$ T-cells specifically has not been evaluated, with most models investigating earlier Tet2 knockouts or in combination with other genetic alterations. Our study has demonstrated that the long-term loss of Tet2 in $CD4^+$ T-cells alone is capable of resulting in a T-cell lymphoma with a T_{FH} immunophenotype (Icos, Bcl6, Pdcd1, Cxcr5 and Il-21) similar to AITL. Pathology review of our $Tet2^{-/-}$ tumors revealed increased CD3 and CD4 expression on the neoplastic cells, which is common in PTCL with a T_{FH} immunophenotype. Interestingly, IHC revealed sheets of large atypical B-cells in the neoplastic spleens ($CD20^+$ and $CD19^+$). In AITL, the TME is often enriched in B-cells, the majority of which are EBV^+[18]. Further,

although extremely rare, composite lymphomas comprising of both AITL and diffuse large B-cell lymphoma have been reported[128]. In our Tet2$^{-/-}$ tumors, all but one profiled, demonstrated equal and overlapping CD19/CD20 staining. However, CD19 was found aberrantly expressed compared to CD20 in one neoplastic spleen. The phenomena of neoplastic T-cells aberrantly expressing CD19 was reported in a single case report of PTCL and more frequently in AML[129,130] and thus we will further investigate the CD19^{+} population in our neoplastic sample.

Other studies have explored the homozygous loss of Tet2 in various cellular populations leading to hematological malignancy development[40,41,95,114-119]. In a cohort of 198 Tet2-null mice, a lethal hematological malignancy was observed in each mouse with survival ranging from three to 22 months, with a myeloid malignancy observed in 92%, a B-cell malignancy in 4.5% and a T-cell malignancy in only 3.5%[116]. Although T-cell lymphoma penetrance was quite low, similar phenotypes were observed (CD3^{+}, CD4^{+} and Pdcd1^{+}) with marked splenomegaly and infiltration in the spleen and liver distorting normal architecture[116]. Thymus infiltration was also frequently observed[116]; however, in our model all thymuses were already diminished in tumor-bearing mice. This difference is likely due to the type of Tet2-knockout and difference in age at lethal stage, as their median age at lethal state was less than a year (0.9)[116] whereas ours was 1.69 years.

Other Tet2-knockout models preferentially resulted in myeloid malignancies with earlier disease onset and increased LSK populations and HSC re-plating capacity[114,115,117]; however, the rare T-cell lymphomas that developed after a longer latency (median 67 weeks) often had a T_{FH} phenotype (Bcl6^{+}, Pdcd1^{+} and Cxcr5^{+}) with liver and lymph node infiltration and clonal detection[115]. Three studies have generated *in vivo* models of Tet2 loss in combination with RHOA mutation[40,41,119]. Common observances included an early autoimmune phenotype evident by skin ulcers, with lethality reached much sooner than Tet2-deficient mice alone[40,41,119]. Although these

models used adoptive cell transfer or repeated ovalbumin stimulation, two of them achieved clonal T-cell lymphoma development with a T_{FH} immunophenotype similar to AITL[40,41]; however, the third never saw malignant transformation as the autoimmunity was too severe resulting in early lethality[119]. Marked splenomegaly was consistently observed in all Tet2-deficient neoplasms in our study and previous reports[40,41,95,114,115,117]. Similar to our findings, T-cell lymphoma tumors were transplantable with accelerated malignancy into NSG[41] and Rag2/Il2rg double knockout mice[40]; however, no tumor cells were detectable ≥180 days when transferred to WT or TCRβ-knockout mice[41]. It would be of interest to determine if our tumors are highly transplantable into other strains. The ability to effectively transplant the tumors increases efficacy in future investigations as multiple tumors could be generated quicker, as primary tumor development is observed after one year.

Similar to other reports, we did not observe changes in total T and B-cell populations pre-neoplasm[115]. We did observe a gradual decrease in the Mac-1/Gr-1 ratio with age, with a more marked decrease in $Tet2^{-/-}$ mice. When looking at the $Mac\text{-}1^{+}/Gr\text{-}1^{+}$ population specifically, we do not observe any changes as the population was always less than 10%. This is reassuring that we are targeting the lymphoid lineage as other groups saw a significant increase of this population with age leading to development of a myeloid neoplasm[114,117].

Sequential RNA-seq of pre-neoplastic $CD4^{+}$ T-cells revealed that long-term loss of Tet2 resulted in an increased number of DEGs. At the later time point, the majority of DEGs were observed to have decreased expression in $Tet2^{-/-}$ $CD4^{+}$ T-cells. This is not surprising as TET2 is known to regulate DNA methylation and DNA methylation is closely associated with gene transcription. This same finding was recently observed in a Tet2 B-cell knockout model[38]. Although we have been able to detect global decreases of 5-hmC in $Tet2^{-/-}$ $CD4^{+}$ T-cells, a phenomena consistently observed in TET2-deficient

cells, completing higher-resolution methylation analysis will enable correlation between altered methylation patterns and gene expression providing further insights into the networks regulated by TET2. Like other groups, our DEGs were enriched in hematopoietic cell lineage[115], cytokine-cytokine interaction[115] and PI3K-AKT signaling signatures[40,41]; these were also observed in our *in vitro* culture system of TET2-deficient human T-cells.

Profiling of neoplastic Tet2$^{-/-}$ CD4^{+} T-cells revealed a number of oncogenic pathway enrichments (PI3K-AKT, NF-κB and JAK-STAT), but of interest was decreased Foxo1 signaling, likely mediated through increased PI3K-AKT. Previously published work found Foxo1 to be decreased in Tet2$^{-/-}$ and Tet2$^{-/-}$; RHOA^{G17V} CD4^{+} T-cells compared to WT[119]. They found that Tet2 loss resulted in increased methylation at the Foxo1 promoter[119]; however, other regions of Foxo1 were not analyzed and warrant further investigation. AKT and MST1 were evaluated as they are upstream of Foxo1 and they found that p-AKT was increased in Tet2$^{-/-}$ cells[119]. AKT is able to tri-phosphorylate Foxo1, resulting in translocation from the nucleus to the cytoplasm where it is inactive. Restoring Foxo1 expression in the Tet2$^{-/-}$; RHOA^{G17V} CD4^{+} T-cells promoted apoptosis and decreased proliferation[119]. Although not evaluated in terms of Tet2, previous work has looked at ICOS and CD28 signaling and found that ICOS is more potent at decreasing levels of Foxo1 and its downstream target Klf2 than CD28[124]. Klf2 directly binds to Cxcr5, a crucial T_{FH} factor; thus, its repression was needed to maintain a T_{FH} phenotype as blocking of ICOS and thus re-expression of Foxo1 and Klf2 reverted the T_{FH} phenotype[124]. Both ICOS and CD28 are important in T-cell activation and signaling; however, in our neoplastic T-cells, we observed a significant increase in Icos expression and no change in CD28. ICOS is characteristically high in T_{FH} cells, and our neoplastic cells have a typical T_{FH} phenotype. Although both CD28 and ICOS regulate PI3K, which regulates downstream AKT and subsequently FOXO1, ICOS has been shown to have

greater AKT activity than CD28[15] and thus may explain the preferential increase of Icos in Tet2$^{-/-}$ CD4^{+} T-cells. Foxo1 also negatively regulates Bcl6, a key transcription factor in T_{FH} differentiation, suggesting another possible need for reduced Foxo1 expression[131].

In conclusion, we have demonstrated that Tet2-loss in CD4^{+} T-cells is sufficient to generate an aggressive T-cell lymphoma at a high penetrance rate compared to other models. We have shown that Tet2-loss alone is capable of skewing CD4^{+} T-cells to a T_{FH}-phenotype, resulting in a neoplasm with atypical B-cells, which is highly similar to AITL. This model will be beneficial for investigating genes epigenetically targeted by Tet2 without effects from other mutations or chronic T-cell stimulation as used by others, as current PTCL models are far and few between.

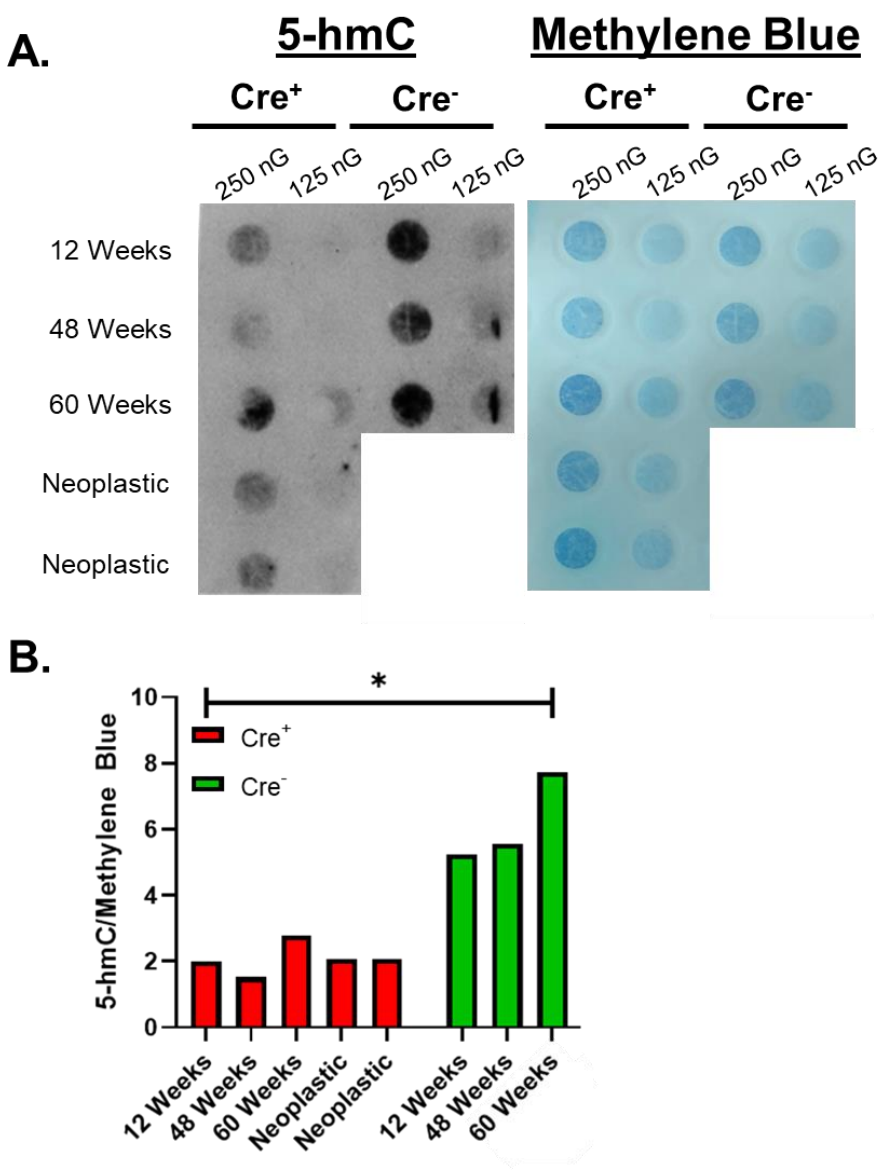

Figure 39: Tet2$^{-/-}$ CD4^{+} T-cells have a global decrease in 5-hydroxymethylcytosine levels.

A. DNA immunoblot detection of global 5-hmC levels (left) in CD4^{+} T-cells of Tet2$^{-/-}$ (Cre^{+}) and WT (Cre^{-}) mice. Methylene blue staining was done as a loading control for DNA on the sample immunobot (right). **B.** Quantification of the 5-hmC dots from the 250 nG inputs only showing a significant reduction in 5-hmC levels in Tet2$^{-/-}$ CD4^{+} T-cells. It appears that DNA in the 125 nG wells was below the detection threshold.

CHAPTER 4: DISCUSSION, CONCLUSIONS AND FUTURE DIRECTIONS

The rarity of PTCLs and the lack of representative model systems have limited our understanding of the underlying pathobiology, ultimately resulting in a lack of therapeutic advancements. Through the work presented here, we have unveiled the chromosomal abnormalities of AITL and two recently identified molecular subgroups of PTCL-NOS, PTCL-GATA3 and PTCL-TBX21. Our cohort of cases was the largest cohort of PTCL-NOS profiled to date. More importantly, our cohort was the first to have molecular subgroup classification. Similarly, our AITL cohort was also the first cohort reported to have been molecularly classified. Our lab previously defined the molecular signatures used for subgroup classification by GEP from microarray data[21,24]. These molecular subgroups were valuable in separating the heterogeneous PTCL-NOS wastebasket entity by identifying the expression of distinct transcription factors representative of the TH_1 and TH_2 lineages and unique oncogenic pathways[21]. A significant difference in OS was observed between these subgroups[21], giving more importance to being able to segregate cases within PTCL-NOS. With supportive findings from other groups, the WHO recognized the PTCL-GATA3 and PTCL-TBX21 molecular subgroups in its 2016 revision of T and NK neoplasm classification[19]. With greater value given to these molecular subgroups, we sought to identify the genomic abnormalities that distinguish these two subgroups and which downstream pathways are altered in the hopes of identifying potential future therapeutic targets unique for each subgroup.

As mentioned, PTCLs are quite rare, so it is difficult to accumulate a significant number of specimens. Consortiums have increased sample availability; however, as with many diseases, FF samples are much more limited than banked FFPE specimens are. Yet, advances in genomic technologies have improved in recent years allowing for profiling of FFPE tissues. A new technology included in our study was the OncoScan

FFPE Assay for detection of CNAs. This assay utilized molecular inversion probe technology optimized for degraded FFPE DNA, as only 40 base pairs of homology are required for probe binding. Further, this assay requires only 80 nG of input DNA, making it an option for samples with low concentration.

Examining the CNAs revealed PTCL-GATA3 to be highly aberrant compared to PTCL-TBX21. Within the PTCL-GATA3 subgroup, frequent alterations of well-known TSs including TP53, PTEN and CDKN2A were observed. Further, mutation profiling of PTCL-GATA3 revealed that all cases with a TP53 mutation also had a heterozygous loss of TP53. Interestingly, we noticed a significant co-occurrence of TP53 and PTEN deletion in PTCL-GATA3. The co-deletion of these two genes is generally uncommon in neoplasms as they are able to regulate each other through different mechanisms; therefore, we sought to delineate their function in T-cell lymphomagenesis by generating a murine model. Briefly, a member of our laboratory has begun initial exploration by generating a murine model with CD4-Cre mediated deletion of Pten and expression of mutant $Trp53^{R172H}$. We observed development of a lethal disease between 8-12 weeks of age with spleen and liver infiltration representative of a mature T-cell lymphoma as characterized by IHC ($CD3^+$, Tdt^- and $CD19^-$). Molecular characterization of the cells by RNA-seq will be valuable in determining if the disease phenotype is similar to that of the PTCL-GATA3 subgroup or TH_2 lineage, specifically. If so, this model will be valuable in exploring potential therapeutic targets, such as targeting mTOR signaling, as we have done in T-cell lines.

PTCL-TBX21 revealed much less CNAs overall, with only a few being recurrent (>20%); suggesting the need of more than genomic instability at the chromosomal level for lymphomagenesis, such as epigenetic mutations in AITL. However, it is important to note that PTCL-TBX21 is still considered to be a heterogeneous subgroup within itself.

This is mainly due to the frequent observation of a cytotoxic subgroup of cases falling within this entity, as we also observed that PTCL-TBX21 cases with an increased amount of CNAs tended to have higher expression of a cytotoxic signature. Unfortunately as detailed above, cases are quite limited and a larger cohort of PTCL-TBX21 is needed to help segregate these subgroups further. When evaluating the mutation data we generated and that previously generated in our lab, we noticed the majority of DNMT3A mutations in PTCL-TBX21 were located in the methyltransferase domain, with many at the well-known DNMT3A^{R882} hotspot. This mutation is frequently observed in MN. In particular, upwards of 60% of AML DNMT3A mutations are located at arginine 882[132], whereas although 40% of AITL harbors DNMT3A mutations, few if any mutations are detected at arginine 882 and no other recurrent sites have been detected. The arginine 882 mutation has been explored in myeloid malignancies and has demonstrated a dominant-negative effect by inhibiting the methyltransferase activity of remaining WT DNMT3A[133]. Further, AML patients with the arginine 882 mutation indicated global hypomethylation[133,134], although some promoter hypermethylation has been reported[134]. Although not yet explored in PTCLs, DNMT3A mutations have been observed in the HSCs and CD34^{+} progenitors of AML patients[135] as well as being frequently observed in the healthy elderly with clonal hematopoiesis[136]. These findings suggest that DNMT3A mutations are likely pre-malignant lesions existing for years before malignancy occurs, likely requiring the accumulation of additional mutations and/or aberrant gene expression due to changes in the methylation landscape. Recently, a small cohort of PTCL tumor samples were microdissected and sequenced and it was observed that of the 19 microdissected tumors four of the cases had the DNMT3A mutation detectable in the CD20^{+} (B-cells) and neoplastic T-cells, supporting that DNMT3A mutations are not restricted solely to the neoplastic population[89]. These findings supplied interest in further exploring the role of DNMT3A mutations in PTCL-

TBX21, specifically. A fellow member of our laboratory has observed that PTCL-TBX21 cases with a DNMT3A mutation and corresponding gene expression data have significant enrichments of cytotoxic gene signatures. These findings were validated by IHC examination of increased CD8 expression. We have begun *in vitro* experimentation to look at the effects of DNMT3A loss versus the specific arginine 882 mutation in murine and human primary T-cells. These experiments will help in revealing the difference between loss of function mutations, which are more so observed in AITL, against the hotspot mutation frequently observed in PTCL-TBX21 in a T-cell context. Using these modified cells, preferential CD4 or CD8 differentiation can be determined, as well as altered methylation patterns due to aberrant DNMT3A. Interestingly, previously work found that mice deficient for Dnmt3a in ~30% of their HSCs and progenitors developed a disease similar to chronic lymphocytic leukemia; however, 12% developed a clonal $CD8^+$ T-cell lymphoma[137]. Creating a murine model with T-cell specific knockout of Dnmt3a may result in higher penetrance of T-cell lymphoma, providing more insight into Dnmt3a's role in T-cell development and differentiation.

AITL was similar to PTCL-TBX21 in that we observed a minimally aberrant genome. Gains of chromosomes 5 and 21 were the most recurrent and tended to co-occur. These aberrations also significantly co-occurred with $IDH2^{R172}$ mutations. As we mentioned earlier, it is difficult to decipher if the gene expression changes we observed were due to chromosomal abnormalities, mutations or an altered epigenome, but more than likely a combination of all three. Since the most recurrent mutations (DNMT3A, RHOA and IDH2) co-occur with TET2 mutation in AITL, we sought to explore the effects of Tet2 loss on T-cells before evaluating its role with the addition of other mutations. To explore the role of Tet2 alone, we generated a conditional knockout model of Tet2 under CD4-Cre control, observing that long-term loss of Tet2 resulted in an aggressive T-cell lymphoma with a T_{FH} phenotype. This disease phenotype shows resemblance to AITL

and may serve as a model system for future investigations into AITL as there is currently no representative cell line or animal model. One contributing factor to the lack of an *in vitro* AITL-like cell line is that AITL relies heavily upon the microenvironment, which has proven difficult to recapitulate in culture in order to provide the required stimuli. Unfortunately, this results in cell lines such as Jurkat and HuT78, both of which are leukemic cell lines, often used as representative PTCL cell lines, however AITL and PTCL-NOS rarely have an associated leukemic phase and thus these are not very representative lines. Previous groups have achieved T-cell lymphomas with Tet2 knockouts; however, the penetrance was quite low as Tet2 was deleted in earlier cell populations most commonly resulting in MNs[95,114-117] or deleted in combination with $RHOA^{G17V}$ mutation[40,41,119], often resulting in severe autoimmune reactions often masking contributions from Tet2 itself.

Comparing our findings from the genomic CN analysis and AITL-like murine models, we observe concordant increases in the PI3K-AKT signaling pathway. This pathway was highly increased in the $Tet2^{-/-}$;$RHOA^{G17V}$ murine models[40,41] and we observed an enrichment in our single-$Tet2^{-/-}$ murine model. In our human genomic study, we observed $IDH2^{WT}$ AITL cases showed significant enrichment of PI3K-AKT activation pathways, with focal losses of PI3K-AKT negative regulators, suggesting that activation of the PI3K-AKT pathway and disturbed metabolic pathways may be unique vulnerabilities that can be exploited in AITL depending on the mutational status of RHOA and/or IDH2. $IDH2^{WT}$ cells may show a more sensitive response to PI3K-mTOR inhibitors, whereas IDH2-mutant cells may be particularly sensitive to alkylating agents[96]. Recently, Cortes et al used duvelisib, a selective small molecular PI3K δ/γ inhibitor, to block the PI3K-AKT-mTOR activation seen in their $Tet2^{-/-}$;$RHOA^{G17V}$ tumors[40]. They observed that blockade with duvelisib resulted in decreased neoplastic infiltration with

reduced proliferation and apoptosis[40]. Duvelisib was recently used to treat relapsed/refractory PTCL in a clinical trial. Improved response rates were observed in the various PTCLs[105], including AITL; however, mutation status was not known for the patients. It would be of interest to have mutation information available to see if response rates differed between different mutation co-occurrences, such as our observation of increased PI3K-AKT in $IDH2^{WT}$ compared to IDH2-mutant suggesting duvelisib may be more effective in $IDH2^{WT}$ cases. Findings such as these support the idea of performing routine targeted-sequencing panels on biopsies. Not only could knowing the mutation status of genes like TET2, DNMT3A, RHOA and IDH2 be useful in therapeutic selection, it would also be valuable in PTCL diagnosis as mutations such as IDH2 are almost exclusively observed in AITL compared to other PTCLs.

In our $Tet2^{-/-}$ murine model we observed a decrease of Foxo1-mediated signaling in our neoplastic $CD4^+$ T-cells, likely due to activation of PI3K-AKT. A previous murine model looked at Foxo1 signaling and found that Tet2 loss resulted in reduced Foxo1 expression and total protein, whereas $RHOA^{G17V}$ alone did not result in loss of expression, but rather showed increased phosphorylation-Foxo1[119]. Phosphorylated Foxo1 is considered to be inactive as it is translocated from the nucleus to the cytoplasm where it is targeted for degradation. As expected, when they evaluated the cells with combined alterations, a more marked reduction in expression and total protein level was observed[119]. These findings led to the hypothesis that Tet2 regulates Foxo1 expression through DNA demethylation, whereas RHOA likely regulates the phosphorylation and localization, in which they observed that Tet2 loss resulted in increased methylation at Foxo1 CpG promoter sites[119]. Although they found that restoring Foxo1 resulted in decreased proliferation and normal $CD4^+$ T-cell subset differentiation, much else remains unknown[119]. It is of value to note, that unlike our $Tet2^{-/-}$ model, the $CD4^+$ T-cells from their $Tet2^{-/-}$;$RHOA^{G17V}$ model did not undergo malignant transformation as RHOA

mutation resulted in an early and lethal inflammatory immune response, as seen by others[40,41,119]. The lack of malignant transformation gives an advantage to our model in being able to track the changes in Foxo1 and both upstream and downstream targets pre- and post-neoplasm.

As it appears that repression of Foxo1 is at least partially responsible for the increased T-cell survival and proliferation we observe in Tet2-deficient cells, there are a number of preliminary experiments and data analyses we propose to perform with our murine $Tet2^{-/-}$ $CD4^{+}$ T-cells. We have generated RNA-seq data on pre-neoplastic and neoplastic $Tet2^{-/-}$ $CD4^{+}$ T-cells with corresponding genome-wide 5-hmC data collected through sodium bisulfite–mediated conversion of 5-hmC to cytosine-5-methylenesulfonate containing-DNA fragments that are then immunoprecipitated. In brief, genomic DNA was sonicated using a Covaris instrument to ~200-400 base pairs, followed by an Ampure bead cleanup. Then, 400 nG of sonicated DNA was combined with 8 pG of sonicated mutant T4 DNA (all hmC). Subsequent library preparation was done with the NEB Ultra II library prep kit using barcoded Illumina adapters. Next, copy strands of the original libraries were made by primer extension amplifying from the P7 end of the DNA. The samples were then modified using T4-BGT to attach an azide-glucose to 5-hmC, followed by attaching PEG-biotin to the azide-glucose via click chemistry reaction. The biotinylated DNA was then pulled down using streptavidin beads, washed and the copy strands were then eluted from the original DNA using NaOH. The eluted DNA was used as the template for library amplification followed by sequencing to obtain the immuno-precipitated samples. For input, the DNA from step 2 was diluted and amplified using duel barcoded Truseq primers. Both the input DNA and 5-hmC enriched DNA was sequenced at 50-base pair single-end to achieve 25 million reads. We collaborated with Chan-Wang Lio at the La Jolla Institute to complete the immunoprecipitation and are currently working on data analysis, but then will be able to

integrate differential methylation peaks with differential gene expression to determine over time what effects Tet2 is having on the epigenome and consequently gene expression. Most previous efforts have focused on promoter-specific regions of select genes, limiting the broader view of Tet2's function. However, more recently it was observed that loss of Tet2 in B-cells resulted in decreased enhancer hydroxymethylation and subsequent loss of expression[38], which is more encouraging for looking at the genome-wide changes.

It will be critical to determine which upstream factors are responsible for increased ICOS and subsequent PI3K-AKT activation, while also monitoring effects on Foxo1 signaling on the Tet2-deficient background. It has been demonstrated that AKT is able to tri-phosphorylate Foxo1, resulting in its cytoplasmic localization and degradation. AKT itself must be phosphorylated at threonine 308 and serine 473 to be completely activated. This activation is highly dependent upon PI3K activity, and importantly PIP_3, PDK1 and mTORC2. Both ICOS and CD28 are important co-stimulatory receptors for the TCR and are known to activate PI3K through subunit binding. Although ICOS and CD28 have similar SH2 binding motifs, ICOS has been shown to attract the p50α subunit of PI3K whereas CD28 recruits the p85 subunit. It has been demonstrated that the p50α subunit results in higher AKT activity by having increased lipid kinase activity and subsequently higher PI3K activity[138], as compared to CD28 co-stimulation since the p50α subunit is more active than the p85 subunit. Interestingly, CD28 activating mutations have been identified in AITL[42]. Exploration into the binding ability of $CD28^{WT}$ and $CD28^{T195P}$ showed no significant difference, which the authors suggested could be due to adaptor proteins (GRB2 and GADS) having higher affinity for the T195P mutant, thus outcompeting PI3K subunits[42]. In our neoplastic $Tet2^{-/-}$ $CD4^{+}$ T-cells, we observe significantly increased expression of Icos with no change in CD28. It would also be of

value to explore Icosl (Icos ligand) expression on cells in the microenvironment to determine if they have a role in the increased Icos expression observed. It will also be of value to determine if *in vitro*, at a pre-neoplastic state, to which extent CD28 or ICOS can activate the PI3K-AKT pathway and subsequently decrease Foxo1. This can be done by culturing naïve $CD4^+$ T-cells from WT or $Tet2^{-/-}$ mice with plate bound anti-CD3 and either anti-CD28 or anti-ICOS. Although not done in context of Tet2, it has been reported that anti-ICOS resulted in a significantly increased amount of phosphorylated-Foxo1:Foxo1 and increased cytoplasmic localization compared to anti-CD28 stimulation[124]. It would be of interest to check the protein levels of PI3K subunits and phosphorylated and total AKT in both culture conditions to determine which stimulation is resulting in greater PI3K-AKT activation in cells deficient for Tet2. However, it is worthwhile to acknowledge that *in vitro* maintenance of primary cells requires the addition of interleukins, which may alter pathway activations; thus, alternative applications such as phospho-flow may be more appropriate for tracking AKT in mice.

Further, Icos has been shown to downregulate Klf2, which is a downstream target of Foxo1[124,139]. It has been shown previously that Icos blockade resulted in increased expression of Klf2, however blockade of CD28 did not result in increased Klf2 expression[124]. Interestingly, they also observed that Icos blockade decreased the amount of $CD4^+$ T-cells with a T_{FH} phenotype, but not the total $CD4^+$ T-cells, thus reverting their T_{FH} phenotype[124]. Further, they observed that Icos represses Klf2 via Foxo1 and Klf2 acts as an activator of S1pr1, Ccr7 and Selplg, while a repressor of Cxcr5[124]. Interestingly, two binding sites for Klf2 have been identified on Cxcr5 suggesting it can directly regulate its expression[124]. The downstream target S1pr1 has been briefly evaluated to determine its role in T_{FH} differentiation[139]. FTY720 treatment was used to neutralize S1pr1 activity, and they were able to conclude that although

downregulation of S1pr1 is necessary for T_{FH} differentiation, it is not the dominate means by which Klf2 regulates T_{FH} cells[139]. In addition, overexpression of Klf2 was evaluated, and as expected, resulted in impairment of T_{FH} differentiation; however, an increase of T-bet^{+} TH_1 cells was observed, suggesting Klf2 expression favors TH_1 differentiation[139].

Bcl6 is the major transcription factor for T_{FH} cells, and its regulation by Foxo1 and Klf2 has been demonstrated to an extent. When Klf2 was overexpressed, increased Prdm1/Blimp-1 was observed with a concordant decrease of Bcl6, and the opposite effect was observed with repression of Klf2[139]. Klf2 promoter binding was identified in Prdm1, however not in the Bcl6 promoter, providing additional support that decreased Bcl6 expression is a secondary effect of Klf2 expression, likely mediated through Prdm1[139]. Foxo1 has also been shown to negatively regulate Bcl6 in T_{FH} differentiation, with the identification of a highly conserved Foxo1 binding site on Bcl6[131]. However, when evaluated in Foxo1-deficient T-cells, Icos stimulation resulted in increased Bcl6 expression in Foxo1-deficient T-cells compared to WT to a greater extent than in combination with CD3, suggesting additional pathways downstream of Icos may also induce Bcl6 expression[131].

It would be of interest to examine the effect of Icos blockade in a PTCL model as it could be used to determine if other factors are upregulated or mutated to account for the loss of Icos in order to maintain the T_{FH} phenotype. Further, relapse is quite common in PTCLs so something that reverts the T_{FH} phenotype may be beneficial initially; however, it is possible that other responses could lead to stimulation and differentiation of the T_{FH} compartment again. Although few details are provided, an anti-ICOS-ligand antibody was tested on two mice in vivo that were transplanted with Tet2$^{-/-}$;RHOA^{G17V} cells, and resulted in decreased tumor proliferation and progression[40]. It would be of value to test this in our Tet2$^{-/-}$ murine model and in corresponding NSG transplants to

see if administration results in no tumor growth or at least decreased tumor burden. MEDI-570, an anti-ICOS antagonistic monoclonal antibody, is currently included in a phase I trial for patients with relapsed/refractory AITL and PTCL with a T_{FH} phenotype; however, no findings have been published yet[140]. The testing of PI3K (duvelisib, copanlisib and idelalisib) and AKT inhibitors could also be of value, but may need to be done in combination with other inhibitors as clinical trials have not found large success with these drugs in aggressive PTCLs. In addition, it is worth remembering that IDH2-mutant AITL cases did not show an increase of PI3K-AKT, therefore those cases may represent a unique subset of AITL that would require different therapeutic approaches. Although the cooperation of Tet2 and RHOA has been investigated in murine models, no data has been published on Tet2 and IDH2 combined murine models, suggesting that it could be a useful model for revealing the alternative oncogenic pathways making up for the lack of PI3K-AKT activation. Further, once the genome-wide methylation data from Tet2 loss is interrogated, demethylating agents can be considered for treatment.

Taken together, we have revealed that the AITL has a minimally aberrant genome as identified by few CN changes, supporting the idea that AITL is likely a disease driven more by an aberrant epigenome as mutations in known epigenetic regulators such as TET2, DNMT3A and IDH2 are frequent. With the lack of an AITL model system, and still much unknown about TET2's role in T-cell transformation, we sought out to establish a murine model with Tet2-deficiency in $CD4^+$ T-cells. We found increased expression of known oncogenic pathways, such as PI3K and AKT, but also observed a decrease in Foxo1 signaling, which has been implicated in T_{FH} differentiation. Our model and the data generated will enable us to further reveal and delineate the effects of aberrant DNA methylation states due to loss of Tet2, providing us

more insight into potential therapeutic targets and the importance of Tet2 mutations in AITL lymphomagenesis in a genetically representative T-cell lymphoma model.

REFERENCES

1. Congdon KL, Reya T. Divide and conquer: how asymmetric division shapes cell fate in the hematopoietic system. *Curr Opin Immunol.* 2008;20(3):302-307.
2. Kondo M. Lymphoid and myeloid lineage commitment in multipotent hematopoietic progenitors. *Immunol Rev.* 2010;238(1):37-46.
3. Iwasaki H, Akashi K. Myeloid lineage commitment from the hematopoietic stem cell. *Immunity.* 2007;26(6):726-740.
4. Lai AY, Kondo M. T and B lymphocyte differentiation from hematopoietic stem cell. *Semin Immunol.* 2008;20(4):207-212.
5. Wu L. T lineage progenitors: the earliest steps en route to T lymphocytes. *Curr Opin Immunol.* 2006;18(2):121-126.
6. Ladi E, Yin X, Chtanova T, Robey EA. Thymic microenvironments for T cell differentiation and selection. *Nat Immunol.* 2006;7(4):338-343.
7. Famili F, Wiekmeijer AS, Staal FJ. The development of T cells from stem cells in mice and humans. *Future Sci OA.* 2017;3(3):FSO186.
8. Ma J, Wang R, Fang X, Sun Z. beta-catenin/TCF-1 pathway in T cell development and differentiation. *J Neuroimmune Pharmacol.* 2012;7(4):750-762.
9. Germain RN. T-cell development and the CD4-CD8 lineage decision. *Nat Rev Immunol.* 2002;2(5):309-322.
10. Misslitz A, Pabst O, Hintzen G, Ohl L, Kremmer E, Petrie HT, Forster R. Thymic T cell development and progenitor localization depend on CCR7. *J Exp Med.* 2004;200(4):481-491.
11. Smith-Garvin JE, Koretzky GA, Jordan MS. T cell activation. *Annu Rev Immunol.* 2009;27:591-619.
12. Luckheeram RV, Zhou R, Verma AD, Xia B. CD4(+)T cells: differentiation and functions. *Clin Dev Immunol.* 2012;2012:925135.
13. Gaud G, Lesourne R, Love PE. Regulatory mechanisms in T cell receptor signalling. *Nat Rev Immunol.* 2018;18(8):485-497.
14. van Berkel ME, Oosterwegel MA. CD28 and ICOS: similar or separate costimulators of T cells? *Immunol Lett.* 2006;105(2):115-122.
15. Chen L, Flies DB. Molecular mechanisms of T cell co-stimulation and co-inhibition. *Nat Rev Immunol.* 2013;13(4):227-242.
16. Vose J, Armitage J, Weisenburger D. International peripheral T-cell and natural killer/T-cell lymphoma study: pathology findings and clinical outcomes. *Journal of clinical oncology : official journal of the American Society of Clinical Oncology.* 2008;26(25):4124-4130.
17. Swerdlow SH, Campo E, Harris NL, Jaffe E, Pileri S, Stein H, Thiele J, Vardiman JW. WHO Classification of Tumours of Haematopoietic and Lymphoid Tissues, Fourth Edition. *Revised*. 2017;2.
18. Lunning MA, Vose JM. Angioimmunoblastic T-cell lymphoma: the many-faced lymphoma. *Blood.* 2017;129(9):1095-1102.
19. Swerdlow SH, Campo E, Pileri SA, Harris NL, Stein H, Siebert R, Advani R, Ghielmini M, Salles GA, Zelenetz AD, Jaffe ES. The 2016 revision of the World Health Organization classification of lymphoid neoplasms. *Blood.* 2016;127(20):2375-2390.
20. Amador C, Greiner TC, Heavican TB, Smith LM, Galvis KT, Lone WG, Bouska A, D'Amore F, Bjerregard Pedersen M, Pileri SA, Agostinelli C, Feldman AL, Rosenwald A, Ott G, Mottok A, Savage KJ, de Leval L, Gaulard P, Lim ST, Ong CK, Ondrejka SL, Song J, Campo E, Jaffe ES, Staudt LM, Rimsza LM, Vose J, Weisenburger DD, Chan WC, Iqbal J. Reproducing the Molecular

Subclassification of Peripheral T-cell Lymphoma-NOS by Immunohistochemistry. *Blood.* 2019.

21. Iqbal J, Wright G, Wang C, Rosenwald A, Gascoyne RD, Weisenburger DD, Greiner TC, Smith L, Guo S, Wilcox RA, Teh BT, Lim ST, Tan SY, Rimsza LM, Jaffe ES, Campo E, Martinez A, Delabie J, Braziel RM, Cook JR, Tubbs RR, Ott G, Geissinger E, Gaulard P, Piccaluga PP, Pileri SA, Au WY, Nakamura S, Seto M, Berger F, de Leval L, Connors JM, Armitage J, Vose J, Chan WC, Staudt LM, Lymphoma Leukemia Molecular Profiling P, the International Peripheral TcLP. Gene expression signatures delineate biological and prognostic subgroups in peripheral T-cell lymphoma. *Blood.* 2014;123(19):2915-2923.
22. de Leval L, Rickman DS, Thielen C, Reynies A, Huang YL, Delsol G, Lamant L, Leroy K, Briere J, Molina T, Berger F, Gisselbrecht C, Xerri L, Gaulard P. The gene expression profile of nodal peripheral T-cell lymphoma demonstrates a molecular link between angioimmunoblastic T-cell lymphoma (AITL) and follicular helper T (TFH) cells. *Blood.* 2007;109(11):4952-4963.
23. Piccaluga PP, Agostinelli C, Califano A, Carbone A, Fantoni L, Ferrari S, Gazzola A, Gloghini A, Righi S, Rossi M, Tagliafico E, Zinzani PL, Zupo S, Baccarani M, Pileri SA. Gene expression analysis of angioimmunoblastic lymphoma indicates derivation from T follicular helper cells and vascular endothelial growth factor deregulation. *Cancer research.* 2007;67(22):10703-10710.
24. Iqbal J, Weisenburger DD, Greiner TC, Vose JM, McKeithan T, Kucuk C, Geng H, Deffenbacher K, Smith L, Dybkaer K, Nakamura S, Seto M, Delabie J, Berger F, Loong F, Au WY, Ko YH, Sng I, Armitage JO, Chan WC. Molecular signatures to improve diagnosis in peripheral T-cell lymphoma and prognostication in angioimmunoblastic T-cell lymphoma. *Blood.* 2010;115(5):1026-1036.
25. Krenacs L, Schaerli P, Kis G, Bagdi E. Phenotype of neoplastic cells in angioimmunoblastic T-cell lymphoma is consistent with activated follicular B helper T cells. *Blood.* 2006;108(3):1110-1111.
26. Wu H, Deng Y, Zhao M, Zhang J, Zheng M, Chen G, Li L, He Z, Lu Q. Molecular Control of Follicular Helper T cell Development and Differentiation. *Front Immunol.* 2018;9:2470.
27. Crotty S. T follicular helper cell differentiation, function, and roles in disease. *Immunity.* 2014;41(4):529-542.
28. Zhu J. T helper 2 (Th2) cell differentiation, type 2 innate lymphoid cell (ILC2) development and regulation of interleukin-4 (IL-4) and IL-13 production. *Cytokine.* 2015;75(1):14-24.
29. Hermann-Kleiter N, Baier G. NFAT pulls the strings during CD4+ T helper cell effector functions. *Blood.* 2010;115(15):2989-2997.
30. Sahoo A, Wali S, Nurieva R. T helper 2 and T follicular helper cells: Regulation and function of interleukin-4. *Cytokine Growth Factor Rev.* 2016;30:29-37.
31. Glatman Zaretsky A, Taylor JJ, King IL, Marshall FA, Mohrs M, Pearce EJ. T follicular helper cells differentiate from Th2 cells in response to helminth antigens. *J Exp Med.* 2009;206(5):991-999.
32. Odejide O, Weigert O, Lane AA, Toscano D, Lunning MA, Kopp N, Kim S, van Bodegom D, Bolla S, Schatz JH, Teruya-Feldstein J, Hochberg E, Louissaint A, Dorfman D, Stevenson K, Rodig SJ, Piccaluga PP, Jacobsen E, Pileri SA, Harris NL, Ferrero S, Inghirami G, Horwitz SM, Weinstock DM. A targeted mutational landscape of angioimmunoblastic T-cell lymphoma. *Blood.* 2014;123(9):1293-1296.
33. Vallois D, Dobay MP, Morin RD, Lemonnier F, Missiaglia E, Juilland M, Iwaszkiewicz J, Fataccioli V, Bisig B, Roberti A, Grewal J, Bruneau J, Fabiani B,

Martin A, Bonnet C, Michielin O, Jais JP, Figeac M, Bernard OA, Delorenzi M, Haioun C, Tournilhac O, Thome M, Gascoyne RD, Gaulard P, de Leval L. Activating mutations in genes related to TCR signaling in angioimmunoblastic and other follicular helper T-cell-derived lymphomas. *Blood.* 2016;128(11):1490-1502.

34. Wang C, McKeithan TW, Gong Q, Zhang W, Bouska A, Rosenwald A, Gascoyne RD, Wu X, Wang J, Muhammad Z, Jiang B, Rohr J, Cannon A, Steidl C, Fu K, Li Y, Hung S, Weisenburger DD, Greiner TC, Smith L, Ott G, Rogan EG, Staudt LM, Vose J, Iqbal J, Chan WC. IDH2R172 mutations define a unique subgroup of patients with angioimmunoblastic T-cell lymphoma. *Blood.* 2015;126(15):1741-1752.
35. Wang M, Zhang S, Chuang SS, Ashton-Key M, Ochoa E, Bolli N, Vassiliou G, Gao Z, Du MQ. Angioimmunoblastic T cell lymphoma: novel molecular insights by mutation profiling. *Oncotarget.* 2017;8(11):17763-17770.
36. Yoo HY, Sung MK, Lee SH, Kim S, Lee H, Park S, Kim SC, Lee B, Rho K, Lee JE, Cho KH, Kim W, Ju H, Kim J, Kim SJ, Kim WS, Lee S, Ko YH. A recurrent inactivating mutation in RHOA GTPase in angioimmunoblastic T cell lymphoma. *Nat Genet.* 2014;46(4):371-375.
37. Schwartz FH, Cai Q, Fellmann E, Hartmann S, Mayranpaa MI, Karjalainen-Lindsberg ML, Sundstrom C, Scholtysik R, Hansmann ML, Kuppers R. TET2 mutations in B cells of patients affected by angioimmunoblastic T-cell lymphoma. *J Pathol.* 2017;242(2):129-133.
38. Dominguez PM, Ghamlouch H, Rosikiewicz W, Kumar P, Beguelin W, Fontan L, Rivas MA, Pawlikowska P, Armand M, Mouly E, Torres-Martin M, Doane AS, Calvo Fernandez MT, Durant M, Della-Valle V, Teater M, Cimmino L, Droin N, Tadros S, Motanagh S, Shih AH, Rubin MA, Tam W, Aifantis I, Levine RL, Elemento O, Inghirami G, Green MR, Figueroa ME, Bernard OA, Aoufouchi S, Li S, Shaknovich R, Melnick AM. TET2 Deficiency Causes Germinal Center Hyperplasia, Impairs Plasma Cell Differentiation, and Promotes B-cell Lymphomagenesis. *Cancer Discov.* 2018;8(12):1632-1653.
39. Yang L, Rau R, Goodell MA. DNMT3A in haematological malignancies. *Nat Rev Cancer.* 2015;15(3):152-165.
40. Cortes JR, Ambesi-Impiombato A, Couronne L, Quinn SA, Kim CS, da Silva Almeida AC, West Z, Belver L, Martin MS, Scourzic L, Bhagat G, Bernard OA, Ferrando AA, Palomero T. RHOA G17V Induces T Follicular Helper Cell Specification and Promotes Lymphomagenesis. *Cancer Cell.* 2018;33(2):259-273 e257.
41. Ng SY, Brown L, Stevenson K, deSouza T, Aster JC, Louissaint A, Jr., Weinstock DM. RhoA G17V is sufficient to induce autoimmunity and promotes T-cell lymphomagenesis in mice. *Blood.* 2018;132(9):935-947.
42. Rohr J, Guo S, Huo J, Bouska A, Lachel C, Li Y, Simone PD, Zhang W, Gong Q, Wang C, Cannon A, Heavican T, Mottok A, Hung S, Rosenwald A, Gascoyne R, Fu K, Greiner TC, Weisenburger DD, Vose JM, Staudt LM, Xiao W, Borgstahl GE, Davis S, Steidl C, McKeithan T, Iqbal J, Chan WC. Recurrent activating mutations of CD28 in peripheral T-cell lymphomas. *Leukemia.* 2016;30(5):1062-1070.
43. Abate F, da Silva-Almeida AC, Zairis S, Robles-Valero J, Couronne L, Khiabanian H, Quinn SA, Kim MY, Laginestra MA, Kim C, Fiore D, Bhagat G, Piris MA, Campo E, Lossos IS, Bernard OA, Inghirami G, Pileri S, Bustelo XR, Rabadan R, Ferrando AA, Palomero T. Activating mutations and translocations in

the guanine exchange factor VAV1 in peripheral T-cell lymphomas. *Proc Natl Acad Sci U S A.* 2017;114(4):764-769.

44. Deng S, Lin S, Shen J, Zeng Y. Comparison of CHOP vs CHOPE for treatment of peripheral T-cell lymphoma: a meta-analysis. *Onco Targets Ther.* 2019;12:2335-2342.
45. Piekarz RL, Frye R, Prince HM, Kirschbaum MH, Zain J, Allen SL, Jaffe ES, Ling A, Turner M, Peer CJ, Figg WD, Steinberg SM, Smith S, Joske D, Lewis I, Hutchins L, Craig M, Fojo AT, Wright JJ, Bates SE. Phase 2 trial of romidepsin in patients with peripheral T-cell lymphoma. *Blood.* 2011;117(22):5827-5834.
46. O'Connor OA, Horwitz S, Masszi T, Van Hoof A, Brown P, Doorduijn J, Hess G, Jurczak W, Knoblauch P, Chawla S, Bhat G, Choi MR, Walewski J, Savage K, Foss F, Allen LF, Shustov A. Belinostat in Patients With Relapsed or Refractory Peripheral T-Cell Lymphoma: Results of the Pivotal Phase II BELIEF (CLN-19) Study. *Journal of clinical oncology : official journal of the American Society of Clinical Oncology.* 2015;33(23):2492-2499.
47. O'Connor OA, Pro B, Pinter-Brown L, Bartlett N, Popplewell L, Coiffier B, Lechowicz MJ, Savage KJ, Shustov AR, Gisselbrecht C, Jacobsen E, Zinzani PL, Furman R, Goy A, Haioun C, Crump M, Zain JM, Hsi E, Boyd A, Horwitz S. Pralatrexate in patients with relapsed or refractory peripheral T-cell lymphoma: results from the pivotal PROPEL study. *Journal of clinical oncology : official journal of the American Society of Clinical Oncology.* 2011;29(9):1182-1189.
48. Dong M, He XH, Liu P, Qin Y, Yang JL, Zhou SY, Yang S, Zhang CG, Gui L, Zhou LQ, Shi YK. Gemcitabine-based combination regimen in patients with peripheral T-cell lymphoma. *Med Oncol.* 2013;30(1):351.
49. Kim SJ, Yoon DH, Kang HJ, Kim JS, Park SK, Kim HJ, Lee J, Ryoo BY, Ko YH, Huh J, Yang WI, Kim HK, Min SK, Lee SS, Do IG, Suh C, Kim WS, Consortium for Improving Survival of Lymphoma i. Bortezomib in combination with CHOP as first-line treatment for patients with stage III/IV peripheral T-cell lymphomas: a multicentre, single-arm, phase 2 trial. *Eur J Cancer.* 2012;48(17):3223-3231.
50. Richardson NC, Kasamon YL, Chen H, de Claro RA, Ye J, Blumenthal GM, Farrell AT, Pazdur R. FDA Approval Summary: Brentuximab Vedotin in First-Line Treatment of Peripheral T-Cell Lymphoma. *Oncologist.* 2019;24(5):e180-e187.
51. Vose J, Armitage J, Weisenburger D, International TCLP. International peripheral T-cell and natural killer/T-cell lymphoma study: pathology findings and clinical outcomes. *Journal of clinical oncology : official journal of the American Society of Clinical Oncology.* 2008;26(25):4124-4130.
52. Parrilla Castellar ER, Jaffe ES, Said JW, Swerdlow SH, Ketterling RP, Knudson RA, Sidhu JS, Hsi ED, Karikehalli S, Jiang L, Vasmatzis G, Gibson SE, Ondrejka S, Nicolae A, Grogg KL, Allmer C, Ristow KM, Wilson WH, Macon WR, Law ME, Cerhan JR, Habermann TM, Ansell SM, Dogan A, Maurer MJ, Feldman AL. ALK-negative anaplastic large cell lymphoma is a genetically heterogeneous disease with widely disparate clinical outcomes. *Blood.* 2014;124(9):1473-1480.
53. Federico M, Rudiger T, Bellei M, Nathwani BN, Luminari S, Coiffier B, Harris NL, Jaffe ES, Pileri SA, Savage KJ, Weisenburger DD, Armitage JO, Mounier N, Vose JM. Clinicopathologic characteristics of angioimmunoblastic T-cell lymphoma: analysis of the international peripheral T-cell lymphoma project. *Journal of clinical oncology : official journal of the American Society of Clinical Oncology.* 2013;31(2):240-246.
54. Xu B, Liu P. No survival improvement for patients with angioimmunoblastic T-cell lymphoma over the past two decades: a population-based study of 1207 cases. *PLoS One.* 2014;9(3):e92585.

55. Iqbal J, Weisenburger DD, Greiner TC, Vose JM, McKeithan T, Kucuk C, Geng H, Deffenbacher K, Smith L, Dybkaer K, Nakamura S, Seto M, Delabie J, Berger F, Loong F, Au WY, Ko YH, Sng I, Armitage JO, Chan WC, International Peripheral TCLP. Molecular signatures to improve diagnosis in peripheral T-cell lymphoma and prognostication in angioimmunoblastic T-cell lymphoma. *Blood.* 2010;115(5):1026-1036.
56. Lemonnier F, Couronne L, Parrens M, Jais JP, Travert M, Lamant L, Tournillac O, Rousset T, Fabiani B, Cairns RA, Mak T, Bastard C, Bernard OA, de Leval L, Gaulard P. Recurrent TET2 mutations in peripheral T-cell lymphomas correlate with TFH-like features and adverse clinical parameters. *Blood.* 2012;120(7):1466-1469.
57. Cairns RA, Iqbal J, Lemonnier F, Kucuk C, de Leval L, Jais JP, Parrens M, Martin A, Xerri L, Brousset P, Chan LC, Chan WC, Gaulard P, Mak TW. IDH2 mutations are frequent in angioimmunoblastic T-cell lymphoma. *Blood.* 2012;119(8):1901-1903.
58. Couronne L, Bastard C, Bernard OA. TET2 and DNMT3A mutations in human T-cell lymphoma. *N Engl J Med.* 2012;366(1):95-96.
59. Iqbal J, Weisenburger DD, Chowdhury A, Tsai MY, Srivastava G, Greiner TC, Kucuk C, Deffenbacher K, Vose J, Smith L, Au WY, Nakamura S, Seto M, Delabie J, Berger F, Loong F, Ko YH, Sng I, Liu X, Loughran TP, Armitage J, Chan WC, International Peripheral TcLP. Natural killer cell lymphoma shares strikingly similar molecular features with a group of non-hepatosplenic gammadelta T-cell lymphoma and is highly sensitive to a novel aurora kinase A inhibitor in vitro. *Leukemia.* 2011;25(2):348-358.
60. Wang T, Feldman AL, Wada DA, Lu Y, Polk A, Briski R, Ristow K, Habermann TM, Thomas D, Ziesmer SC, Wellik LE, Lanigan TM, Witzig TE, Pittelkow MR, Bailey NG, Hristov AC, Lim MS, Ansell SM, Wilcox RA. GATA-3 expression identifies a high-risk subset of PTCL, NOS with distinct molecular and clinical features. *Blood.* 2014;123(19):3007-3015.
61. Piccaluga PP, Fuligni F, De Leo A, Bertuzzi C, Rossi M, Bacci F, Sabattini E, Agostinelli C, Gazzola A, Laginestra MA, Mannu C, Sapienza MR, Hartmann S, Hansmann ML, Piva R, Iqbal J, Chan JC, Weisenburger D, Vose JM, Bellei M, Federico M, Inghirami G, Zinzani PL, Pileri SA. Molecular profiling improves classification and prognostication of nodal peripheral T-cell lymphomas: results of a phase III diagnostic accuracy study. *Journal of clinical oncology : official journal of the American Society of Clinical Oncology.* 2013;31(24):3019-3025.
62. Dobay MP, Lemonnier F, Missiaglia E, Bastard C, Vallois D, Jais JP, Scourzic L, Dupuy A, Fataccioli V, Pujals A, Parrens M, Le Bras F, Rousset T, Picquenot JM, Martin N, Haioun C, Delarue R, Bernard OA, Delorenzi M, de Leval L, Gaulard P. Integrative clinicopathological and molecular analyses of angioimmunoblastic T-cell lymphoma and other nodal lymphomas of follicular helper T-cell origin. *Haematologica.* 2017;102(4):e148-e151.
63. Kuilman T, Velds A, Kemper K, Ranzani M, Bombardelli L, Hoogstraat M, Nevedomskaya E, Xu G, de Ruiter J, Lolkema MP, Ylstra B, Jonkers J, Rottenberg S, Wessels LF, Adams DJ, Peeper DS, Krijgsman O. CopywriteR: DNA copy number detection from off-target sequence data. *Genome Biol.* 2015;16:49.
64. Boi M, Rinaldi A, Kwee I, Bonetti P, Todaro M, Tabbo F, Piva R, Rancoita PM, Matolcsy A, Timar B, Tousseyn T, Rodriguez-Pinilla SM, Piris MA, Bea S, Campo E, Bhagat G, Swerdlow SH, Rosenwald A, Ponzoni M, Young KH, Piccaluga PP, Dummer R, Pileri S, Zucca E, Inghirami G, Bertoni F. PRDM1/BLIMP1 is

commonly inactivated in anaplastic large T-cell lymphoma. *Blood.* 2013;122(15):2683-2693.

65. Hartmann S, Gesk S, Scholtysik R, Kreuz M, Bug S, Vater I, Doring C, Cogliatti S, Parrens M, Merlio JP, Kwiecinska A, Porwit A, Piccaluga PP, Pileri S, Hoefler G, Kuppers R, Siebert R, Hansmann ML. High resolution SNP array genomic profiling of peripheral T cell lymphomas, not otherwise specified, identifies a subgroup with chromosomal aberrations affecting the REL locus. *British journal of haematology.* 2010;148(3):402-412.
66. Lin WM, Lewis JM, Filler RB, Modi BG, Carlson KR, Reddy S, Thornberg A, Saksena G, Umlauf S, Oberholzer PA, Karpova M, Getz G, Mane S, Garraway LA, Dummer R, Berger CL, Edelson RL, Girardi M. Characterization of the DNA copy-number genome in the blood of cutaneous T-cell lymphoma patients. *J Invest Dermatol.* 2012;132(1):188-197.
67. Nakagawa M, Nakagawa-Oshiro A, Karnan S, Tagawa H, Utsunomiya A, Nakamura S, Takeuchi I, Ohshima K, Seto M. Array comparative genomic hybridization analysis of PTCL-U reveals a distinct subgroup with genetic alterations similar to lymphoma-type adult T-cell leukemia/lymphoma. *Clin Cancer Res.* 2009;15(1):30-38.
68. Yamagishi M, Nakano K, Miyake A, Yamochi T, Kagami Y, Tsutsumi A, Matsuda Y, Sato-Otsubo A, Muto S, Utsunomiya A, Yamaguchi K, Uchimaru K, Ogawa S, Watanabe T. Polycomb-mediated loss of miR-31 activates NIK-dependent NF-kappaB pathway in adult T cell leukemia and other cancers. *Cancer Cell.* 2012;21(1):121-135.
69. Ehrentraut S, Schneider B, Nagel S, Pommerenke C, Quentmeier H, Geffers R, Feist M, Kaufmann M, Meyer C, Kadin ME, Drexler HG, MacLeod RA. Th17 cytokine differentiation and loss of plasticity after SOCS1 inactivation in a cutaneous T-cell lymphoma. *Oncotarget.* 2016;7(23):34201-34216.
70. Piva R, Pellegrino E, Mattioli M, Agnelli L, Lombardi L, Boccalatte F, Costa G, Ruggeri BA, Cheng M, Chiarle R, Palestro G, Neri A, Inghirami G. Functional validation of the anaplastic lymphoma kinase signature identifies CEBPB and BCL2A1 as critical target genes. *The Journal of clinical investigation.* 2006;116(12):3171-3182.
71. An J, Fujiwara H, Suemori K, Niiya T, Azuma T, Tanimoto K, Ochi T, Akatsuka Y, Mineno J, Ozawa H, Ishikawa F, Kuzushima K, Yasukawa M. Activation of T-cell receptor signaling in peripheral T-cell lymphoma cells plays an important role in the development of lymphoma-associated hemophagocytosis. *International journal of hematology.* 2011;93(2):176-185.
72. Kadin ME, Cavaille-Coll MW, Gertz R, Massague J, Cheifetz S, George D. Loss of receptors for transforming growth factor beta in human T-cell malignancies. *Proc Natl Acad Sci U S A.* 1994;91(13):6002-6006.
73. Trapnell C, Roberts A, Goff L, Pertea G, Kim D, Kelley DR, Pimentel H, Salzberg SL, Rinn JL, Pachter L. Differential gene and transcript expression analysis of RNA-seq experiments with TopHat and Cufflinks. *Nat Protoc.* 2012;7(3):562-578.
74. Johnson WE, Li C, Rabinovic A. Adjusting batch effects in microarray expression data using empirical Bayes methods. *Biostatistics.* 2007;8(1):118-127.
75. Carter SL, Cibulskis K, Helman E, McKenna A, Shen H, Zack T, Laird PW, Onofrio RC, Winckler W, Weir BA, Beroukhim R, Pellman D, Levine DA, Lander ES, Meyerson M, Getz G. Absolute quantification of somatic DNA alterations in human cancer. *Nat Biotechnol.* 2012;30(5):413-421.
76. de Figueiredo AF, Capela de Matos RR, Othman MA, Liehr T, da Costa ES, Land MG, Ribeiro RC, Abdelhay E, Silva ML. Molecular cytogenetic studies

characterizing a novel complex karyotype with an uncommon 5q22 deletion in childhood acute myeloid leukemia. *Mol Cytogenet.* 2015;8:62.
77. Fang J, Barker B, Bolanos L, Liu X, Jerez A, Makishima H, Christie S, Chen X, Rao DS, Grimes HL, Komurov K, Weirauch MT, Cancelas JA, Maciejewski JP, Starczynowski DT. Myeloid malignancies with chromosome 5q deletions acquire a dependency on an intrachromosomal NF-kappaB gene network. *Cell Rep.* 2014;8(5):1328-1338.
78. Zhu J, Yamane H, Paul WE. Differentiation of effector CD4 T cell populations (*). *Annu Rev Immunol.* 2010;28:445-489.
79. Weinstein JS, Lezon-Geyda K, Maksimova Y, Craft S, Zhang Y, Su M, Schulz VP, Craft J, Gallagher PG. Global transcriptome analysis and enhancer landscape of human primary T follicular helper and T effector lymphocytes. *Blood.* 2014;124(25):3719-3729.
80. Song MS, Salmena L, Pandolfi PP. The functions and regulation of the PTEN tumour suppressor. *Nat Rev Mol Cell Biol.* 2012;13(5):283-296.
81. Leiserson MD, Wu HT, Vandin F, Raphael BJ. CoMEt: a statistical approach to identify combinations of mutually exclusive alterations in cancer. *Genome Biol.* 2015;16:160.
82. Vallois D, Dupuy A, Lemonnier F, Allen G, Missiaglia E, Fataccioli V, Ortonne N, Clavert A, Delarue R, Rousselet MC, Fabiani B, Llamas-Gutierrez F, Ogawa S, Thome M, Ko YH, Kataoka K, Gaulard P, de Leval L. RNA fusions involving CD28 are rare in peripheral T-cell lymphomas and concentrate mainly in those derived from follicular helper T cells. *Haematologica.* 2018;103(8):e360-e363.
83. Califano D, Sweeney KJ, Le H, VanValkenburgh J, Yager E, O'Connor W, Jr., Kennedy JS, Jones DM, Avram D. Diverting T helper cell trafficking through increased plasticity attenuates autoimmune encephalomyelitis. *The Journal of clinical investigation.* 2014;124(1):174-187.
84. Marsland BJ, Soos TJ, Spath G, Littman DR, Kopf M. Protein kinase C theta is critical for the development of in vivo T helper (Th)2 cell but not Th1 cell responses. *J Exp Med.* 2004;200(2):181-189.
85. Newman AM, Liu CL, Green MR, Gentles AJ, Feng W, Xu Y, Hoang CD, Diehn M, Alizadeh AA. Robust enumeration of cell subsets from tissue expression profiles. *Nat Methods.* 2015;12(5):453-457.
86. Sundrud MS, Grill SM, Ni D, Nagata K, Alkan SS, Subramaniam A, Unutmaz D. Genetic reprogramming of primary human T cells reveals functional plasticity in Th cell differentiation. *J Immunol.* 2003;171(7):3542-3549.
87. Amador C, Greiner TC, Heavican T, Lone W, Smith L, Bouska A, Yu J, Mottok A, Rosenwald A, Ott G, Ondrejka S, Rimsza L, Weisenburger D, Chan WC, Iqbal J. An Immunohistochemistry Algorithm Subclassifies PTCL-NOS into Gene Expression Profiling Defined Molecular Subgroups with High Accuracy. Paper presented at: 107TH Annual United States and Canadian Academy of Pathology; 3/20/2018, 2018; Vancouver, BC, Canada.
88. Wang C, McKeithan TW, Gong Q, Zhang W, Bouska A, Rosenwald A, Gascoyne RD, Wu X, Wang J, Muhammad Z, Jiang B, Rohr J, Cannon A, Steidl C, Fu K, Li Y, Hung S, Weisenburger DD, Greiner TC, Smith L, Ott G, Rogan EG, Staudt LM, Vose J, Iqbal J, Chan WC. IDH2R172 mutations define a unique subgroup of patients with angioimmunoblastic T-cell lymphoma. *Blood.* 2015.
89. Nguyen TB, Sakata-Yanagimoto M, Asabe Y, Matsubara D, Kano J, Yoshida K, Shiraishi Y, Chiba K, Tanaka H, Miyano S, Izutsu K, Nakamura N, Takeuchi K, Miyoshi H, Ohshima K, Minowa T, Ogawa S, Noguchi M, Chiba S. Identification

of cell-type-specific mutations in nodal T-cell lymphomas. *Blood Cancer J.* 2017;7(1):e516.
90. Nelson M, Horsman DE, Weisenburger DD, Gascoyne RD, Dave BJ, Loberiza FR, Ludkovski O, Savage KJ, Armitage JO, Sanger WG. Cytogenetic abnormalities and clinical correlations in peripheral T-cell lymphoma. *British journal of haematology.* 2008;141(4):461-469.
91. Schlegelberger B, Zwingers T, Hohenadel K, Henne-Bruns D, Schmitz N, Haferlach T, Tirier C, Bartels H, Sonnen R, Kuse R, et al. Significance of cytogenetic findings for the clinical outcome in patients with T-cell lymphoma of angioimmunoblastic lymphadenopathy type. *Journal of clinical oncology : official journal of the American Society of Clinical Oncology.* 1996;14(2):593-599.
92. Fujiwara SI, Yamashita Y, Nakamura N, Choi YL, Ueno T, Watanabe H, Kurashina K, Soda M, Enomoto M, Hatanaka H, Takada S, Abe M, Ozawa K, Mano H. High-resolution analysis of chromosome copy number alterations in angioimmunoblastic T-cell lymphoma and peripheral T-cell lymphoma, unspecified, with single nucleotide polymorphism-typing microarrays. *Leukemia.* 2008;22(10):1891-1898.
93. Thorns C, Bastian B, Pinkel D, Roydasgupta R, Fridlyand J, Merz H, Krokowski M, Bernd HW, Feller AC. Chromosomal aberrations in angioimmunoblastic T-cell lymphoma and peripheral T-cell lymphoma unspecified: A matrix-based CGH approach. *Genes Chromosomes Cancer.* 2007;46(1):37-44.
94. Schlegelberger B, Zhang Y, Weber-Matthiesen K, Grote W. Detection of aberrant clones in nearly all cases of angioimmunoblastic lymphadenopathy with dysproteinemia-type T-cell lymphoma by combined interphase and metaphase cytogenetics. *Blood.* 1994;84(8):2640-2648.
95. Li Z, Cai X, Cai CL, Wang J, Zhang W, Petersen BE, Yang FC, Xu M. Deletion of Tet2 in mice leads to dysregulated hematopoietic stem cells and subsequent development of myeloid malignancies. *Blood.* 2011;118(17):4509-4518.
96. Wang P, Wu J, Ma S, Zhang L, Yao J, Hoadley KA, Wilkerson MD, Perou CM, Guan KL, Ye D, Xiong Y. Oncometabolite D-2-Hydroxyglutarate Inhibits ALKBH DNA Repair Enzymes and Sensitizes IDH Mutant Cells to Alkylating Agents. *Cell Rep.* 2015;13(11):2353-2361.
97. Manso R, Gonzalez-Rincon J, Rodriguez-Justo M, Roncador G, Gomez S, Sanchez-Beato M, Piris MA, Rodriguez-Pinilla SM. Overlap at the molecular and immunohistochemical levels between angioimmunoblastic T-cell lymphoma and a subgroup of peripheral T-cell lymphomas without specific morphological features. *Oncotarget.* 2018;9(22):16124-16133.
98. Sugio T, Miyawaki K, Kato K, Sasaki K, Yamada K, Iqbal J, Miyamoto T, Ohshima K, Maeda T, Miyoshi H, Akashi K. Microenvironmental immune cell signatures dictate clinical outcomes for PTCL-NOS. *Blood Adv.* 2018;2(17):2242-2252.
99. Liang J, Saad Y, Lei T, Wang J, Qi D, Yang Q, Kolattukudy PE, Fu M. MCP-induced protein 1 deubiquitinates TRAF proteins and negatively regulates JNK and NF-kappaB signaling. *J Exp Med.* 2010;207(13):2959-2973.
100. Mihaylova MM, Shaw RJ. The AMPK signalling pathway coordinates cell growth, autophagy and metabolism. *Nat Cell Biol.* 2011;13(9):1016-1023.
101. Trotman LC, Pandolfi PP. PTEN and p53: who will get the upper hand? *Cancer Cell.* 2003;3(2):97-99.
102. Stambolic V, MacPherson D, Sas D, Lin Y, Snow B, Jang Y, Benchimol S, Mak TW. Regulation of PTEN transcription by p53. *Mol Cell.* 2001;8(2):317-325.

103. Mayo LD, Dixon JE, Durden DL, Tonks NK, Donner DB. PTEN protects p53 from Mdm2 and sensitizes cancer cells to chemotherapy. *J Biol Chem.* 2002;277(7):5484-5489.
104. Freeman DJ, Li AG, Wei G, Li HH, Kertesz N, Lesche R, Whale AD, Martinez-Diaz H, Rozengurt N, Cardiff RD, Liu X, Wu H. PTEN tumor suppressor regulates p53 protein levels and activity through phosphatase-dependent and -independent mechanisms. *Cancer Cell.* 2003;3(2):117-130.
105. Horwitz SM, Koch R, Porcu P, Oki Y, Moskowitz A, Perez M, Myskowski P, Officer A, Jaffe JD, Morrow SN, Allen K, Douglas M, Stern H, Sweeney J, Kelly P, Kelly V, Aster JC, Weaver D, Foss FM, Weinstock DM. Activity of the PI3K-delta,gamma inhibitor duvelisib in a phase 1 trial and preclinical models of T-cell lymphoma. *Blood.* 2018;131(8):888-898.
106. Waickman AT, Powell JD. mTOR, metabolism, and the regulation of T-cell differentiation and function. *Immunol Rev.* 2012;249(1):43-58.
107. Delgoffe GM, Pollizzi KN, Waickman AT, Heikamp E, Meyers DJ, Horton MR, Xiao B, Worley PF, Powell JD. The kinase mTOR regulates the differentiation of helper T cells through the selective activation of signaling by mTORC1 and mTORC2. *Nat Immunol.* 2011;12(4):295-303.
108. Song J, Salek-Ardakani S, So T, Croft M. The kinases aurora B and mTOR regulate the G1-S cell cycle progression of T lymphocytes. *Nat Immunol.* 2007;8(1):64-73.
109. Feng Z, Zhang H, Levine AJ, Jin S. The coordinate regulation of the p53 and mTOR pathways in cells. *Proc Natl Acad Sci U S A.* 2005;102(23):8204-8209.
110. de Leval L, Gaulard P. Cellular origin of T-cell lymphomas. *Blood.* 2014;123(19):2909-2910.
111. Heavican TB, Bouska A, Yu J, Lone W, Amador C, Gong Q, Zhang W, Li Y, Dave BJ, Nairismagi ML, Greiner TC, Vose J, Weisenburger DD, Lachel C, Wang C, Fu K, Stevens JM, Lim ST, Ong CK, Gascoyne RD, Missiaglia E, Lemonnier F, Haioun C, Hartmann S, Pedersen MB, Laginestra MA, Wilcox RA, Teh BT, Yoshida N, Ohshima K, Seto M, Rosenwald A, Ott G, Campo E, Rimsza LM, Jaffe ES, Braziel RM, d'Amore F, Inghirami G, Bertoni F, de Leval L, Gaulard P, Staudt LM, McKeithan TW, Pileri S, Chan WC, Iqbal J. Genetic drivers of oncogenic pathways in molecular subgroups of peripheral T-cell lymphoma. *Blood.* 2019.
112. Sakata-Yanagimoto M, Enami T, Yoshida K, Shiraishi Y, Ishii R, Miyake Y, Muto H, Tsuyama N, Sato-Otsubo A, Okuno Y, Sakata S, Kamada Y, Nakamoto-Matsubara R, Tran NB, Izutsu K, Sato Y, Ohta Y, Furuta J, Shimizu S, Komeno T, Sato Y, Ito T, Noguchi M, Noguchi E, Sanada M, Chiba K, Tanaka H, Suzukawa K, Nanmoku T, Hasegawa Y, Nureki O, Miyano S, Nakamura N, Takeuchi K, Ogawa S, Chiba S. Somatic RHOA mutation in angioimmunoblastic T cell lymphoma. *Nat Genet.* 2014;46(2):171-175.
113. Ko M, An J, Pastor WA, Koralov SB, Rajewsky K, Rao A. TET proteins and 5-methylcytosine oxidation in hematological cancers. *Immunol Rev.* 2015;263(1):6-21.
114. Moran-Crusio K, Reavie L, Shih A, Abdel-Wahab O, Ndiaye-Lobry D, Lobry C, Figueroa ME, Vasanthakumar A, Patel J, Zhao X, Perna F, Pandey S, Madzo J, Song C, Dai Q, He C, Ibrahim S, Beran M, Zavadil J, Nimer SD, Melnick A, Godley LA, Aifantis I, Levine RL. Tet2 loss leads to increased hematopoietic stem cell self-renewal and myeloid transformation. *Cancer Cell.* 2011;20(1):11-24.

115. Muto H, Sakata-Yanagimoto M, Nagae G, Shiozawa Y, Miyake Y, Yoshida K, Enami T, Kamada Y, Kato T, Uchida K, Nanmoku T, Obara N, Suzukawa K, Sanada M, Nakamura N, Aburatani H, Ogawa S, Chiba S. Reduced TET2 function leads to T-cell lymphoma with follicular helper T-cell-like features in mice. *Blood Cancer J.* 2014;4:e264.
116. Pan F, Wingo TS, Zhao Z, Gao R, Makishima H, Qu G, Lin L, Yu M, Ortega JR, Wang J, Nazha A, Chen L, Yao B, Liu C, Chen S, Weeks O, Ni H, Phillips BL, Huang S, Wang J, He C, Li GM, Radivoyevitch T, Aifantis I, Maciejewski JP, Yang FC, Jin P, Xu M. Tet2 loss leads to hypermutagenicity in haematopoietic stem/progenitor cells. *Nat Commun.* 2017;8:15102.
117. Quivoron C, Couronne L, Della Valle V, Lopez CK, Plo I, Wagner-Ballon O, Do Cruzeiro M, Delhommeau F, Arnulf B, Stern MH, Godley L, Opolon P, Tilly H, Solary E, Duffourd Y, Dessen P, Merle-Beral H, Nguyen-Khac F, Fontenay M, Vainchenker W, Bastard C, Mercher T, Bernard OA. TET2 inactivation results in pleiotropic hematopoietic abnormalities in mouse and is a recurrent event during human lymphomagenesis. *Cancer Cell.* 2011;20(1):25-38.
118. Scourzic L, Couronne L, Pedersen MT, Della Valle V, Diop M, Mylonas E, Calvo J, Mouly E, Lopez CK, Martin N, Fontenay M, Bender A, Guibert S, Dubreuil P, Dessen P, Droin N, Pflumio F, Weber M, Gaulard P, Helin K, Mercher T, Bernard OA. DNMT3A(R882H) mutant and Tet2 inactivation cooperate in the deregulation of DNA methylation control to induce lymphoid malignancies in mice. *Leukemia.* 2016;30(6):1388-1398.
119. Zang S, Li J, Yang H, Zeng H, Han W, Zhang J, Lee M, Moczygemba M, Isgandarova S, Yang Y, Zhou Y, Rao A, You MJ, Sun D, Huang Y. Mutations in 5-methylcytosine oxidase TET2 and RhoA cooperatively disrupt T cell homeostasis. *The Journal of clinical investigation.* 2017;127(8):2998-3012.
120. Dobin A, Davis CA, Schlesinger F, Drenkow J, Zaleski C, Jha S, Batut P, Chaisson M, Gingeras TR. STAR: ultrafast universal RNA-seq aligner. *Bioinformatics.* 2013;29(1):15-21.
121. Anders S, Pyl PT, Huber W. HTSeq--a Python framework to work with high-throughput sequencing data. *Bioinformatics.* 2015;31(2):166-169.
122. Bolotin DA, Poslavsky S, Mitrophanov I, Shugay M, Mamedov IZ, Putintseva EV, Chudakov DM. MiXCR: software for comprehensive adaptive immunity profiling. *Nat Methods.* 2015;12(5):380-381.
123. Gong Q, Wang C, Zhang W, Iqbal J, Hu Y, Greiner TC, Cornish A, Kim JH, Rabadan R, Abate F, Wang X, Inghirami GG, McKeithan TW, Chan WC. Assessment of T-cell receptor repertoire and clonal expansion in peripheral T-cell lymphoma using RNA-seq data. *Sci Rep.* 2017;7(1):11301.
124. Weber JP, Fuhrmann F, Feist RK, Lahmann A, Al Baz MS, Gentz LJ, Vu Van D, Mages HW, Haftmann C, Riedel R, Grun JR, Schuh W, Kroczek RA, Radbruch A, Mashreghi MF, Hutloff A. ICOS maintains the T follicular helper cell phenotype by down-regulating Kruppel-like factor 2. *J Exp Med.* 2015;212(2):217-233.
125. Feng Y, Li X, Cassady K, Zou Z, Zhang X. TET2 Function in Hematopoietic Malignancies, Immune Regulation, and DNA Repair. *Front Oncol.* 2019;9:210.
126. Jaiswal S, Fontanillas P, Flannick J, Manning A, Grauman PV, Mar BG, Lindsley RC, Mermel CH, Burtt N, Chavez A, Higgins JM, Moltchanov V, Kuo FC, Kluk MJ, Henderson B, Kinnunen L, Koistinen HA, Ladenvall C, Getz G, Correa A, Banahan BF, Gabriel S, Kathiresan S, Stringham HM, McCarthy MI, Boehnke M, Tuomilehto J, Haiman C, Groop L, Atzmon G, Wilson JG, Neuberg D, Altshuler D, Ebert BL. Age-related clonal hematopoiesis associated with adverse outcomes. *N Engl J Med.* 2014;371(26):2488-2498.

127. Xie M, Lu C, Wang J, McLellan MD, Johnson KJ, Wendl MC, McMichael JF, Schmidt HK, Yellapantula V, Miller CA, Ozenberger BA, Welch JS, Link DC, Walter MJ, Mardis ER, Dipersio JF, Chen F, Wilson RK, Ley TJ, Ding L. Age-related mutations associated with clonal hematopoietic expansion and malignancies. *Nat Med.* 2014;20(12):1472-1478.
128. Suefuji N, Niino D, Arakawa F, Karube K, Kimura Y, Kiyasu J, Takeuchi M, Miyoshi H, Yoshida M, Ichikawa A, Sugita Y, Ohshima K. Clinicopathological analysis of a composite lymphoma containing both T- and B-cell lymphomas. *Pathol Int.* 2012;62(10):690-698.
129. Rizzo K, Stetler-Stevenson M, Wilson W, Yuan CM. Novel CD19 expression in a peripheral T cell lymphoma: A flow cytometry case report with morphologic correlation. *Cytometry B Clin Cytom.* 2009;76(2):142-149.
130. Francis J, Dharmadhikari AV, Sait SN, Deeb G, Wallace PK, Thompson JE, Wang ES, Wetzler M. CD19 expression in acute leukemia is not restricted to the cytogenetically aberrant populations. *Leuk Lymphoma.* 2013;54(7):1517-1520.
131. Stone EL, Pepper M, Katayama CD, Kerdiles YM, Lai CY, Emslie E, Lin YC, Yang E, Goldrath AW, Li MO, Cantrell DA, Hedrick SM. ICOS coreceptor signaling inactivates the transcription factor FOXO1 to promote Tfh cell differentiation. *Immunity.* 2015;42(2):239-251.
132. Yuan XQ, Peng L, Zeng WJ, Jiang BY, Li GC, Chen XP. DNMT3A R882 Mutations Predict a Poor Prognosis in AML: A Meta-Analysis From 4474 Patients. *Medicine (Baltimore).* 2016;95(18):e3519.
133. Russler-Germain DA, Spencer DH, Young MA, Lamprecht TL, Miller CA, Fulton R, Meyer MR, Erdmann-Gilmore P, Townsend RR, Wilson RK, Ley TJ. The R882H DNMT3A mutation associated with AML dominantly inhibits wild-type DNMT3A by blocking its ability to form active tetramers. *Cancer cell.* 2014;25(4):442-454.
134. Qu Y, Lennartsson A, Gaidzik VI, Deneberg S, Karimi M, Bengtzen S, Hoglund M, Bullinger L, Dohner K, Lehmann S. Differential methylation in CN-AML preferentially targets non-CGI regions and is dictated by DNMT3A mutational status and associated with predominant hypomethylation of HOX genes. *Epigenetics.* 2014;9(8):1108-1119.
135. Corces-Zimmerman MR, Hong WJ, Weissman IL, Medeiros BC, Majeti R. Preleukemic mutations in human acute myeloid leukemia affect epigenetic regulators and persist in remission. *Proc Natl Acad Sci U S A.* 2014;111(7):2548-2553.
136. Buscarlet M, Provost S, Zada YF, Barhdadi A, Bourgoin V, Lepine G, Mollica L, Szuber N, Dube MP, Busque L. DNMT3A and TET2 dominate clonal hematopoiesis and demonstrate benign phenotypes and different genetic predispositions. *Blood.* 2017;130(6):753-762.
137. Haney SL, Upchurch GM, Opavska J, Klinkebiel D, Hlady RA, Roy S, Dutta S, Datta K, Opavsky R. Dnmt3a Is a Haploinsufficient Tumor Suppressor in CD8+ Peripheral T Cell Lymphoma. *PLoS Genet.* 2016;12(9):e1006334.
138. Fos C, Salles A, Lang V, Carrette F, Audebert S, Pastor S, Ghiotto M, Olive D, Bismuth G, Nunes JA. ICOS ligation recruits the p50alpha PI3K regulatory subunit to the immunological synapse. *J Immunol.* 2008;181(3):1969-1977.
139. Lee JY, Skon CN, Lee YJ, Oh S, Taylor JJ, Malhotra D, Jenkins MK, Rosenfeld MG, Hogquist KA, Jameson SC. The transcription factor KLF2 restrains CD4(+) T follicular helper cell differentiation. *Immunity.* 2015;42(2):252-264.

140. Amatore F, Gorvel L, Olive D. Inducible Co-Stimulator (ICOS) as a potential therapeutic target for anti-cancer therapy. *Expert Opin Ther Targets.* 2018;22(4):343-351.